Process-oriented ore-body characterization of the Ag-polymetallic Rupice Deposit, Bosnia and Herzegovina (ULiège)

Auteur : Vujevic, Ivan
Promoteur(s) : Pirard, Eric
Faculté : Faculté des Sciences appliquées
Diplôme : Master en ingénieur civil des mines et géologue, à finalité spécialisée en "geometallurgy (EMERALD)
Année académique : 2022-2023
URI/URL : http://hdl.handle.net/2268.2/19391

University of Liège - School of Engineering and Computer Science

Process-oriented ore-body characterization of the Ag-polymetallic Rupice deposit, Bosnia and Herzegovina

Presented by Ivan Vujević

This thesis is submitted in partial fulfilment of the requirements for the EMerald triple Degree of:

‹‹ Master in Mining and Geological Engineering ›› from University of Liège

‹‹ Master in Sciences de la Terre et des Planètes Environnement ›› from L'École Nationale Supérieure de Géologie, University of Lorraine, Nancy

‹‹›Master of Science – Major: Geosciences›› from Luleå University of Technology

Academic supervisor:

PIRARD Eric
BOROJEVIĆ-ŠOŠTARIĆ Sibila

Industry supervisor:

SMOLONOGOV Sergei
VELIGRAKIS Theodore
MATIĆ Marko

Academic Year 2022-2023

Introduction

ABSTRACT

The ongoing global need for necessary raw materials has resulted in increased awareness within the European Union, highlighting the importance of securing new sources of crucial minerals. In this context, the Rupice polymetallic deposit emerges as an outstanding discovery in Bosnia and Herzegovina, acquired by Adriatic Metals Plc. in 2017. This deposit holds special significance as the primary hard rock mine to be opened in the region in over three decades.

Located within the metallogenic province of Vareš, the Rupice deposit displays a diverse polymetallic mineralization consisting of silver (Ag), gold (Au), zinc (Zn), lead (Pb), copper (Cu), barite ($BaSO_4$), and various other elements. Its geological context within the metallogenic zone, combined with a history of varied mining activities, contributes to its complex structural and mineralogical characteristics. In response to this intricate geological pattern, this research sets out on a comprehensive process-oriented orebody characterization of the Rupice deposit. The primary objectives of the study are threefold: firstly, to unravel the mineral composition of the deposit, identify all mineral phases and observe textures; secondly, to interpret the distribution and connections of valuable metals, particularly Ag and Sb, within distinct mineral phases; and thirdly, to delve into the role played by trace elements, including germanium, mercury, phosphorus, and arsenic, in the mineralization processes. The analytical work was conducted in the University of Zagreb and University of Liege and included: optical microscopy core scanning (SWIR), SEM-EDS, LIBS and XRD.

By addressing these multifaceted research objectives, we strive to provide valuable insights that contribute to the broader understanding of polymetallic deposits, further enhancing the knowledge base necessary for effective resource management and sustainable mining practices.

Acknowledgments

First and foremost, I want to thank God for giving me the opportunity to experience these amazing past few months. There would be nothing without you.

I would like to thank the company officials, including Sergei Smolonogov, Theodore Veligrakis and Marko Matić, for opening the doors of their company to us, hosting me and my colleague Ema Vokić for two months and being really inspiring human beings. You have helped me a lot and I learned a lot from every one of you.

To the researchers and professors at University of Zagreb and University of Liege. I would not have done it without your support. Special thanks goes to Marina Cabidoche, Simon Nachtergaele, and dr. Hassan Bouzahzah, for spending countless hours with me and helping me in every step along the way.

To my mentors, prof. Eric Pirard and prof. Sibila Borojević- Šoštarić. You have shown me what it takes to conduct real-life research. Thank you for sharing your knowledge, time and effort into trying to help me solve the bumps along the way.

To my Emerald friends. I wouldn't have done it without you guys. You have been there alongside me these last two years. Special thanks goes to Charis, Marcel, Melissa, Silum, Chiedza, Oguzhan, Hasseeb, for your endless support. We laughed together, cried together, now it is time to celebrate.

Mojoj obitelji. Ne bih bio ovdje bez vas. Svaki korak koji sam napravio, svaku prepreku koju sam prošao, sve je ovo zbog vas. Hvala majko, hvala oče, hvala braćo i moja sestro.

Mojoj Eleni, ovo je za tebe.

Sve mogu u onome koji me ojača!

Table of Contents

TABLE OF FIGURES

LIST OF TABLES

1. Introduction & objectives

The Rupice polymetallic deposit, located in the central part of Bosnia and Herzegovina, is a current prospect under concession by Adriatic Metals plc., since 2017. Situated within the metallogenic region of Vareš, with its long history of Pb-Zn-Fe-Mn-Hg-Ba mining operations, it represents one of the biggest Pb-Zn-Ag discoveries in what is shaping up to be a highly prospective metallogenic province. The deposit exhibits complex geological, structural, and mineralogical characteristics, created as a result of multiple phases of over thrusting, related to the Alpine Wilson cycle in Dinarides. The motivation behind this research is to conduct a process-oriented orebody characterization of the Rupice deposit, enabling a deeper understanding of its geochemical and mineralogical features. The Rupice deposit, with rich polymetallic mineralization (21.1 Mt at 156 g/t Ag, 1.2 g/t Au, 4.3% Zn, 2.8% Pb, 0.4% Cu, 27% BaSO4, Press release July 2023. Adriatic Metals Plc.), encompasses a diverse range of ore-bearing minerals, including galena, sphalerite, chalcopyrite, pyrite, bournonite, boulangerite, freibergite and barite. However, the complex nature of the deposit poses challenges in terms of optimal extraction and processing methods, resource estimation accuracy, and economic viability assessment.

Accurate orebody characterization is essential for efficient mining operations and effective resource management. It provides crucial insights into the deposit's geological structure, mineral distribution, and metallurgical behaviour. Previous studies conducted by Adriatic Metals plc. have made initial contributions to the understanding of the Rupice deposit. With over 280 drillholes in place as of July 2023., the company was able to produce a geological model of the ore body. The dimensions are roughly 900 x 350 meters, with a thickness ranging from 0,3 meters up to 60 meters. A preliminary mineralogical study was performed, and main ore-bearing and gangue mineral phases were identified. However, there is still a knowledge gap regarding the detailed mineralogical characterization of the ore body, as well as establishing the genetic model of the deposit.

This study seeks insights into the orebody's composition, structure, and minerals/elements distribution via detailed analyses of its geological and mineralogical features. A process-oriented approach aids our effort to achieve an understanding of the Rupice deposit which will improve resource estimation accuracy while facilitating extraction and processing optimization.

Research objectives

The following research objectives and main questions were outlined:

1. What is the mineralogical composition of the Rupice deposit, and how does it vary spatially within the orebody?
2. How does the Ag and Au deportment in the orebody look like and what mineral phases are responsible for their concentration?
3. What role do the trace elements, such as germanium, mercury, phosphorous and arsenic play in the mineralisation?
4. How can a process-oriented approach enhance the understanding of the Rupice deposit, particularly in terms of optimizing mining and processing methods with regards to penalty elements?

To address these research questions and achieve the objectives, the following tasks were conducted:

1. Perform a comprehensive mineralogical analysis of the deposit:
   - Collect representative samples from different sections of the orebody.
   - Conduct mineralogical identification and quantification using techniques such as ore microscopy, X-ray diffraction (XRD), SEM-EDS, LIBS and mineral liberation analysis (MLA).
   - Analyse the spatial distribution of different minerals within the deposit.
2. Assess the metallurgical characteristics of the minerals:
   -Evaluate the liberation characteristics of the minerals through particle size analysis and mineral liberation analysis
   - Asses the deportments of Ag, Au, Sb, Cu, based on automated mineralogical study
3. Conduct a statistical approach to data processing:
   - Provide general statistical information on the data
   - Evaluate potential links in the correlation plots
   - Conclude based on different clustering techniques a possible link with the known lithologies
4. Apply a process-oriented approach to orebody characterization:
   - Integrate the lithological, mineralogical, and metallurgical data to develop a comprehensive understanding of the deposit.
   - Evaluate the implications of the orebody characteristics on the selection of mining methods, ore processing techniques, and overall resource utilization.

By accomplishing these research objectives and addressing the corresponding questions, this study aims to contribute to the knowledge and understanding of the Rupice polymetallic deposit, providing valuable insights for the mining industry, and paving the way for optimized mining practices and sustainable resource management.

1.2. Limitations

It is important to acknowledge the limitations that may impact the research and the interpretation of its findings:

1. Sample Size and Representation:
   - The study will rely on 40 representative samples due to logistical and resource constraints.
   - The extent to which the samples represent the overall variability of the deposit may be subject to certain limitations (objectivity of the analysis, applicability to the existing extent of mineralisation due to constant exploration activities discovering and extending the ore body, with a change in chemistry (Adriatic metals press release, July 2023).
2. Time and Resource Constraints:
   - The research is conducted within a six months' timeframe and with analytical methods that were available for use (SEM-EDS, Ore microscopy, XRD, LIBS, Core scanning, Automated mineralogy) , which may influence the depth of the analysis.
   - Some aspects of the deposit's characterization require further research beyond the scope of this study, such as the structural analysis of the deposit, it's constraints for the mineralisation, and a detailed analysis of the trace elements in the ore body and its relevance for the in the genetic model of the deposit.
3. Data Availability:
   - The availability of historical data and access to specific information related to the Rupice deposit is limited, due to the geopolitical conflicts in the 1990s, which resulted in closure of every active mining in the Bosnia and Herzegovina
   - The research heavily relies on existing data sources and collaboration with industry stakeholders to gather the necessary information.
4. Generalizability:
   - The findings of this study will be specific to the Rupice polymetallic deposit and may not be directly applicable to other ore deposits or regions.
   - The geological, mineralogical, and metallurgical characteristics of the Rupice deposit may vary from other polymetallic deposits, limiting the generalizability of the research findings.

By clearly defining the scope of the study and acknowledging its limitations, the research outcomes will be presented within a well-defined context, providing a comprehensive understanding of the Rupice polymetallic deposit while recognizing the boundaries and constraints of the investigation.

2. Literature review

2.1. Geotectonical and geodynamic setting

The Rupice mine is situated in the Dinarides fold-thrust belt, which spans approximately 700 km in a northwest-southeast direction. They are a folded, thrusted, and imbricated belt located between the Southern Alps in the northwest and the Hellenides in the south and southeast (see Figure 1; modified after Schmid et al., 2020). The geology of the Dinarides is characterized by a complex tectonic history that includes multiple phases of subduction, collision, and extension, represented by the Alpine Wilson cycle in the Dinarides, and its stages: 1) Early intra-continental rifting (Permian); 2) Triassic advanced rifting; 3) Jurassic oceanization; 4) Cretaceous subduction; 5) Paleogene collision; and 6) Neogene post-collision and extension (L. A. Palinkaš et al., 2008). The region has been the focus of numerous geological studies due to its geological complexity and potential for mineral resources.

Schmid et al. (2008, 2020), defines the tectonic units as: 1) Adriatic microplate, consisting of Paleo-Mesosoic platform carbonates from the Adriatic carbonate platform; 2) High Karst & Dalmatian unit from the most external Dinarides, represented by Late Triassic – Cretaceous carbonate platform facies; 3) Composite nappes, comprised of three distinct units, namely East Bosnian-Durmitor (including Rupice deposit), Drina-Ivanjica and Jadar-Kopaonik unit; 4) Ophiolites and suture zones, with Sava suture zone and Western Vardar ophiolitic unit being relevant for the region of interest.

The Dinaridic part of the Alpine orogeny was formed because of prolonged convergence between the Adriatic microplate and Eurasia, which began in the Mid-Jurassic period (Schmid et al., 2020). The Dinarides can be divided into two main segments: the internal and external Dinarides. The internal Dinarides consist of multiple composite nappes (see Figure 1), including ophiolites derived from the Western Vardar Ophiolitic unit of the Neotethys. These ophiolites were obducted onto the continental slope deposits of the Adriatic passive margin during the Late Jurassic (Robertson et al., 2009). Subsequently, the convergence between Adria and Eurasia led to the north-eastward subduction of the remaining oceanic lithosphere beneath the units derived from Europe (for more details, refer to Schmid et al., 2020; Van Hinsbergen et al., 2020). The collision between the continents resulted in Maastrichtian-Paleocene deformation and metamorphism of Upper Cretaceous trench deposits in the Sava Suture Zone (Ustaszewski et al., 2010), followed by nappe-stacking within the internal Dinarides (Schmid et al., 2020). Shortening processes continued throughout the Paleogene, with the deformation front continuously propagating south-westward, eventually reaching the Adriatic Mesozoic carbonate platform in the Middle Eocene period. In the external Dinarides, this foreland propagation is evidenced by the syn-

orogenic deposition of turbiditic deposits from the Mid-Upper Eocene to locally the Oligocene (referred to as the "External Dinarides Flysch"; see Figures 1 and 2). These deposits are sometimes interbedded with coarse-grained conglomerate-bearing formations known as the Promina Beds (Figure 1); (Mrinjek et al., 2012).

During the Miocene epoch, extensive lacustrine deposits developed within various intramontane basins of different sizes and origins in the Dinarides (e.g., Andrić et al., 2017; de Leeuw et al., 2012). Tectonically, the external Dinarides can be further divided into the more internally located High Karst unit and the more externally positioned Dalmatian unit (Figure 1; Schmid et al., 2020). Rupice deposit (red star on Figure 1) is situated in the narrow part of the East-Bosnian Durmitor nappe. Three kilometres of aerial distance separates this unit from the obducted Western Vardar ophiolites, suggesting a complex tectonic environment.

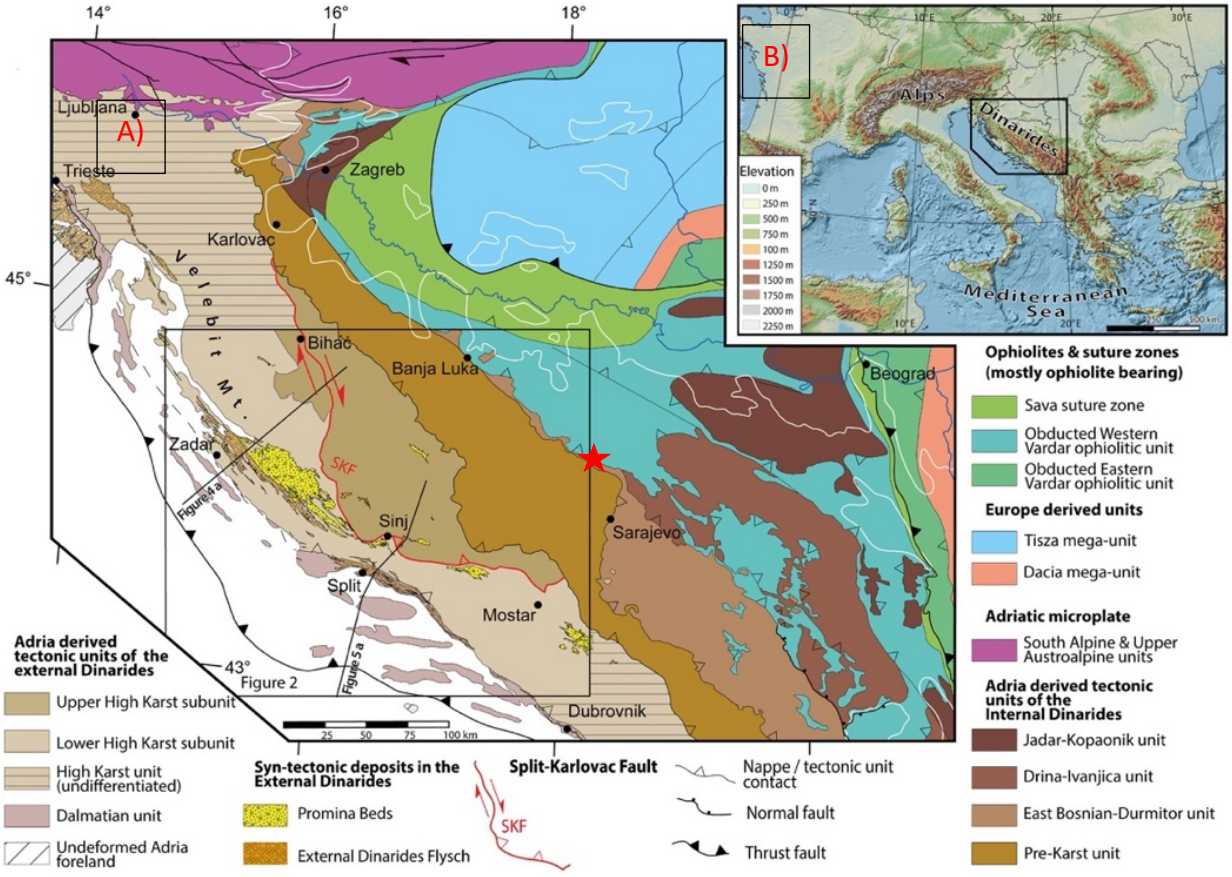

Figure 1. Tectonic map of the Dinarides, (Map (A) after (Schmid et al., 2020,), Map (B) after (Balling et al., 2021)- Red star marks the Rupice deposit

2.3. Regional Geology

Vareš metallogenic district is a part of the East-Bosnian Durmitor nappe, a composite thrust sheet that consists of Paleozoic and Mesozoic formations. The basal part of the nappe includes Paleozoic and Triassic-Jurassic strata, while the upper part consists of ophiolitic units that were obducted during the Late Jurassic to earliest Cretaceous (Schmid et al., 2008).
The nappe is characterized by its complex geological history. It was formed through the detachment of Paleozoic and Mesozoic formations from the Adriatic passive margin during Cenozoic times . The deposition of radiolarites started in the Middle Jurassic when the Triassic-Early Jurassic carbonate platform sank below the Carbonate Compensation Depth (CCD). The radiolarites were later overlain by a Late Jurassic ophiolitic tectonic mélange, known as the "Diabase-Radiolarite Formation," which was deposited during the obduction of the Western Vardar Ophiolite Units.

The East Bosnian-Durmitor nappe is a composite unit that also includes more internal tectonic units such as the Lim Paleozoic and overlying Triassic-Jurassic strata (Schmid et al., 2008). It is characterized by out-of-sequence thrusting, with a thrust that post-dates the Late Jurassic obduction of the Western Vardar Ophiolitic Unit over the East Bosnian-Durmitor Unit. This thrust juxtaposes the more external East Bosnian-Durmitor composite thrust sheet against the more internal Drina-Ivanjica Unit, which is also a composite tectonic unit (Fig x – fali nam slika East Bosnian Durmitor nappe sa svim jedinicama koje opisujete. Vidjeti u literaturi i dodati neku od karata; još jednom provjeriti poziciju Rupica).

The East Bosnian-Durmitor nappe is considered to be a far-travelled thrust sheet, with a displacement of more than 45 km. It corresponds to the "Zone Serbe" of previous geological studies (Hrvatović & † Pamić, 2005; Ustaszewski et al., 2010). The nappe has been extensively studied and mapped using various geological maps and research papers, including the 1:100,000 Geological Map of former Yugoslavia (Osnovna Geološka Karta SFRJ) and the work of Kräutner & Krstić (2002, 2006).

2.2. The Advanced intracontinental rifting of the Dinarides

The geology of the Dinarides is constrained by the Alpine Wilson cycle. Such a cycle, which got its name after J.Tuzo Wilson (1908-1993), is based upon plate tectonics , and tells a “story” about an ocean's opening and closing stages. The major stages of the Alpine Wilson cycle in the Dinarides are (Palinkaš et al., 2008): 1) Early intra-continental rifting (Permian); 2) Triassic advanced rifting; 3) Jurassic oceanization; 4) Cretaceous subduction; 5) Paleogene collision; and 6) Neogene post-collision and extension followed by orogenic collapse. Each of these stages represents a specific geological environment and consequentially, specific ore deposits related to them (Palinkaš et al., 2016).

Advanced intra-continental rifting stage, specific to Middle Triassic, is represented by various types of ore deposits, several of which are in the Vareš metallogenic district (including Rupice). One type of deposit is the carbonate-hosted, low-temperature, Pb-Zn deposits found within the carbonate platform formations, known as Mississippi Valley Type (MVT) or Bleiberg-Mežica Type deposits. These deposits are in the Middle Triassic formations of the External Dinarides, which is a passive continental margin of the Adriatic microplate. The Pb-Zn deposits in this region exhibit distinct characteristics, such as an anomalous modal age of lead ranging from 310 to 490 million years (Palinkaš, 1985.). The paragenesis of these deposits is simple, consisting mainly of Pb-Zn minerals without significant copper content. The fluid inclusion studies conducted on these deposits indicate the dominance of Ca2+ in the ore-bearing fluids, the presence of biogenic sulphur in the sulphides, and a low temperature of formation ranging from 100 to 200ºC (Borojević Šoštarić et al., 2004). These deposits are believed to have originated from deeply seated basinal connate brines that were expelled during the Middle Triassic advanced rifting. The depositional environment within the carbonate platform, devoid of significant tectono-magmatic events, explains the low temperature of fluids and the simple sulphide paragenesis observed in these deposits. Some notable examples of these deposits include the Topla Pb-Zn deposit in the northern Karavanke Alps, the Mežica Pb-Zn deposit in the same region, and the Sv. Jakob Pb-Zn deposit on Medvednica Mountain in the southwestern part of the Zagorje-Mid-Transdanubian zone. Another type of deposit associated with the advanced Tethyan rifting stage is the sedimentary-exhalative (SEDEX) deposits of iron (Fe), manganese (Mn), barite (Ba), polysulphide, and mercury (Hg). These deposits are widespread in the Dinarides and are part of the Mid-Triassic volcano sedimentary sequences. They originated from seafloor hydrothermal exhalations in longitudinal troughs formed by advancing Tethyan rifting. These deposits are typically found within tuffs, tuffites, cherts, clastics, and occasionally limestone and dolostones. The mineralization is often interstratified with extrusive submarine volcanics. The depositional environment and local redox conditions led to the formation of various reducing and oxidizing parageneses, including pyrite, cinnabar, base metal sulphides, sulfosalts, barite, siderite, hematite, and Mn-oxides.

Within the Vareš metallogenic district in Central Bosnia, advanced rifting magmatism resulted in the formation of spilites, ophitic basalts, and diabases, interlayered with Ladinian sedimentary rocks (Operta, 2014). This region hosts various deposits related to the magmatism, including cinnabar deposits, Mn-oxide deposits, monomineralic and polymetallic barite deposits, and siderite-hematite deposits. These deposits are located within a sigmoid-shaped curved belt, stretching approximately 25 km in length and 2 to 5 km in width, extending from the Srednje-Draževići area in the south to Vareš-Borovica in the northwest. The geological formation consists of Lower Triassic shales, sandstones, and limestones, Anisian limestones, and Ladinian spilites interlayered with pyroclastic rocks, cherts, shales, Fe-Mn shales, and locally covered by Upper Triassic carbonates (Palinkaš et al., 2008).

The Vareš deposits, including Smreka, Droškovac, and Brezik, are significant examples of Mid-Triassic mineralization during the advanced Tethyan rifting phase. These deposits exhibit hydrothermal, stratiform siderite-hematite-chert beds within the Anisian and Ladinian sequences. The mineralization shows vertical zoning, reflecting changes in redox conditions during deposition. The sequence begins with bituminous shales containing pyrite and base metal sulphides, followed by barite and siderite deposition under reducing conditions. Overlying clastics, oolithic limestone, and hematite shale with hematite ± chert beds indicate an oxidizing environment. The major minerals in these deposits include siderite, manganese-rich hematite, barite, pyrite, marcasite, chalcopyrite, galena, sphalerite, tetrahedrite, and Pb-sulfosalts. In the Srednje-Borovica-Rupice-Veovača area, ore-bearing dolostones and intra-formational ore-breccias are found. These mineralized rocks, ranging from 60 to 120 meters in thickness, contain barite, galena, sphalerite, pyrite, marcasite, arsenopyrite, chalcopyrite, bournonite, tetrahedrite, stibnite, cinnabar, and other minerals. The Rupice deposit consists of massive ore bodies containing iron sulphides with barite or massive barite bodies. The Veovača deposit contains ore-breccia or ore-conglomerates cemented by barite and Pb-Zn sulphides. Other deposits within the region include the Draževići cinnabar deposit, Čevljanovići manganese deposit, Bužim manganese deposit, Mt. Ivanščica manganese occurrence, and the renowned Idrija mercury deposit. The Idrija deposit is the second-largest mercury deposit globally and is associated with fault zones in Permo-Carboniferous to Upper Ladinian formations. The ore beds in this deposit consist of cinnabar-pyrite beds in the Upper Ladinian organic-rich Skonca Formation. The ore minerals include cinnabar, metacinnabar, native mercury, pyrite, and barite. The genesis of the Idrija deposit is linked to Ladinian rifting and hydrothermal fluid mineralization along subvertical faults. Fluid inclusion data indicate a temperature range of 160 to 220 °C and low to moderate salinity (Palinkaš et al., 2004).

Undoubtedly, the metallogeny of Dinarides has great economic potential, as new investments and exploration efforts show (i.e. Rupice mine). However, the region is still largely under-explored, with potential for both greenfield and brownfield exploration projects in the

future. Borojević Šoštarić et al., 2022., provided a comprehensive SWOT analysis of the Adria region (corresponding to Dinarides, Hellenides and Vardar zone), and its countries. The region has mineral resource potential, human resource potential to accommodate the complete value chain through higher academic institutions. The resources are unevenly distributed between the countries, and there is a disbalance in the economical point of view between them, although they share similar economic “troubles”, formerly being part of the same country of Yugoslavia. Authors suggest more comprehensive exploration activities, followed by the compliance of the resources and reserves with the international (JORC, PERC), and EU legislations.

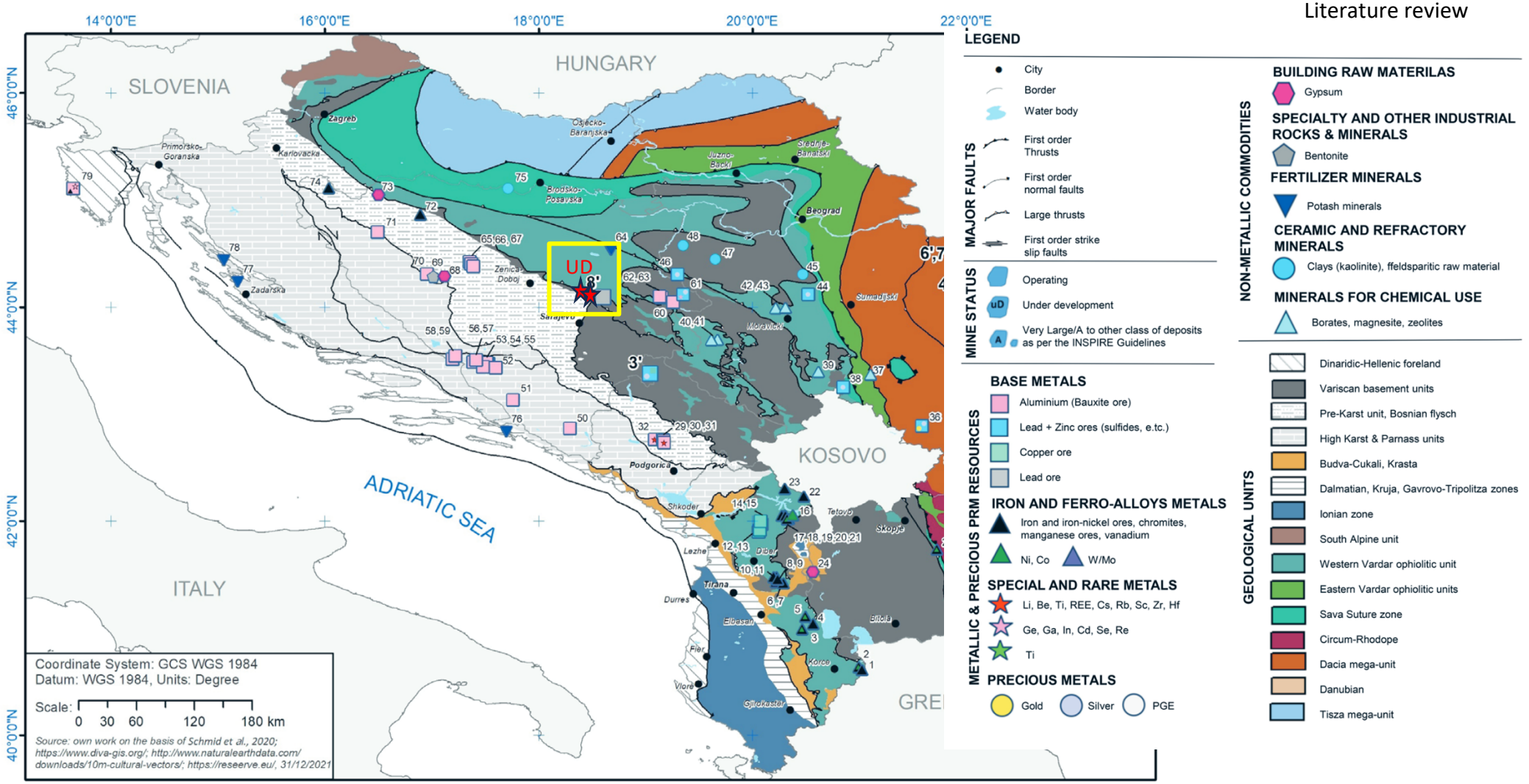

Figure 2. Simplified metallogenic map of the Dinarides. From (Borojević Šoštarić et al., 2022), modified after (Schmid et al., 2020). Red stars mark the locations of Rupice deposit (left), and Veovača deposit (right) UD – under development.

2.2.3. Vareš metallogenic district

Rupice deposit is a part of the Vareš region, which has been historically known for its mining potential. There is evidence of Roman culture in these areas, specifically related with the mining and smelting activities of the iron ore. In the early 15th century oral tradition is telling stories of the old village owners selling iron ore to the Turkish generals. First written evidence of mining in this region comes in early 17th century, with the Church monks represented by Pavao Pelicarić mentioning the district of Vareš, as well as local iron mines and smelters. In the early 1800-s, Austro-Hungarian monarchy started to rule over these areas, providing technological and cultural advancements in the field of geology and mining, which resulted in prosperity of the Vareš region (Hrvatović, 2022). Its significance increased in 1891, when the first steel-making plant commenced in Vareš, and lasted long after the second world war, in 1945, up until 1992 when all mining activity in the region collapsed due to bad investments, and geopolitical circumstances.

First geological knowledge of the Vareš area comes with A.Conrad in 1870. Some thirty years later, following his works, Austrian geologist Friedrich Katzer conducted the first geological survey of Bosnia and Herzegovina (Katzer, 1903). Published map 1:200 000 clearly marked the areas in and around Vareš as ore-bearing. By delineating middle and upper Jurassic in the village of Borovica (some 5km NW form the city of Vareš), he highlighted the occurrence of iron and lead bearing minerals.

Following the results of the surveying, extensive geological investigations have been conducted in the Vareš region in the next half a century, focusing on the Triassic sedimentary zone and particularly on the exploration of complex sulphide ores containing lead, zinc, and barite (Operta, 2006). These research efforts have spanned several decades, albeit with occasional breaks. The primary objective of these studies has been to identify the distribution of sulphide deposits within the stratigraphic column, analyse their mineralogical composition, examine their genetic characteristics, and determine their chemical composition (Atanacković et al., 1968; Ramović, 1955, 1962; Trubelja, 1969; Veljković, 1973, 1989). The tectonic units of the Dinarides were best compiled on the geological 1:100 000 maps of former Yugoslavia (**Error! Reference source not found.**; ,Pamić et al., 1978).

In the zone of Triassic sediments in the Vareš area, around 30 mineral and ore occurrences have been recorded in the Smreka, Brezik, Droškovac, Veovača, Orti, Rupice, Juraševac-Brestić, Selište, Kraljeva jama, and Smailova šuma localities (Operta, 2014). These deposits can be separated in two distinct categories: iron deposits and polymetallic (Pb, Zn, Au, Cu, Ag) deposits (Hrvatović, 2022).

Iron ore was mined at three localities in the Vareš area: Smreka, Brezik and Droškovac. While Smreka and Brezik were open pit mines, Droškovac started like an open pit, but due to the morphology of the orebody it quickly became an underground operation. Ore was mined at these localities since 1891, with an almost continuous production until its ending point in

1992 (Hrvatović, 2022). Smreka was the largest deposit with reserves of approximately 150 million tons. After the completion of mining operations, a lake with dimensions of 350 meters and depth of 150 meters was formed at the open pit, but no reclamation effort was done at either of those three mine sites.

Significant polymetallic deposits comprised of lead-zinc-barite ore are present in the Borovica-Vareš zone. These deposits were known since the Romans, and artisanal mining sites can be locally found in the area. A more comprehensive research and exploratory work has been done in the period between 1878-1941. (Hrvatović, 2022). Veovača deposit is located east of Vareš in Triassic sediments and contains several types of ore: breccia with barite, sphalerite, marcasite, and pyrite, as well as dark barite with sphalerite, galena, and occasionally marcasite. Exploitation at the Veovača deposit began in 1983, with a break in the period 1987-1988 (due to instability of the flotation tailings) and was finally discontinued in 1991 due to the inability to market sulphide concentrates due to the presence of mercury and financial over-indebtedness (Operta, 2014).

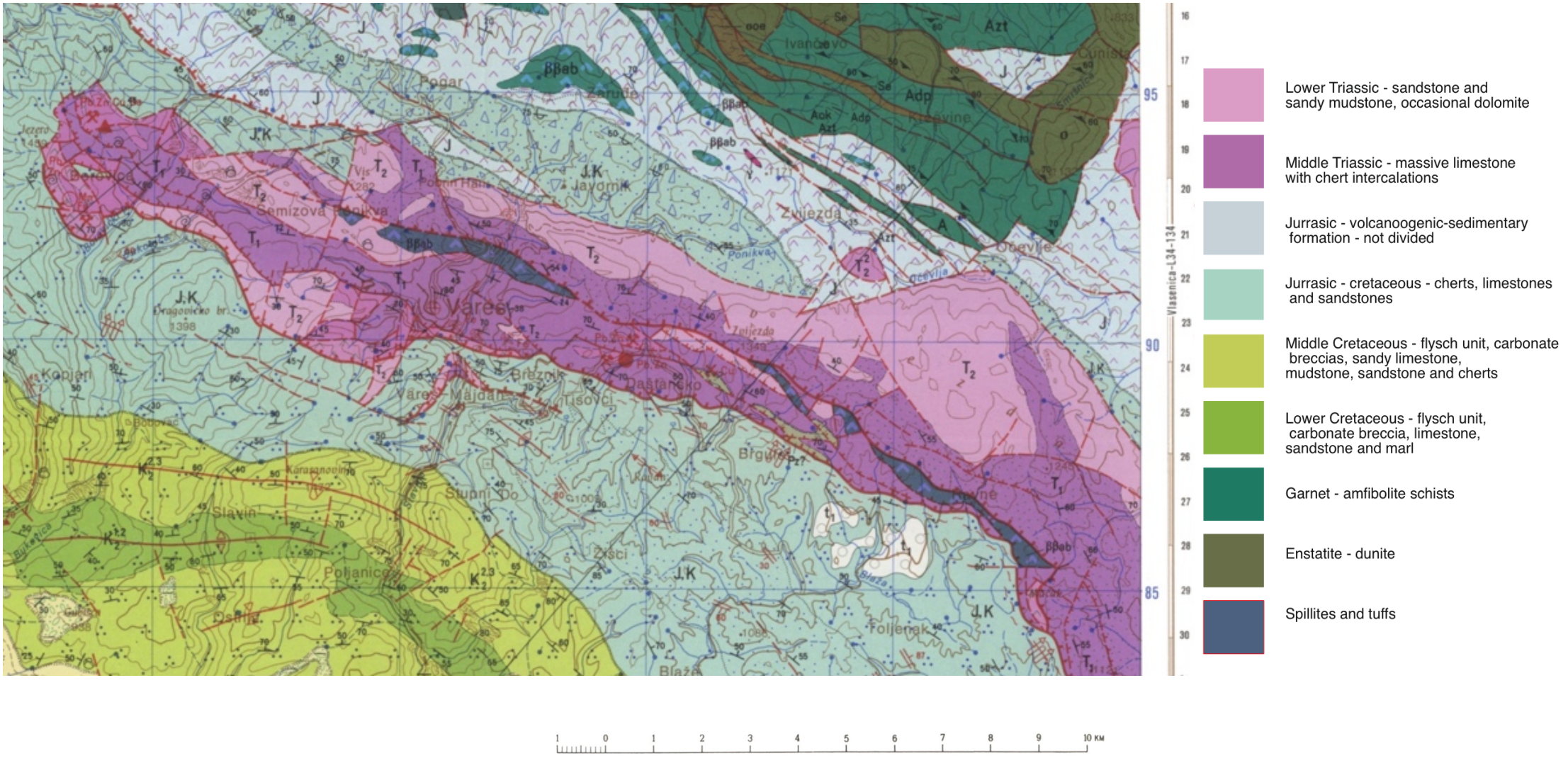

Figure 3.Geological map of Vareš area, modified after (Pamić et al., 1978)

Rupice deposit

Rupice project encompasses a concession area of 41 square kilometres, centred around the town of Vareš. This town is situated in the Vareš municipality of the Zenica-Doboj Canton in Bosnia and Herzegovina. It is approximately 45km NW from Sarajevo, the capital of Bosnia and Herzegovina.

Exploratory activities in the Rupice area began in 1952 and were conducted on and off until 1990. Initially, the focus was on identifying barite mineralisation, but later shifted to polymetallic mineralization. Various exploration methods were employed, including geophysical surveys (IP – chargeability), surface excavations (costeans), exploratory tunnels (exploration adits), and drilling. These investigations indicated the presence of polymetallic mineral deposits at Rupice and Juraševac-Brestić. Chargeability anomalies were identified extending southeast between Rupice and Juraševac-Brestić, but these trends have not been confirmed through drilling. Similarly, other anomalies in the Gornja Borovica and Donja Borovica areas have not been explored further through drilling, with prospective plans for future investigation (Adriatic Metals Plc. Corporate presentation, 2022.).

Figure 4. Map of exploration concessions of Adriatic Metals plc. in the Vareš municipality. (Location of Rupice mine in red sphere) (from Adriatic Metals Plc. Corporate presentation, 2022.)

In 2018, Adriatic metals plc., under their newly acquired concession, conducted drilling at BR-17-18, which was located on the boundary of the original concession area. This drilling successfully intercepted 66 meters of high-grade mineralization. As a result, the company sought to expand the concession boundary and is currently conducting drilling in the northern plunge of the deposit. Recent drilling has yielded thick sections of high-grade mineralization to the north and southeast, towards Juraševac-Brestić. In 2019., first mineral resource estimates were published, based on JORC code. They concluded Indicated and inferred mineral resource estimates at 12.0 Mt at 149 g/t Ag, 1.4g/t Au, 4.1% Zn and 2.6% Pb. Pre-feasibility study was published in the late 2022, followed by a definitive feasibility study in 2021. Results are summarised in the table below (Adriatic Metals Plc. Definitive Feasibility study of the Rupice deposit, 2021.).

Table 1. Mineral resource and reserves, Rupice definitive feasibility study, 2021.

Rupice Mineral Resources, August 2020 (PFS)									
		Grades							
JORC Classification	(Mt)	AgEq (g/t)*	ZnEq (%)	Ag (g/t)	Zn (%)	Pb (%)	Cu (%)	Au (g/t)	Sb (%)
Indicated	9,5	450	18,6	176	4,9	3,1	0,5	1,6	0,2
Inferred	2,5	111	4,6	49	0,9	0,7	0,2	0,3	0,1
Rupice Mineral Reserves, August 2021 (DFS)									
Probable	7,3	485	13,0	202	5,7	3,6	1,9	0,6	0,2

*AgEq - Silver equivalent was calculated using conversion factors of 37.31 for Zn, 28.6 for Pb, 72.0 for Au, 118.2 for Cu and 118.2 for Sb. A cut-off grade of 50 g/t of AgEq was applied. The applied formula was: AgEq = Ag (g/t) * 89 % * 88 % + 37.3 * Zn(%) * 91% * 75% + 28.6 * Pb(%) *92% * 87% + 72.0 * Au(g/t) * 64% * 77% + 118.2 * Sb(%) * 95% * 84% + 118.2 * Cu(%) * 94% * 16% (Rupice definitive feasibility study, 2021.

Since then, more than 280 drillholes have successfully delineated a major part of the *Main orebody.* In 2022, in the NW part of the concession, exploratory drilling hit another massive sulphide mineralisation zone. Mineralisation is present in two zones, the Lower and *Upper load*, with a distinct correlation between the higher grade of mineralisation in the lower zone and the occurrence of the upper zone. The NW part exhibits less deformation compared to Rupice Main orebody. Besides that, the NW part is more copper and gold rich, with less barite (Adriatic Metals press release July 2023.). Within the massive sulphide boundaries of the deposits, there is evidence of differential shearing, which has given rise to a large sigmoidal structure containing polymetallic mineralization. Most of the deformation primarily occurs along shears that wrap around the edges of the mineralization. This aligns with the

understanding that the deposit is situated within a regional-scale compressional low angle thrust environment. The central part of the Rupice deposit shows thickening due to thrust-related folding, where mineralized widths of up to 65 meters true thickness can be observed.

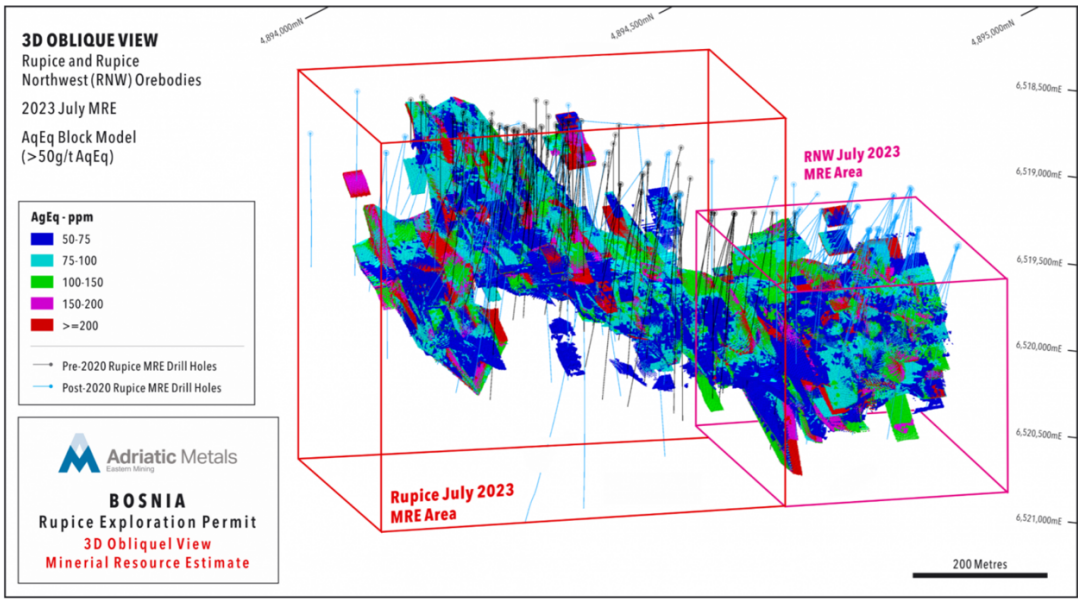

Figure 5. 3D mineral resource estimate of the Rupice orebodies

Rupice is positioned stratigraphically higher than RNW, with a siliceous chert unit rich in iron oxides (GYD) separating the two. At their extremities, Rupice and RNW overlap for approximately 80 meters, forming an area known as the 'GAP'. Within the GAP region, both Rupice and the NW part lenses exhibit a transition from being predominantly massive to dolomitic breccia and finally to disseminated sulphides. It is less structurally deformed, with an expected continuation in the Kakanj municipality. Initially thought to be another lens of the broader mineralised system, since then the so-called *Gap* between the two orebodies has been narrowed down to less than 20 meters, with mineralisation shortening towards the main orebody. New and updated mineral resource estimation defines 21.1 Mt at 156 g/t Ag, 1.2 g/t Au, 4.3% Zn, 2.8% Pb, 0.4% Cu, 27% $BaSO_4$. (Adriatic Metals press release July 2023.)

As of April 2023., the mine is in development stage, with access roads to and from the mine and processing plant being built. Access to underground workings will be via two ramps, so called Upper access portal and Lower access portal. Mining will be performed using transversal and longitudal longhole open stoping method. The delineation between the two variations is dependable on the thickness of the orebody, with 20m being the limit. Cut- off grades for high grade domains were 10% for Zn, 3% for Pb, 25% for BaSO4, 1% for Cu, 2.5g/t for Au, and 110g/t for Ag.

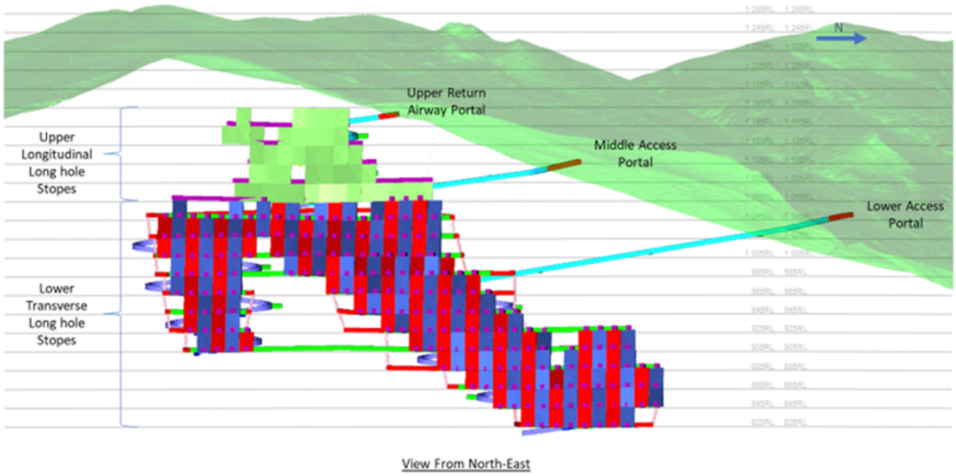

Figure 6. Mine plan of Rupice deposit (Obtained from the Adriatic metals plc. DFS, 2021)

The production rate of the Rupice Underground Mine is specifically designed to align with the capacity of the Vareš Processing Plant, which is set at 800,000 tonnes per year (Adriatic Metals Plc. DFS, 2021). Processing of the ore will start at the Rupice mine site, with crushing and stockpiling of the ore in three categories: low, medium and high-grade ore. Processing plant is being built on the brownfield site, with thickener pools being re-used from previous processing works, in Yugoslavian times. The Vareš Processing Plant receives crushed ore through a coarse ore hopper. This crushed ore is then conveyed and stored in two separate crushed ore bins before being processed in the ball mill grinding circuit. The ball mill grinding circuit consists of a ball mill and cyclones. The overflow from the cyclones is directed to the sequential flotation circuit. The sequential flotation circuit is comprised of two stages. The first stage involves silver-lead flotation and regrinding, while the second stage involves zinc flotation and regrinding. The purpose of these stages is to separate and concentrate the silver-lead and zinc minerals from the ore. The flotation process generates two saleable concentrates, namely the silver-lead concentrate and the zinc concentrate Figure 7. These concentrates are then subjected to thickening, filtration, and transported to the shipping dock of Ploče via train line.

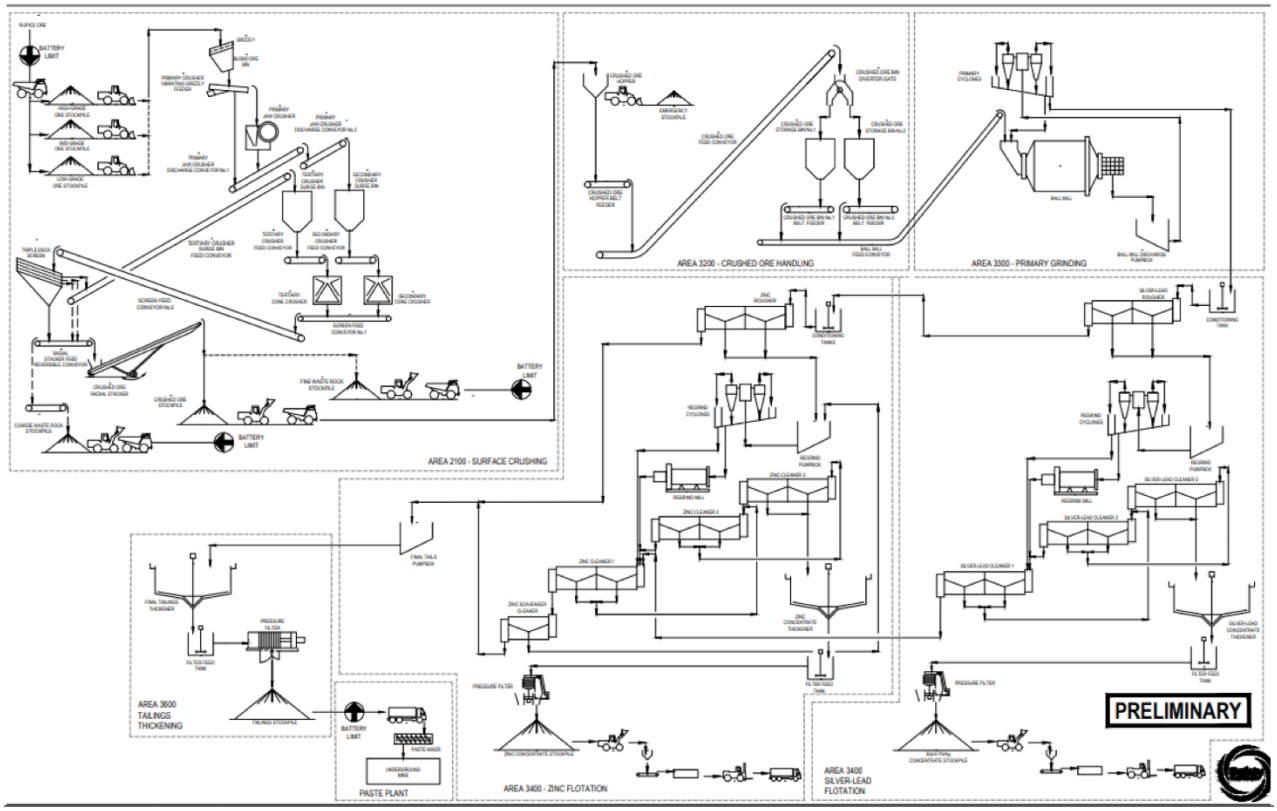

Figure 7. Preliminary process flowsheet (DFS, 2021.)

Economic mineralisation in the Rupice deposit is presented by a single tabular lens, with current drillings giving some insight about a potential of another lens, indicating presence of potential clusters (Figure 8). Its thickness goes from 0,5-60m, with the width of 250m. In the Rupice deposit, mineralised dolomitic breccias hosts the ore, and can be observed on the outer flanks of the orebody, with thickness between 2-25m. They are heterogeneous and constructed of clasts from different lithologies, mostly chert, shale, sandstone, and dolomites. Mineralisation is visible as the infill of the space between the clasts, as well as different stages of carbonate replacement by the sulphide minerals (mostly pyrite, in the matrix Gn+Sph). Central part of the orebody consists of massive barites, with lead, zinc, and copper sulphides. Its thickness goes from 0,5-60m. Going from the central part of the orebody to the outer flanks, tectonically more deformed lithological units occur (Geology Synopsis by Aleksa Vujinović, Adriatic Metals Plc. 2022.).

Through exploratory drilling and comprehensive geological mapping, it has been determined that the deposit is situated within a duplex structure that comprises multiple planes of overthrust. Within these duplex structures, the rocks exhibit intense tectonic deformation, which is evident from the presence of shale (fissility and lamination), isocular folds, cleavage, faults, cracks, and numerous clayey zones identified during the exploration drilling and geological mapping processes. Mineralisation is structurally controlled, with two subparallel strike-slip faults delineating the longitudinal axis of the deposit. Among these

faults, the largest one forms the boundary zone of the deposit in the northeast, where movements exceeded 100 meters. The productive structure of the deposit displays significant deformation, particularly in the southwest and southeast sections, where suspension structures have been documented. The most prominent structural-tectonic features of the deposit include folds, duplex structures, and faults. A concrete structural model has not yet been established, and together with 20 oriented drill cores until April 2023, a more comprehensive understanding of the tectonic assemblages and deformation phases is not to be expected soon (OREFIND tm. Vareš Structural report, 2018.).

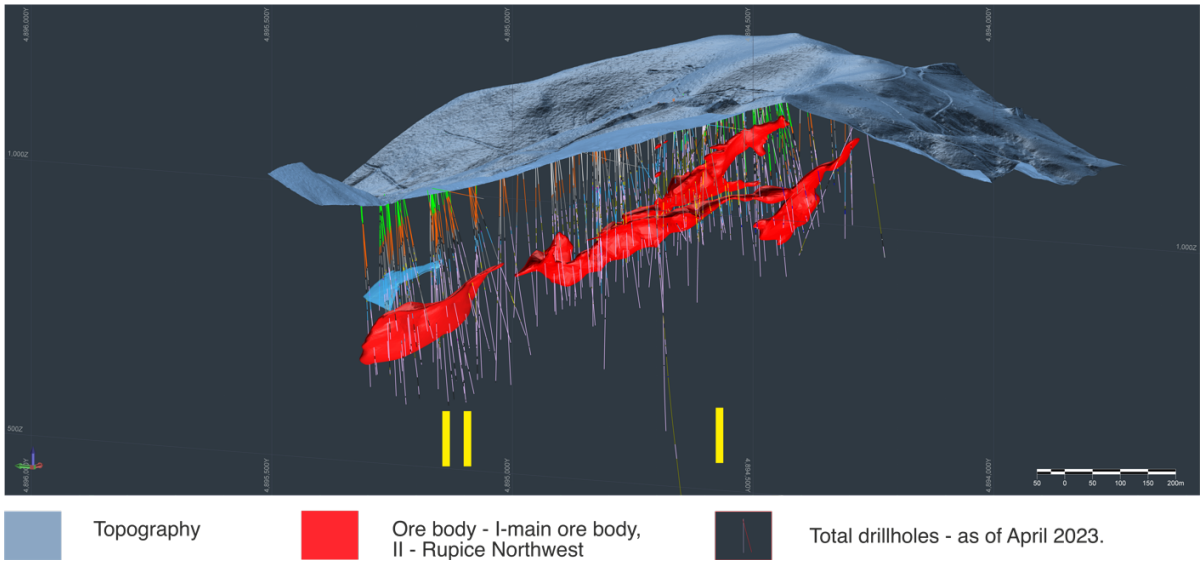

Figure 8. Ore body model of the Rupice deposit, with extensive drillholes shown (until April 2023.) (picture obtained from Adriatic Metals plc.)

3. Materials and Methods

3.1. Materials

Sampling campaign was conducted at the Adriatic Metals plc. exploration team facility in Vareš, Bosnia and Herzegovina. Prior to sampling, a thorough drill core mapping was performed. Over a 2-month period, a total of 108 samples were collected, consisting of ¼ of a drill core (avg. size 10x3 cm), drill core cuttings and chippings, of various sizes. Out of those 108 samples, 40 samples were mineralised, and upon closer inspection sent to the University of Liège for further analysis. List of the samples collected, and analysis performed in ULiège is shown in the Table 2.

During the sampling campaign, three distinct ore types were observed based on the optical properties and can be classified in two major groups: massive mineralisation and dolomitic breccia mineralisation. First ore type is massive barite (figure 9a), with minor sulphide phases (Gn+Sph+Py+Sulph+Cpy). Second ore type is massive sulphides, with minor barite (figure 9b). Third ore type is dolomitic breccia, with sulphide veins (Gn+Sph+BaSO4) (figure 9c).

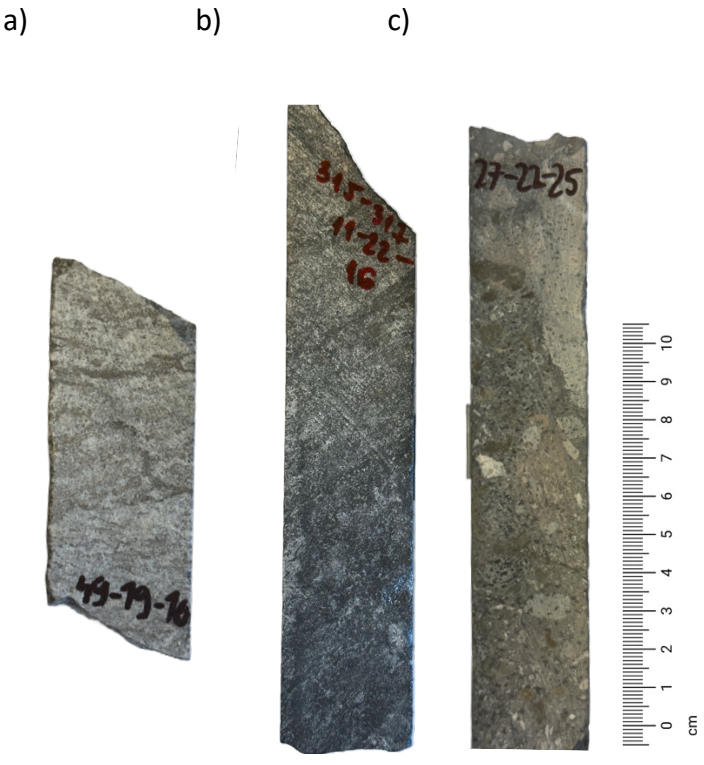

Figure 9. Three distinct ore types: a) massive barite with minor sulphides, b) massive sulphide with minor barite, c) dolomitic breccia with partial sulphide replacement

Table 2. List of samples collected, and the analysis performed at ULiege, and RGNf (composite sample)*

No	Sample ID	Lab-ID	From [m]	To [m]	Length [m]	Sample description	Ore petrology	SEM-EDS	LIBS	XRD	XRF	Automated mineralogy
1	NW-BR-21-22-03		211,6	211,7	0,1	Chert with carbonate veins, chloritization in cracks						
2	NW-BR-21-22-04	2	213	213,1	0,1	Massive sulphides with coarse grained idiomorphic barite blades	+	+		+ (2*)	+	+(2*)
3	NW-BR-21-22-05		213,7	213,8	0,1	Dolomitic breccia with Qtz and Ba veins				+	+	
4	NW-BR-21-22-06	1	215,9	216	0,1	Dolomitic breccia with sulphide veins and veinlets	+	+		+		
5	NW-BR-21-22-07		224	224,4	0,4	Dolomitic breccia with disseminated Py and Ba veins						
6	NW-BR-21-22-08		226,9	227,3	0,4	Dolomitic breccia with disseminated Py				+		
7	NW-BR-21-22-09		235	235,1	0,1	Interlayering of chert (grey) and shale (greenish)				+		
8	NW-BR-11-22-01		206,50	206,60	0,1	Mineralised breccia- Py in fragments					+	
9	NW-BR-11-22-02		210,10	210,20	0,1	Mineralised breccia- disseminated Sph + Gn + Cpy/py					+	
10	NW-BR-11-22-13	7	211,5	211,8	0,3	Upper zone of NW mineralisation, dolomitic breccia with sulphide veins	+	+		+ (2*)		+ (2*)
11	NW-BR-11-22-14	+	254,8	254,9	0,1	Dolomite with sulphide veins (Sph+Gn)						
12	NW-BR-11-22-15		259	259,1	0,1	Dolomite with sulphide veins (Sph+Gn+Brt)						
13	NW-BR-11-22-03		299,70	299,80	0,1	Marl with Barite fragments				+	+	
14	NW-BR-11-22-04		301,00	301,10	0,1	Fault zone				+		
15	NW-BR-11-22-05	3	305,00	305,10	0,1	Massive mineralisation, barite rich	+	+	+		+	
16	NW-BR-11-22-06	4	314,00	314,10	0,1	Massive sulphides, with subordinate barite	+	+	+	+ (1*)		+ (1*)
17	NW-BR-11-22-16	11	316,50	317,00	0,5	Massive sulphides, minor barite	+	+	+			
18	NW-BR-11-22-17		329,00	329,20	0,2	Massive sulphides, minor barite						
19	NW-BR-11-22-07	+	330,00	330,10	0,1	Mineralised breccia with disseminated Py and Ba veins						

20	NW-BR-11-22-08	+	332,60	332,70	0,1	Mineralised breccia with disseminated Py					+	
21	NW-BR-11-22-09	+	337,60	337,80	0,2	Interlayering of chert (grey) and shale (greenish)					+	
22	NW-BR-11-22-18		347,00	347,10	0,1	Dolomite with mineralised veins (idiomorpfic Brt+Sph+Gn)						
23	NW-BR-11-22-10	5	345,90	346,00	0,1	Massive sulphides heavily tectonised and recrystalysed	+	+		+	+	
24	NW-BR-11-22-11	6	347,00	347,10	0,1	Coarse grained sulphide grains in shale matrix, heavily tectonised	+	+			+	
25	MOB-BRD-27-22-13	15	319,60	319,80	0,20	Massive sulphides with carbonate veins as overprints	+	+	+			
26	MOB-BRD-27-22-14	+	336,80	336,90	0,10	Dolomitic breccia with sulphide veins						
27	MOB-BRD-27-22-19		349,10	349,20	0,10	Reddish marl with Py						
28	MOB-BRD-27-22-20	8	353,10	353,25	0,15	Massive barite, with minor sulphides	+	+	+			
29	MOB-BRD-27-22-21	+	355,90	356,10	0,20	Dolomitic breccia with sulphide veins, matrix supported			+			
30	MOB-BRD-27-22-22		356,20	356,40	0,20	Dolomitic breccia with sulphide veins, matrix supported						
31	MOB-BRD-27-22-23	16	356,60	356,80	0,20	Dolomitic breccia (clast supported) with massive sulphide mineralisation as stockwerk	+	+		+ (2*)		+ (2*)
32	MOB-BRD-27-22-24		358,00	358,20	0,20	Dolomitic breccia - clast supported, with sulphide overprint, radial Tth						
33	MOB-BRD-27-22-25		358,50	358,70	0,20	Dolomitic breccia - clast supported, with sulphide overprint, radial Tth						
34	MOB-BR-49-19-11		229,40	229,60	0,20	Marl with sulphide overprint						
35	MOB-BR-49-19-12	12	244,70	244,80	0,10	Dolomitic breccia with massive Py+Sulfosalts	+	+				
36	MOB-BR-49-19-13	9	247,70	247,80	0,10	Massive sulphides - Sph+Py+Gn+Cpy, minor Brt	+	+				
37	MOB-BR-49-19-14		252,00	252,20	0,20	Massive sulphides - Sph+Gn+Py						
38	MOB-BR-49-19-15	13	252,20	252,40	0,20	Massive sulphides - Sph+Gn+Py - increas of Brt	+	+		+(3*)		+(3*)
39	MOB-BR-49-19-16	10	252,50	252,70	0,20	Massive sulphides - Sph+Gn+Py - barite rich	+	+	+			
40	MOB-BR-49-19-17	14	255,70	255,80	0,10	Massive sulphides, barite rich, fine grained	+	+				

3.2. Methods

The internship at the Adriatic Metals Plc. facility in Vareš, took place from February until April 2023. The primary objective of the internship was to get familiar with the lithological units, main ore -bearing mineral phases, and the structural context of the deposit. Drill core mapping and complex data analysis of the company's datasets were performed daily, with a goal of better understanding the deposit, and its main ore-forming processes. This is described in the Figure 10 as 'PHASE 1' and 'PHASE 2'. Complementary to core mapping, parts of the cores were analysed using the portable XRF gun, provided by the company. ICP-MS data was provided to us, for all the drill cores that were mapped, and sampled. The geochemical analysis was done by the company, on core halves, for every meter of the mineralisation, including the contacts with the hanging wall and the footwall of the mineralisation. Mapping was performed simultaneously following the geochemical data, to monitor changes in elemental distribution by depth.

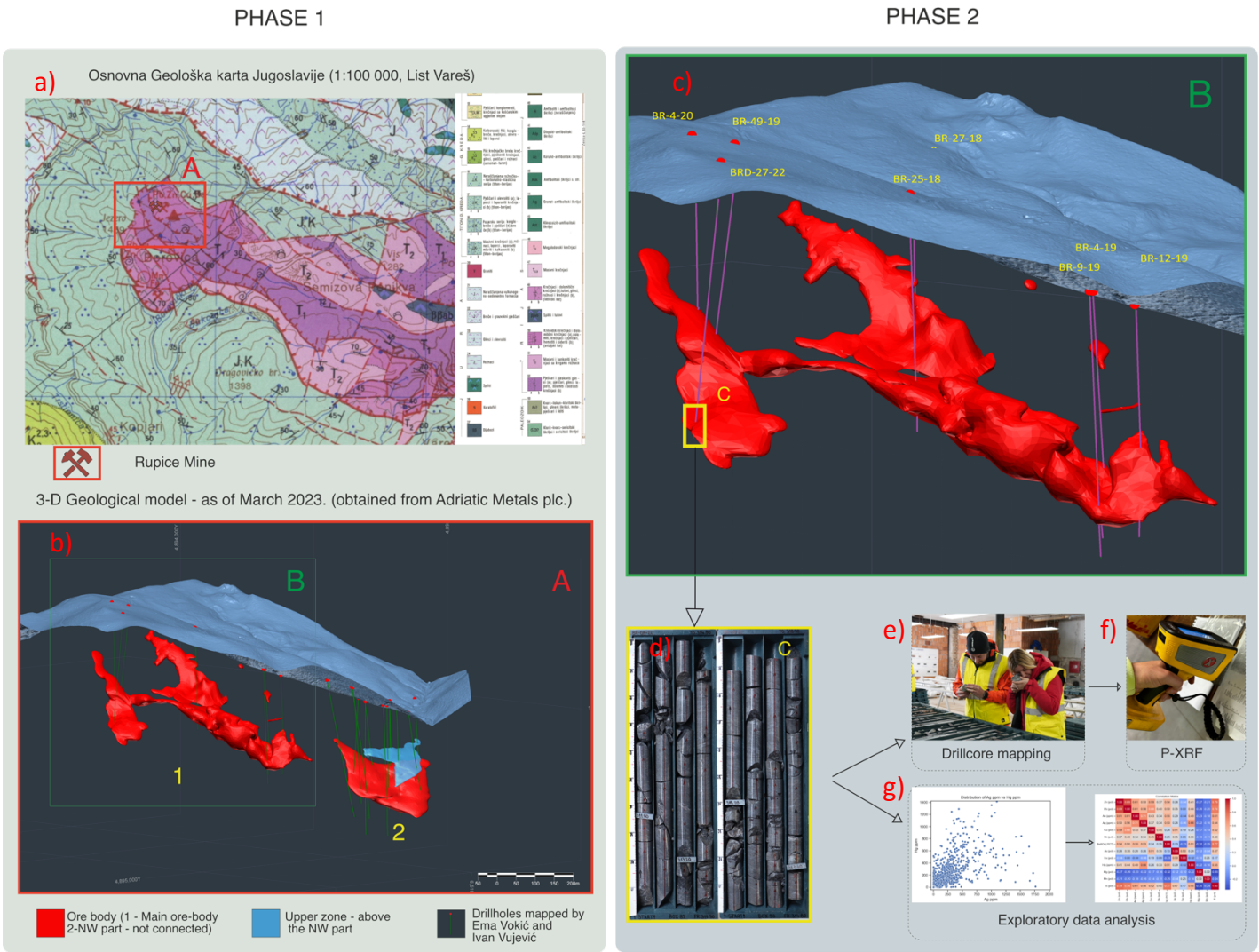

Figure 10. Sequence of analysis, starting from Phase 1 (left), and continuing with Phase 2 (right) a) Geological map of the Vareš area, red square marks the location of the rupice mine site, b) geological 3D model of the Rupice deposit, two ore-bodies are visible, main ore body and the NW part (as of April 2023.), c)close up of the main ore body with all the drillholes that were mapped during the sampling campaign, d) core tray for the BRD-27-22 core, section of massive mineralisation, e) drillcore mapping during the February-April internship at the Vareš site, f) geochemical analysis using the portable XRF gun, curtesy of the Adriatic Metals Plc., g) statistical analysis of the assay data provided by the company, preliminary results and conclusions

Geochemical assays were used additionally for exploratory data analysis, using python programming language. General statistical parameters were obtained, and several different plots were created, with a goal of understanding the lithological constraints of the assays, and the correlation between them.

A total of 40 mineralised samples were collected and sent to the University of liege laboratory for further analysis. A set of analytical techniques was carefully chosen by the supervisors, to enable representaitve and conclusive results, which align with the set objectives of the thesis. The methodological summary of the analytical work is shown in the Figure 11.

As observed, it can be devided in three parts: PHASE 3, PHASE 4 and PHASE 5 in the figure XYZ. Phase 3 consists of a comprehensive mineralogical analysis of 16 samples, using ore microscopy and SEM-EDS at University of Liége. Main objective of this phase is to recognise all mineral phases present in the samples, note and observe different textures and establish the sequence of mineralisation. The SEM-EDS nalysis was performed under help and guidance of prof. Hassan Bouzahzah, researcher at the GEMME laboratory of the ULIEGE.

Phase 4 encompasses trace element analysis, using the LIBS (Laser Induced Breakdown Spectroscopy) prototype, developed as a part of the SCReeN project, which is devoted to develpoing techniques of monitoring, detecting and characterising Critical Raw Materials (CRM) in Belgium, but also in the European Union. The analysis is performed on 8 core cuttings, which represent mirrored samples, prepared for the PHASE 3 (A).

Phase 5 has an objective of looking into elemental deportments of the main elements present in the orebody. 3 composite samples were prepared, based on three distinct ore types, defined by core mapping at the Vareš exploration team facility, earlier this year. Atuomated mineralogy was performed, using the Zeiss Mineralogic system, implemented in the SEM device. Prior to the analysis, a novel sample preparation technique was used to prepare the samples, using carbon black, mixed with the sillicon resin. This Method ensures almost no segregation of the particles in the sample, makin the analysis more objective, and liberation more precise. XRD was performed on the same samples, to compare the semi-quanitification with the automated mineralogy results.

Figure 11. Methodological summary of the analytical techniques used for the set objectives of the Thesis work

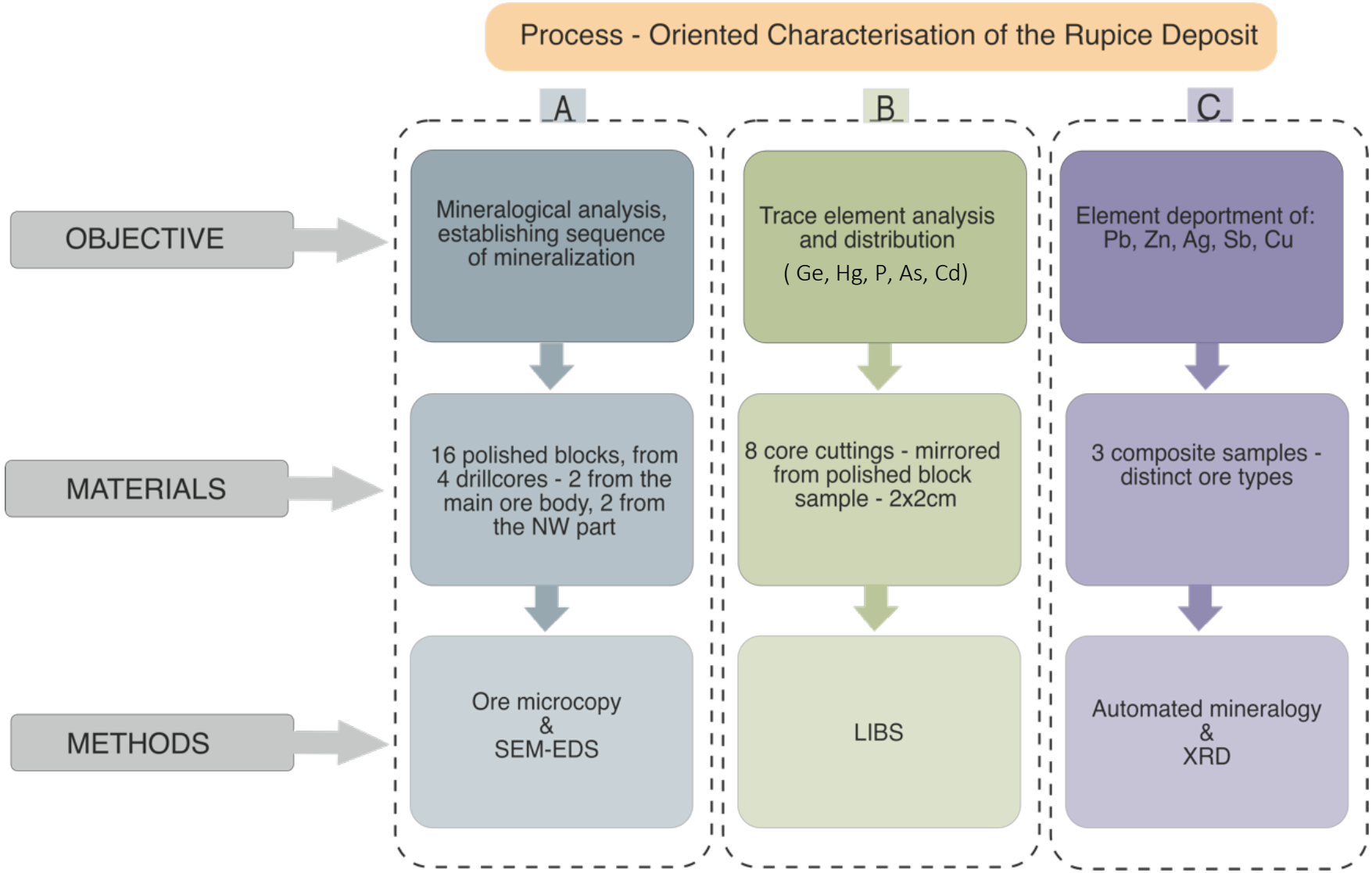

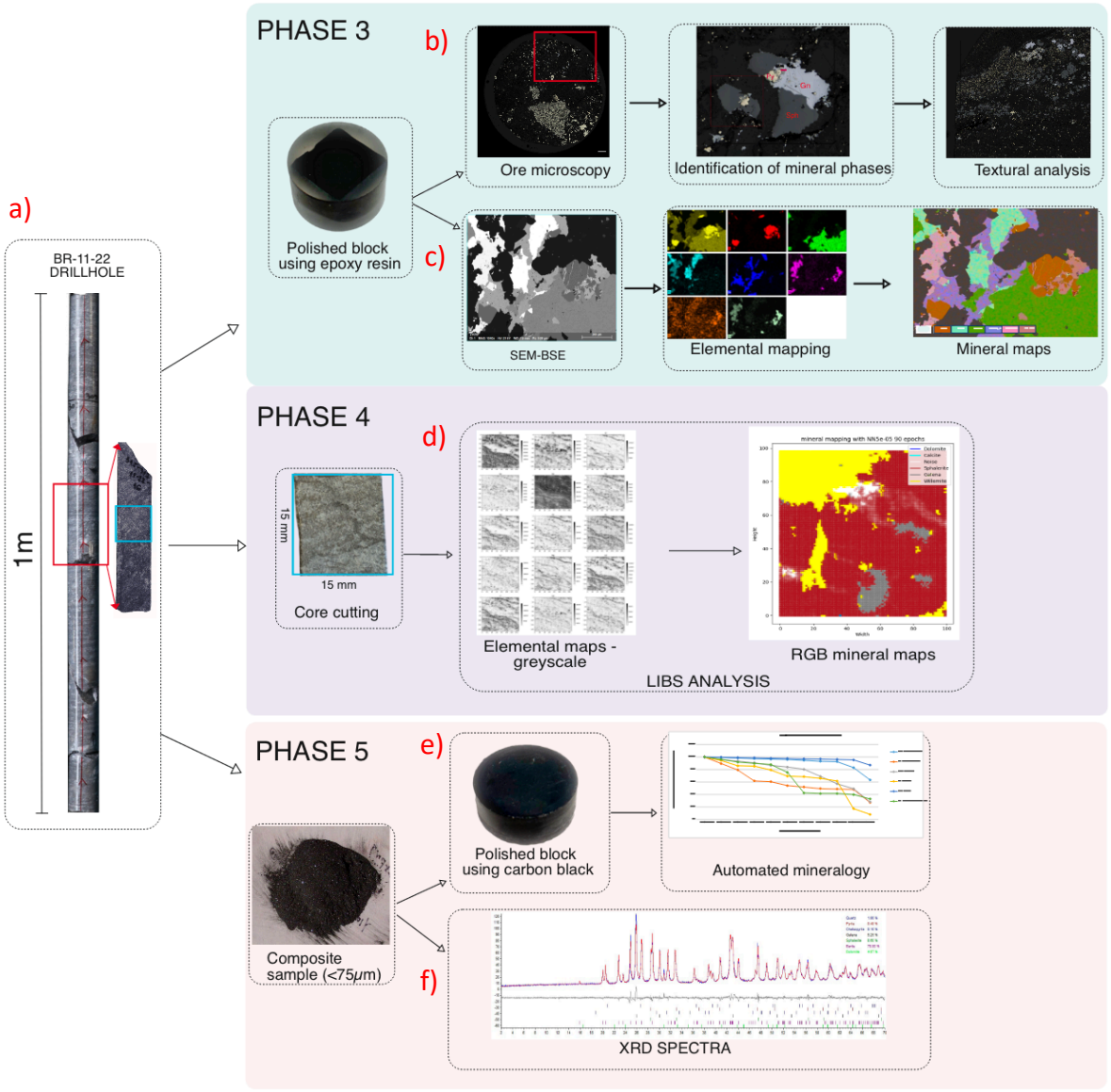

Figure 12. Sequence of analytical work, divided in three phases, a) drill core mapping and sample selection, b)polished block preparation for the microscopy, through which different mineral phases were analysed, ore textures observed, c) SEM-EDS analysis on the polished blocks, EDS used for elemental mapping, which when element-to – mineral conversion is applied, can be made into mineral maps, d) LIBS analysis on the core cuttings of 15x15 mm, elemental and RGB mineral maps are the final product, e) polished block preparation for automated mineralogy on three composite samples previously crushed, ground and subsampled. A.M. was used for bulk mineralogy, liberation analysis and mineral associations, f) XRD on the composite samples was conducted, in order to compare the mineral deportment with the automated mineralogy.

3.2.1 Mineralisation characterization

Core scanning

The core scanning experiment involved the use of a hyperspectral imaging instrument, which is a device that captures images of an object in multiple wavelengths of light. The instrument used in this experiment was a Hyspex Neo SWIR 384 camera, courtesy of the GeMMe laboratory of the university of Liege, which is a high-performance camera that can measure the spectral reflectance of an object in the shortwave infrared (SWIR) region, from 1000 nm to 2500 nm. The camera has a spatial resolution of 384 pixels, which means that it can capture 384 distinct points along a line. The camera was positioned at 1 m from the core sample, which was mounted on a rotating platform. The camera scanned the core sample line by line, creating a hyperspectral image cube that contained both spatial and spectral information. The data collected by the camera were then used for mineral classification, which is the process of identifying and mapping the different minerals present in the core sample. The classification was based on the comparison of the spectra of each pixel in the image cube with the reference spectra of four classes: dolomite, chlorite, galena, and background. The reference spectra were taken from the NASA Jet Propulsion Laboratory spectral library, which is a collection of spectra of various materials measured under laboratory conditions. The classification algorithm used in this experiment was the spectral angle mapper (SAM), which is a simple and fast method that calculates the angle between two spectra and assigns each pixel to the class with the smallest angle. The SAM algorithm does not require any prior knowledge of the spectral properties of the classes, but it assumes that the spectra are linearly independent and that there is no spectral mixing. To improve the quality of the classification, the data were pre-processed with the standard normal variate (SNV) method, which is a technique that removes the effects of unequal illumination and enhances the spectral features by transforming each spectrum to have zero mean and unit variance.

Ore microscopy

Drill core quarters, and cuttings were cut using the appropriate saw to the 3cm diameter circles. In total, 16 samples were prepared, and moulded using the silicon based EPOFIX resin. Samples in the resin were put in the vacuum to ensure minimal concentration of air bubbles present in them. After several stages of air drying and hardening, samples were put to the Struers Tegramin rotary polishing machine, for several stages of polishing. Each stage consisted of a specific diamond mesh size, which results in the difference in the amount of material scraped from the sample, and specific time frame, adjusted accordingly. Water based diamond suspension is constantly injected to ensure the wetness of the surface, and the contact of the samples and the diamond mesh. In total, 16 polished blocks were cleaned using the ultrasonic bath, to remove excess residue from the diamond mesh, and dried using the air compression gun. Every sample was thoroughly looked at under microscope to make sure the polishing was done accordingly, and all the contacts between mineral grains were sharp.

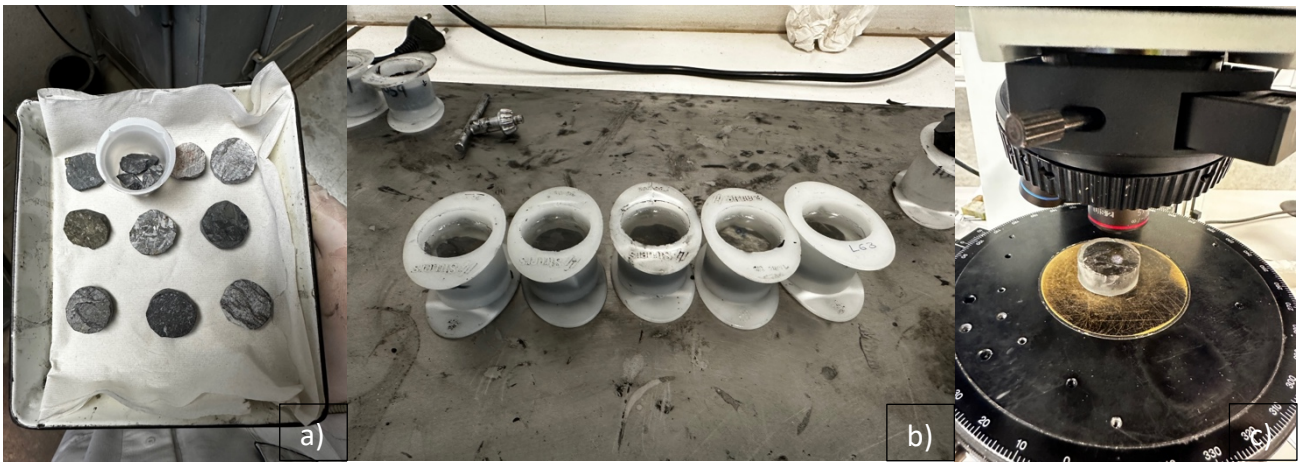

Figure 13. Three step sample preparation for optical microscopy and SEM-EDS. A) core quarters cut in 3cm diameter round shapes, b) EPOFIX resin and moulds in which the samples were put, c) optical microscopy of the samples, checking if the cutting was done properly

Microscopical analysis was performed using the Zeiss Axioimager M2m from the GeMMe laboratory from the University of Liege, paired with the AxioCam ICc 5, for the 16 samples. Sample mapping was conducted using Cytomine software, implemented in the microscope. Image capturing, stitching, and uploading the complete sample database was done as a part of the sample preparation.

Figure 14. Zeiss Axioimager M2m

LIBS

A custom-made LIBS system was designed at the Geological Survey of Belgium as a part of the SCReeN project to scan the whole core sample with a rectangular laser grid. A Quantel Viron laser was used with these parameters: 10 Hz frequency, 15 mJ energy, 9 ns pulse duration and 100-200 µm spot size. The spot size was achieved with a 50 mm focal distance planoconvex lens. The laser set-up was attached to a microscope table that could be moved in X, Y and Z directions. The table movement was programmed with an in-house GUI to follow parallel lines and the laser was only activated when the table moved left. The laser spatial sampling resolution was set to 0.1 mm. An air-circulation path was also installed to push the dust away from the sample to an air filter. The air-cleaner was turned on during the LIBS acquisition to prevent dust from settling on the sample surface. The light from the plasma

decay was collected with glass fibres and sent to a high-resolution rack of 4 AvaSpec ULS4096CL-EVO spectrometers. The rack measured the light from 195.53 nm to 575.38 nm. The spectral resolution of the whole set-up was around 0.025 nm, which allowed for excellent peak discrimination.

LIBS mapping was accomplished by coordinating the sample's movement with the laser, operating at a maximum repetition rate of 20 Hz. Simultaneously, the LIBS spectrum was recorded at each point on the map using a single-shot measurement technique. The mapping parameters consisted of a grid of 400 x 100 pixels, with each pixel measuring 250 µm, resulting in a scanned area of 15 x 15 mm. The time required for scanning this area is approximately 60 minutes at a laser repetition rate of 10 Hz, or 30 minutes at 20 Hz. Subsequently, a hyperspectral datacube was generated using Python/Java scripting within the Fiji/ImageJ image analysis software environment (e.g., Rueden et al., 2017). From the datacube, LIBS images were extracted after subtracting the background and addressing spectral interferences as necessary. Despite the intricate nature of LIBS spectra, the issue of peak overlap due to spectral interference was not a major concern for most elements. Corrections for overlap were primarily employed to enhance the elemental images. To identify lines with optimal intensity and minimal peak overlap, a range of reference materials and freely available atomic emission tables (Kramida et al., 2019) were utilized. For the recognition and classification of sample litholoy, convolutional neural networks were used.

SEM-EDS/EDX

A comprehensive examination was conducted to investigate present mineral phases using a ZEISS (Sigma 300) Scanning Electron Microscope (SEM), from the GeMMe laboratory from the University of Liege, equipped with two Bruker xFlash 6|30 X-ray energy dispersion spectrometers (EDS). The SEM-EDS analyses were performed by utilizing a probe current of 2.3 nA and an accelerating voltage of 20 kV, maintaining a working distance of 8.5 mm. To identify the main ore-bearing and gangue minerals, and the neighbouring elements, a manual spot analysis was carried out. When comparing the EDS and LIBS spot size, there is a discrepancy with regards to measurement accuracy and precision (9.4 µm for EDS compared to 200 µm for LIBS) Prior to the analysis, all the samples were carbon coated to increase the signal-to-noise ratio for producing higher quality images.

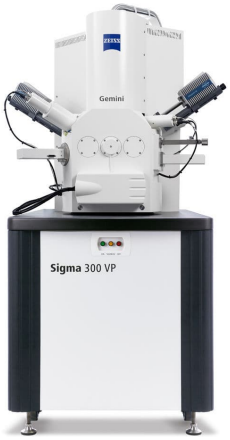

Figure 15. ZEISS (Sigma 300) Scanning Electron Microscope (SEM)

3.2.2. Process-oriented characterization

Automated mineralogy

Zeiss Mineralogic system is a software that provides automated quantitative mineral analysis by combining high-resolution scanning electron microscopy (SEM) with energy-dispersive spectroscopy (EDS) and artificial intelligence (AI). The system can identify and quantify minerals in real-time, based on their chemical composition, morphology, texture, and liberation. The system can also classify lithology, ore types, and trace elements, and generate reports and visualizations of the results. Zeiss Mineralogic system from the University of Liege, GeMMe laboratory was used for this analysis.

The Zeiss Mineralogic system works by using different methods of mineral classification, depending on the sample texture and application. For maximum accuracy, it uses a standards-based quantitative EDS technique that measures the stoichiometry of all minerals and compares them with reference standards. For the fastest analysis speeds, it uses a backscattered electron detector (BSD) grayscale technique that assigns minerals based on their brightness levels. It can also combine both techniques with grain size, shape, and intra-granular porosity-based mineral classification to achieve textural quantification. Additionally, it can include element ratio rules to discriminate end members of a solid solution or correlative workflows to integrate data from other analytical techniques such as uXRF, EPMA, or LA-ICP-MS.

5. Results

4.1. Macroscopic determination of the Rupice ore body

The Rupice ore body is massive, with distinct changes, from massive barite and minor sulphide, to massive sulphide and minor barite. The mineralisation is fine grained (<100 µm), and difficult to differentiate without magnifier (Figure 17, Figure 18). This resulted in the distinction of three main ore types, as previously mentioned. The structural control factor is evident, as the ore body is constrained by two major fault zones.

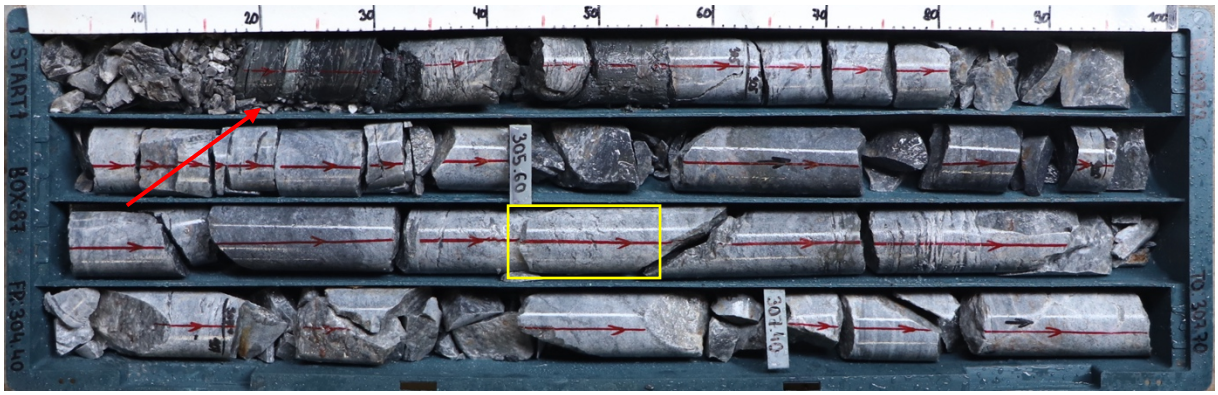

Figure 16. MACROPHOTO: Drillhole BR-08-22, with a clearly visible contact between the fault zone and the massive mineralisation (RED ARROW)

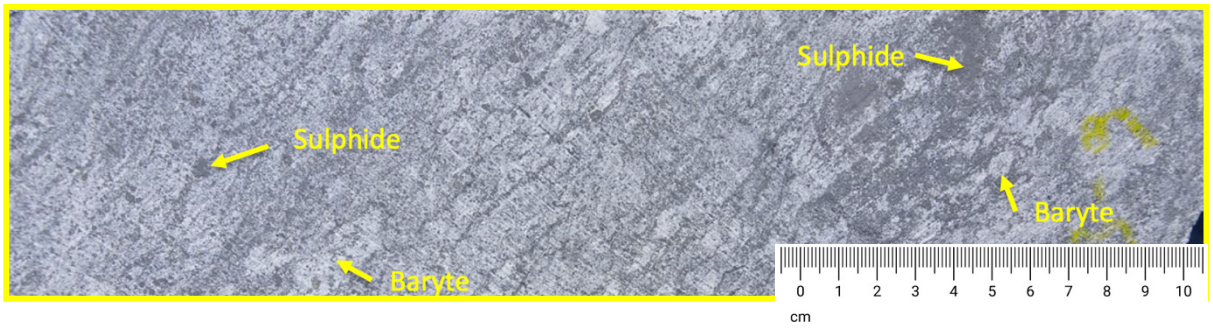

Figure 17. . MACROPHOTO: Ore type 1 – massive barite with minor sulphide (Gn+Sph+Sulph.+Py+Cpy)

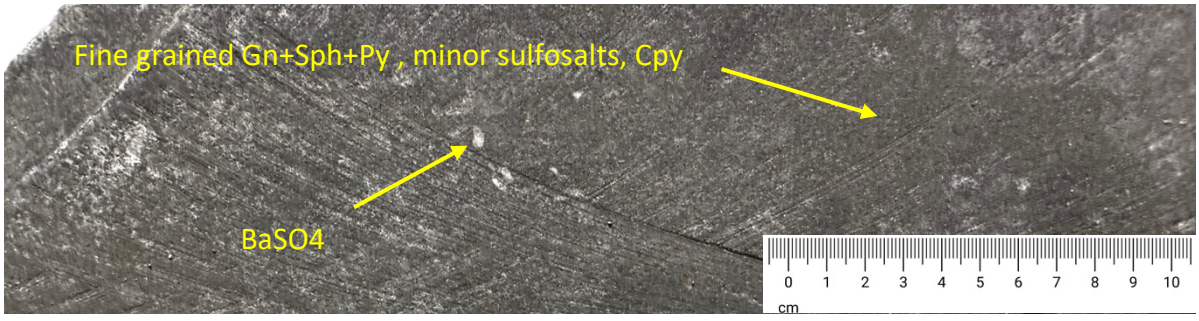

Figure 18. MACROPHOTO: Ore type 2 – massive sulphide (Gn+Sph+Sulf.+Py+Cpy) with minor barite

Coarser grained mineral phases are evident at the outer zones of the orebody, in the shape of sulphide veins and veinlets in dolomitic breccia (Figure 19). The veins show no signs of zonation, as multiple mineralisation phases overprinted one another, making it difficult to distinguish if there was a zonation during crystallisation.

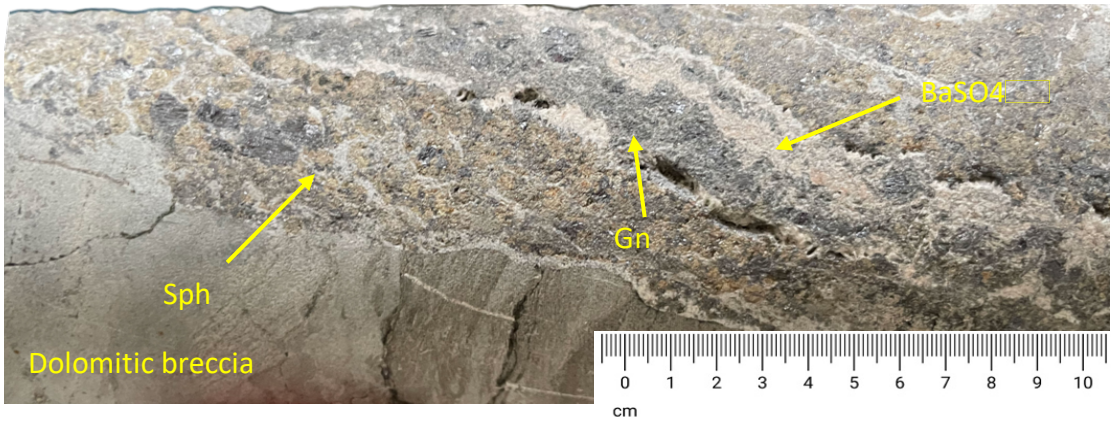

Figure 19. MACROPHOTO: Ore type 3 – Dolomitic breccia with sulphide vein (Gn+Sph+BaSO4)

Core scanning

Core scanning analysis was conducted for the first batch of 17 samples. The only constraint was the width of the conveyor belt, otherwise more would fit. When taking a closer look and comparing the samples one by one with their macro photo, common traits are evident. Main ore and gangue phases are recognised, such as galena/ dolomite/calcite/barite (Figure 20).

Massive barite ore, which tends to be finer grained compared to the dolomitic breccia ore type. General mapping of barite was done well, but the sulphide veinlets are not mapped. The existence of calcite is also doubtful, as it hasn't been identified in the microscopical sample.

Massive sulphide sample (Figure 20b), when compared to its macro photo, is difficult to compare. Some distributions of barite are similar, while there is no differentiation of sulphide phases. The mapping of calcite is questionable, as no calcite or dolomite phases have been observed in the microscopical analysis of that sample.

The dolomitic breccia ore type is reasonably well mapped, with the resolution and overprinting calcite veins not being recognised. Contact between the dolomite and sulphide phases is clear and resembles the original one. The differentiation of sulphides presents another challenge, as SWIR generally struggles to note the difference. In this case, everything related to sulphides was named 'galena'. The colour scheme is:

- Blue: dolomite
- Green: calcite
- Red: chlorite
- Cyan (light blue): muscovite
- Yellow: barite
- Pink: galena
- Black: conveyor belt material

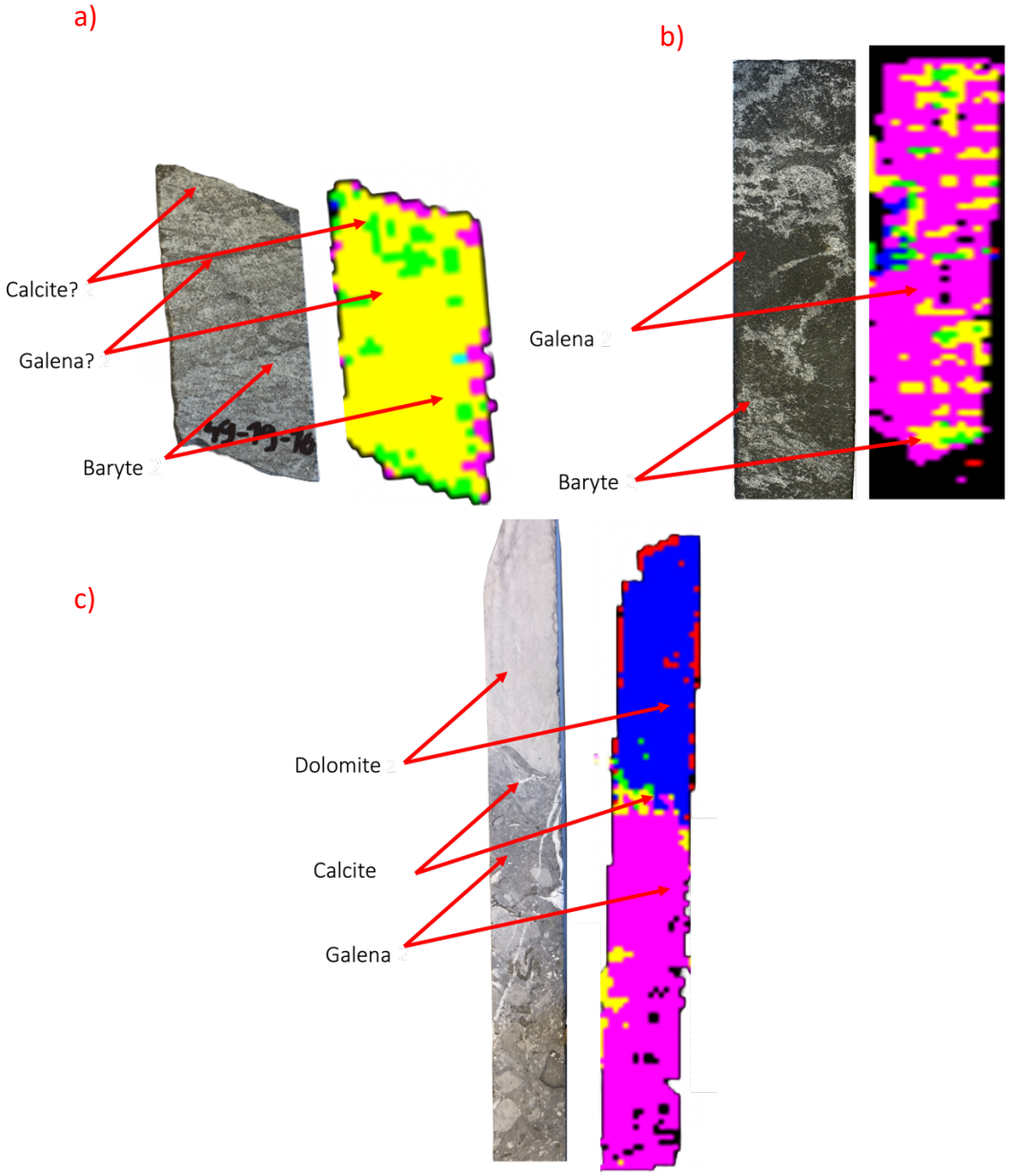

Figure 20. Comparison of macro-photo and core scanning results for some drill core samples, a) massive barite ore, b) massive sulphide ore, c) dolomitic breccia ore type

4.2. Microscopic determination of the Rupice ore body

Ore microscopy

A total of 16 samples were prepared as polished blocks for ore microscopy and SEM-EDS analysis at the university of Liége (Table 2). Samples were taken from 4 drillholes in total, two from the main ore body (MOB), and two from the Rupice Northwest (NW).

Using the optical microscope from GeMMe laboratory at University of Liege, mineralogical analysis was conducted, with an objective of identifying all the mineral phases present in the samples, analysing textures, inclusions, possible exsolutions, suppressions and determining the ratios between mineral phases. As previously mentioned, three main ore types are distinguished: massive barite, massive sulphide and dolomitic breccia sulphides (dolomitic breccia). Main ore-bearing mineral phases are galena, sphalerite, chalcopyrite, pyrite, cinnabar and sulfosalts, while the gangue is barite, dolomite, apatite, quartz, and muscovite.

Massive barite ore type

Pyrite is present in various forms and sizes, ranging from idiomorphic, to xenomorphic in habitus. Idiomorphic pyrite (Py 1) is 10-100 µm in size and is suppressed by every other main ore phase (Figure 21.a). It occupies less than 1 vol. % of the samples. Xenomorphic pyrite (Py 2) has a size of 20-200 µm and is intergrown with the main ore phase (Gn+Sulfosalts+/- Cpy). Framboidal pyrite is observed in every sample, with spherical grains 10-75 µm in size being related with the later stage of mineralisation (vein filling, and as overprint). Framboidal pyrite represents less than 1 vol. % of the samples, being even less observed than the idiomorphic or xenomorphic phases. Framboids cemented together during growth can exhibit colloidal texture (Figure 21b). As a later stage of recrystallisation, transformation from pyrite to marcasite is observed (Figure 21c). Marcasite is very rarely observed, constituting to less than 1 % of all the samples, and when comparing its abundance to the other pyrite phases, it is the least present phase.

Main zinc bearing phase, sphalerite, has hypidiomorphic habitus. Grain size ranges from 40 µm up to 500 µm. Sphalerite is commonly finer grained in massive barite (< 200 µm) and occupies between 2 and 15 vol. %. Often exhibits inclusions of barite, and pyrite, occasionally chalcopyrite (Figure 21.e). Sphalerite is frequently suppressed by Gn+sulfosalts phase, making it genetically younger than them.

Chalcopyrite has xenomorphic to hypidiomorphic habitus. Grain size vary from 20-200 µm. Cpy is present in massive barite samples in amount below1 vol. %. The later ore stages, that include galena, sulfosalts and barite (Brt 1), are supressing Cpy (Figure 21.a,g,h), making it one of the earlier stages of mineralisation, possibly timewise similar with sphalerite crystallisation.

Fine-grained galena (25-200 µm) is present as xenomorphic grains and occupy 2-9 vol. % of the massive barite ore. Galena is intergrown with the Ag-Sb-As bearing sulfosalts and pyrite (Py 2), suppressing the earlier pyrite stage (Py 1). Often, galena is observed as space and fracture filling of the earlier sphalerite mineralisation stage (Figure 21b,h). Distinct triangular pits in several samples exhibit ductile deformation.

Sulfosalts are rare xenomorphic grains, 10-100 µm in size, and occupying between 1-2 vol. % of the samples. Spatial association with Gn+ Py1+Cpy is evident in majority of the samples.

Cinnabar has hypidiomorphic habitus and ranges between 20-100 µm. It is observed in only one sample, and its abundance was below1 vol. %. It is observed as fracture and cracks filling, within? brecciated barite veins (Figure 21i).

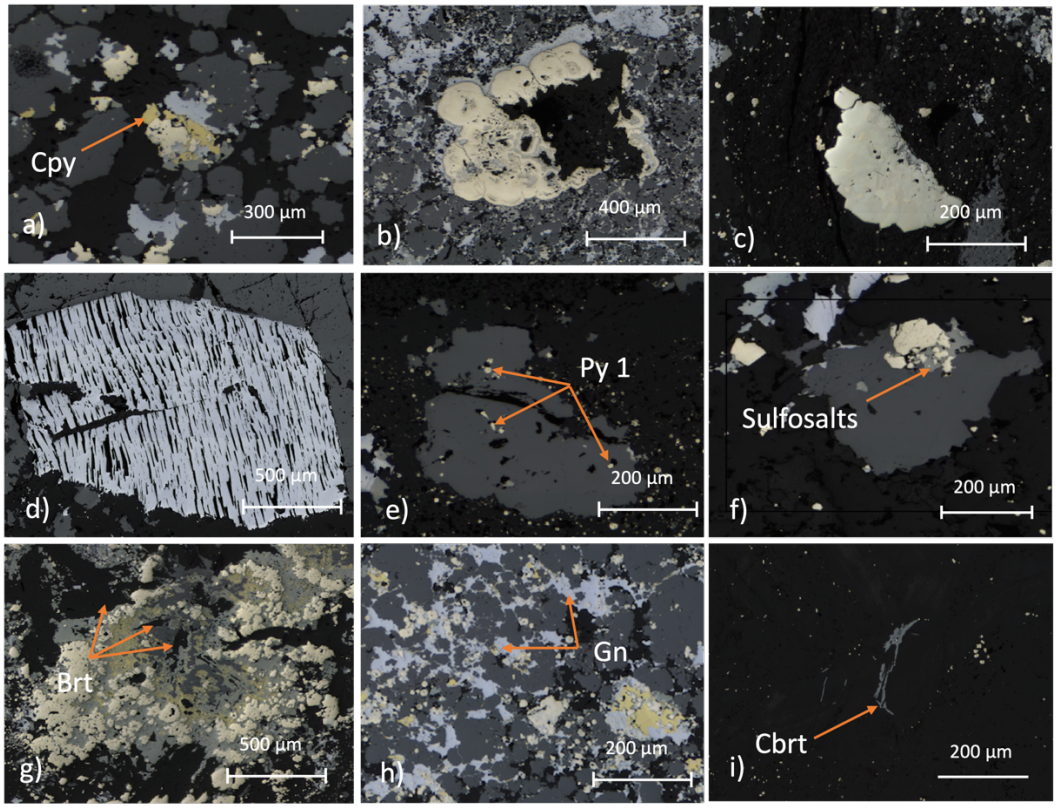

Figure 21. Microscopical images of massive barite samples. a) Py 1 partially recrystallized to marcasite, b) colloidal texture of Pyrite (Py 1), c) Gn and Sph intergrowth, d) hypidiomorphic grain of Gn showing ductile deformation (triangular pits), e) Py and Brt inclusions in Sph. f) Sph grain suppressed by Gn+Sulfosalts + Py 2, g) Suppression of Cpy, Py 1 and Sph by sulfosalts and Barite 1, h) association of Py 1, Cpy, sulfosalts and Gn

Massive sulphide ore type

In the massive sulphide ore type, pyrite displays a range of appearances, from idiomorphic to xenomorphic habitus, comprising 2 to 10 vol. % of the sample. Idiomorphic pyrite (Py 1) (20-80 µm in size) is closely linked to the Gn+sulfosalts+/-Cpy ore-bearing stage. Xenomorphic pyrite (Py 2; 20-200 µm in size) is intergrown with the Gn+Sulfosalts+/- Cpy ore phase (Figure 22a). Framboidal pyrite contains spherical grains (10-75 µm in size) associated with later-stage mineralization (vein filling and overprint) (Figure 22b). Colloidal pyrite texture is also observable, as well as the transformation from pyrite to marcasite (Figure 22b). Barite idiomorphic blades are found on recrystallized pyrite/marcasite grains, with sulphides crystallizing within the barite blades, causing suppression (Figure 22c).

Sphalerite exhibits a hypidiomorphic to xenomorphic habitus, occupying 1-65 vol. % and possessing a grain size of 50-3000 µm. It's commonly suppressed by Gn and Brt in later mineralization stages. A later Galena+ Sulfosalt phase leads to hydrothermal brecciation of sphalerite grains (Figure 22a, b). Suppression of earlier idiomorphic pyrite grains by Sph is evident (Figure 22.c).

Chalcopyrite displays a xenomorphic to hypidiomorphic habitus, with grain sizes ranging from 25-300 µm. It comprises 1 to 6 vol. % of massive sulphides and is associated with Py1, Gn, and sulfosalts (Figure 22.a, e). Occasional inclusions within sphalerite grains are observed (Figure 22.d).

Galena features xenomorphic to hypidiomorphic grains with sizes ranging from 50-500 µm, constituting 1-25 vol. % of massive sulphides. Galena appears as fracture filling and associates with sulfosalts, Py 1, and Cpy (Figure 22.a).

Sulfosalts occupy 1-3 vol. % in massive sulphides, exhibiting xenomorphic to hypidiomorphic characteristics with grain sizes from 10-200 µm. An association with Gn +/- Cpy and Py 1 is apparent (Figure 22a, e).

Barite demonstrates a hypidiomorphic to idiomorphic habitus, occupying 10 - 30 vol. % of samples, with grain sizes ranging from 100 to 2000 µm. Barite overlays the primary ore stage (Cpy+Sph+Gn+Sulfosalts+Py 2). Idiomorphic barite blades are present within colloidal pyrite, suppressed by sulphides (Gn+Sph+sulfosalts) (Figure 22c).

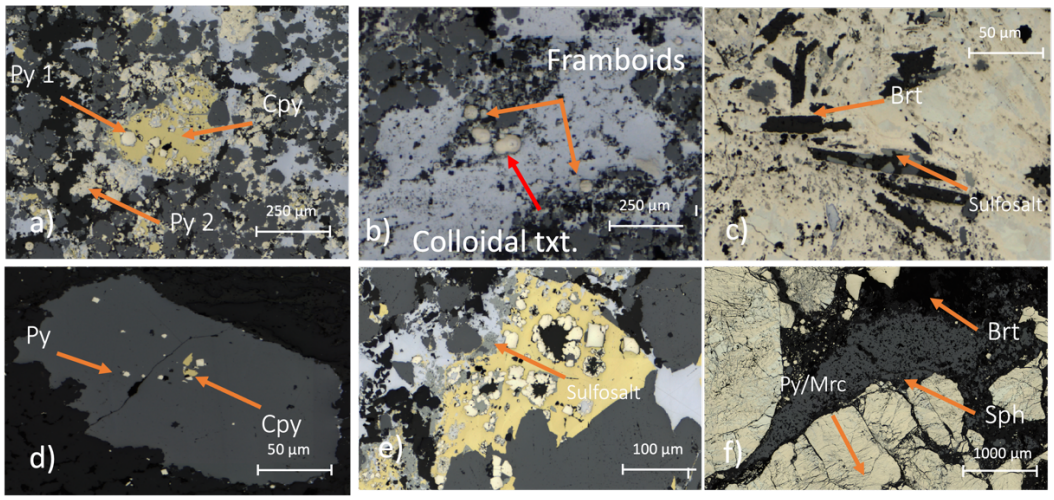

Figure 22. Massive sulphide ore. a) Py 1 – idiomorphic, suppressed by Cpy+Gn+Sulfosalts, Py 2- xenomorphic, associated with Cpy+Gn+Sulfosalts, b) Framboidal and collodial texture of pyrite on the boundaries between Gn and Sph (darker), c) Idiomorphic Brt blades as inclusions in Py/marcasite grain. Recrystallisation of sulfosalts and sphalerite observed d) Py and Cpy inclusions in Sph grain, e) Py 1+Cpy+Gn+Sulfosalts complex, Py suppressed by Brt fluid (black), f) Cataclastic texture of pyrite, breakdown to marcasite. Suppression by Sph and later stage barite (Brt 1)

Dolomitic breccia

Pyrite is present in the dolomitic breccia ore with varying forms and grain sizes, ranging from <10 µm up to 2500 µm. It exhibits different textural characteristics, including cataclastic, framboidal (as shown in Figure 23a), and colloform. Late stage brecciation of colloform textures is evident (Figure 23b). Idiomorphic pyrite (Py 1) grains are completely enclosed by quartz-rich fluid (Figure 23c), and a transformation of pyrite (Py 1) into marcasite is observed (Figure 23d).

Sphalerite exhibits a range of grain sizes (40 – 2500 µm) and occupies 1 - 50 vol. % of the sample. It displays a cataclastic texture, with cracks and fractures often filled by Gn/Py/Brt/Sulfosalts. Suppression by galena, sulfosalts, and barite indicates earlier phase of mineralisation.

Chalcopyrite is observed in a single sample of dolomitic breccia ore, with grain sizes ranging from 50-200 µm and a hypidiomorphic habitus. Evidence of hydrothermal brecciation by sulfosalts is present (Figure 23e).

Galena exhibits a grain size of 50-2000 µm and idiomorphic to xenomorphic habitus. It comprises 1-15 vol. % of the samples. Coarser grains display ductile deformation (Figure 23f) and are associated with sulfosalts, Cpy and Py 1.

Sulfosalts exhibit hypidiomorphic to xenomorphic habitus, with grain sizes of 50-500 µm, and occupy 1 - 15 vol. %. They tend to intergrow with pyrite, galena, and chalcopyrite (Figure 23e).

Barite, characterized by a grain size between 200 – 1000 µm and a hypidiomorphic habitus, constitutes 1% to 40 vol. % of dolomitic breccia ore. It overprints all previous stages of mineralization.

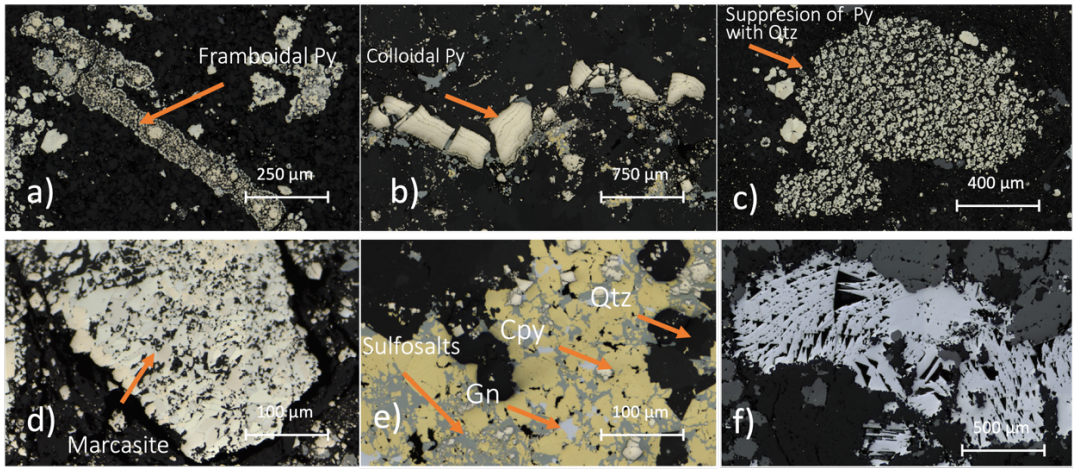

Figure 23. Dolomitic breccia ore type. a) colloform Py texture, Gn/Sph/sulfosalts cement, b) brecciated colloidal pyrite texture, c) Py 1 dissolved by Qtz rich fluid, marcasitisastion of Py, d) Idiomorphic barite grains recrystallised on colloidal Py grain, e) Hydrothermally brecciated Cpy, sulfosalt rich fluid (black grains Qtz?), f) Py 1+Gn+sulfosalts complex, Cpy not present, g) ductile deformation of triangular pits, grain of Galena

SEM-EDS

Massive barite

Among the three ore types, pyrite is least abundant in massive barite ore (< 2% vol.). Texturally, it is represented by framboidal and colloform forms. Colloform pyrite often becomes cemented by galena, sphalerite, and barite in later mineralization stages. Multiple end members of iron sulphides are detected in the colloform and framboidal pyrite, such as: greigite (Fe 56,5 wt. %, S 43,5 wt. %, chemical formula: $Fe^{2+}Fe^{3+}{}_2S_4$), pyrite (Fe 46,7 wt. %, S 53,3 wt. %, chemical formula FeS_2), pyrrhotite (Fe 62,3 wt.%, S 37,7 wt. %, chemical formula: $Fe_{(1-x)}$ S). The colloform texture reveals the initial idiomorphic pyrite grain (Py 1), shown in Figure 24a and b. Framboidal pyrite exist in various orders (spheres, disorganized), suggesting different stages of formation. There seems to be a connection between disorganised framboidal grains and occurrence of greigite, and fully formed spheres, and pyrite. Pyrrhotite is likely related with later stages of growth, observed in the outer rims of framboids and colloforms. Arsenic is detected in every iron sulphide sample, with 1-6 wt.%. Commonly observed traces of Cu (1-2 wt. %) and Sb (<1 wt. %) in framboids and colloform texture. Idiomorphic pyrite (Py 1) is associated with the Gn+sulfosalts+Cpy ore stage and exhibits breakdown to marcasite in most coarse grains (>150 µm).

Chalcopyrite (Cu 36-40 wt. %, Fe 30-34 wt. %, S 17-30 wt. %) is often suppressed by galena and As-Sb-Ag-bearing sulfosalts. Shows traces of Sb (<1 wt. %) and Ba (1-2 wt. %). Sphalerite's hypidiomorphic to xenomorphic grains are finer-grained (<200 µm) compared to the other ore types. Zn constitutes from 64-70 wt. % in sphalerite, S 30-34 wt. % and Fe 0-3 wt. %. Trace elements include Cu (1-4 wt. %), Sb (1-2 wt. %) , Pb (1-2 wt. %), Ba (up to 4 wt. %) and Sr (up to 2 wt. %). Iron is often below detection limit, suggesting additional, low-Fe phase. Chalcopyrite is rarely observed as inclusions in the sphalerite grains.

Point analysis of sulfosalt grains reveals different phases, mineral from the tetrahedrite group, (tennantite ($(Cu,Fe)_{12}As_4S_{13}$) or freibergite ($(Ag,Cu,Fe)_{12}(Sb,As)_4S_{13}$), bournonite ($PbCuSbS_3$), and boulangerite ($Pb_5Sb_4S_{11}$). Tetrahedrite group consists of Cu, from 38-44 wt. %, Sb from 15-27 wt. %, S 20-22 wt. %, Zn 6-8 wt. %, As 1-10 wt. %, and Ag 1-5 wt. %. Often detected traces of Fe (1-3 wt. %). Zonation of freibergite grains is commonly seen, due to changes in Ag, As, and Sb stoichiometry (Figure 24d). Higher As (3 wt. %), an lower Ag (1 wt. %) ans Sb (24 wt. %) comprise the darker part of the grain, while lower As (1 wt. %), and higher Ag (4 wt. %) and Sb (26 wt. %) make up for the lighter part. They surround Py 1 (idiomorphic) grains, along with galena and chalcopyrite. Bournonite (Pb 40 wt. %, Cu 15 wt. %, Sb 12-14 wt. %, and S 20-22 wt. %) has a significant amount of As (9-10 wt. %) present in all the grans analyzed.

Galena associates closely with sulfosalts and idiomorphic pyrite, often filling fractures and cracks in pyrite grains or framboids (Figure 24a). consists of pb (86-87 wt. %) and S (12-13 wt. %). Commonly found traces of Sb (0,5-2 wt. %) and Cu (1 wt. %). Fe (2-3 wt. %) and Zn (2-4 wt. %) rarely detected.

Barite (Ba 53-58 wt. %, S 11-15 wt. % and O 25-28 wt. %) appears in two mineralization stages. Barite 1, coarse-grained (>250 µm), fills cavities and breccia of earlier sulphide mineralization. Commonly detected Sr (1-9 wt. %), Zn (1-3 wt. %) and rarely Cu (2-3 wt. %) and Fe (1-3 wt. %), P (up to 1 wt. %), Ca (1-2 wt. %). Barite 2 cements earlier brecciated stages, including brecciated Barite 1 (Figure 24e), displaying a banded texture with nanoscale intercalations of apatite and Fe-bearing barite (Figure 24f).

Two phases of apatite ($Ca_5(PO_4)_3F$) are present. Apatite 1, idiomorphic (Figure 24h), is closely linked to the main ore-bearing stage (Gn+Sulf.+Py1/Py2+Cpy) and suppressed by sulfosalts. Consists of Ca, (40-41 wt. %), P (15-17 wt. %), O 3(4-35 wt. %) and F (3-5 wt. %). Traces of Fe (0,5-2 wt. %) and Si (1 wt. %) were detected. Apatite 2, as described earlier, features nanoscale intercalations with Fe-bearing Barite 2, indicating a later mineralization stage. It has a higher wt. % of Ca (44-45 wt. %), while P is a bit lower, at 14 wt. %. Fe is variable in Apatite 2, going up to 17 wt. %.

Cinnabar (HgS) is found as xenomorphic grains, infilling the brecciated banded texture of apatite 2 + barite 2 (Figure 24e), present in only one sample, at a level of <1%. Hg constitutes between 80-84 wt. %, while S is at 15 wt.%. Traces of barite (2-3 wt. %) rarely observed.

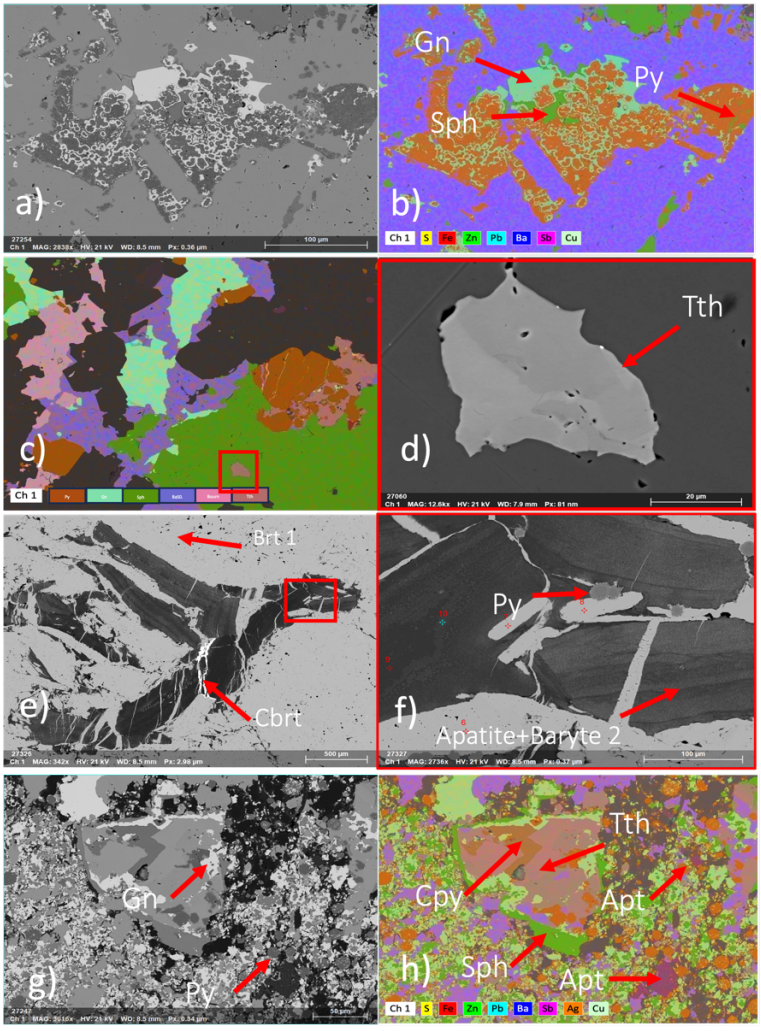

Figure 24. Massive Barite ore type. SEM-BSE image (greyscale), SEM-EDS elemental map (multi-colour).

Massive sulphides

Presence of pyrite in massive sulphide ore is associated with the galena+sulfosalts+/-chalcopyrite ore stage. Idiomorphic pyrite (Py 1) suppressed by Gn+Sulfosalt, while the hypidiomorphic pyrite (Py 2) appears to be of similar genetic timeline as the Gn+Sulfosalt ore stage. Py 2 (S – 44-48 wt. %, Fe – 48-52 wt. %) has traces of Cu (0,3-1 wt. %), As (1-3 wt. %) and Sb (0,2-1 wt. %). The textural attributes are characterized by framboidal and colloform pyrite. (Figure 25. a-c) Framboidal pyrite is frequently bound together by galena, sphalerite, and barite, occurring during the later stages of mineralization. Colloform pyrite texture exhibits evidence of pyrite breakdown into pyrrhotite, as the stoichiometry of pyrite (S – 50-53 wt. %, Fe – 44-47 wt. %) changes to one of pyrrhotite (Fe – 60-63 wt. %, S – 37-40 wt. %). The breakdown is visible as changes in darker (pyrrhotite rich) to brighter (pyrite rich) parts going inside the colloform texture outwards.

The presence of chalcopyrite is linked to the Gn+Sulfosalt+Py 1 ore stage in massive sulphide ore. Cu in Cpy is from 34-38 wt. %, Fe 32-35 wt. % and S 26-32 wt. %. Minor traces of As (<1 wt. %) and Sb (<2 wt. %) are rarely detected, usually where sulfosalts are in contact with Cpy.

Sphalerite grains with hypidiomorphic to xenomorphic characteristics appear finer grained (<200 µm) in comparison to the other two ore types. Zn constitutes from 64-68 wt. % in sphalerite, S 24-30 wt. % and Fe 1-5 wt. %. Traces of Pb (2-4 wt. %), Sr (<1 wt. %) and Ba (<3 wt. %) are detected in some samples. Occasionally, these grains exhibit veinlets that are filled with Cpy (Figure 22. (d)). Many instances also show inclusions of Cpy and Py 1.

Tetrahedrite (subgroup: Freibergite) is the main group of sulfosalts related with the massive sulphide ore. They associate with Gn, Cpy and Py 1 (Figure 25. g-i). Stoichiometry is as follows: Cu, 35-43 wt. %, Sb, 15-28 wt. %, S, 20-24 wt. %, Ag, 1-5 wt. %, As, 1-13 wt. %. Fe (0,5-3 wt. %), and Zn (6-7 wt. %) were also detected.

Galena (Pb – 85-89 wt. %, S – 19-22 wt. %) tends to closely associate with sulfosalts and idiomorphic pyrite, sometimes with chalcopyrite. It is often infilling fractures and cracks within pyrite grains or framboids (depicted in Figure 25. d-f). Commonly observed elements include Zn (1-3 wt. %), and Fe (2-3 wt. %), while Cu (<1 wt. %) is rarely detected.

Barite (Ba 54-58 wt. %, S 11-16 wt. % and O 25-28 wt. %) is observed as hypidiomorphic to xenomorphic, with a single mineralisation phase in massive sulphide ore type. It has a coarse grain size (>250 µm) and is related with cavity infill of brecciated grains formed during the earlier sulphide mineralization. It overprints all preceding mineral phases. Commonly detected with barite is Sr (1-6 wt. %), and rarely Cu (1-2 wt. %) and Fe (1-3 wt. %).

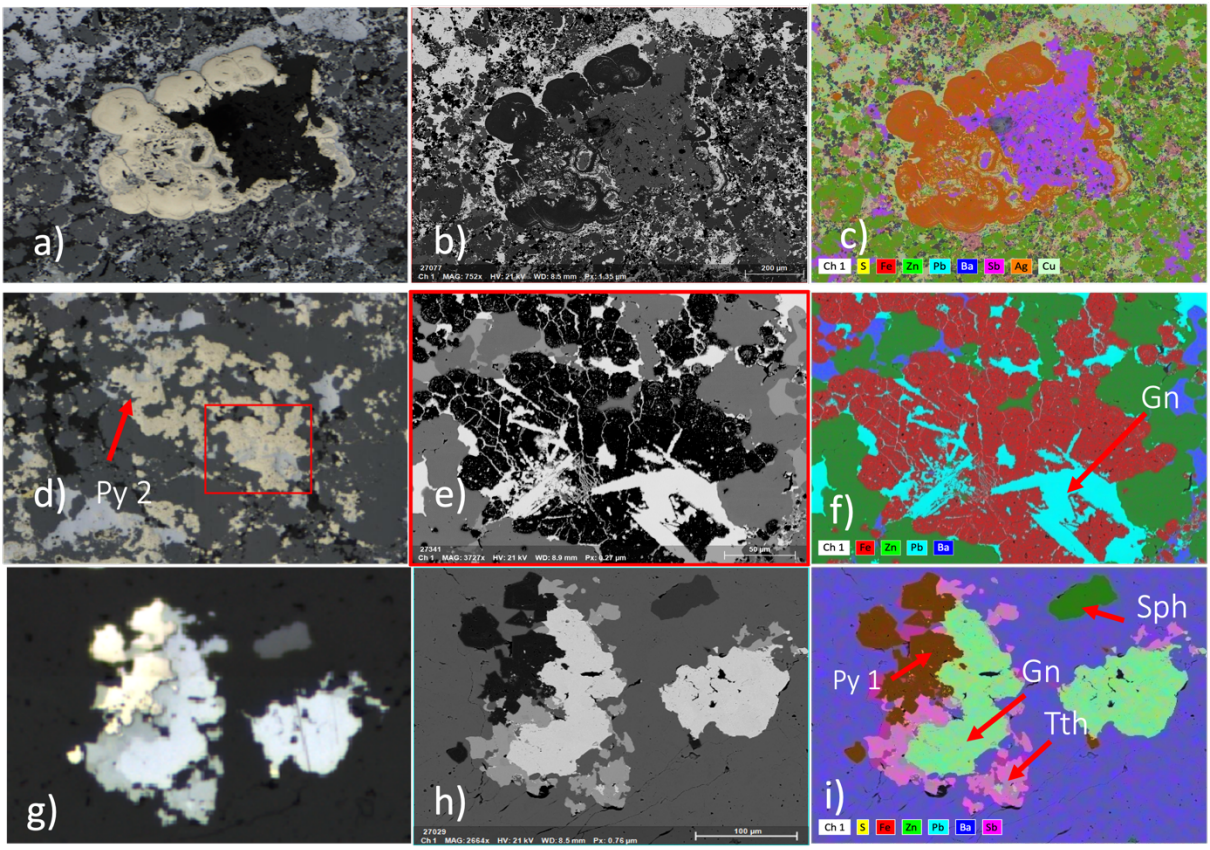

Figure 25. Massive sulphide ore type, Ore microscopy pictures (LEFT), SEM-BSE image (CENTRE), SEM-EDS elemental map (RIGHT).

Dolomitic breccia

Pyrite in dolomitic breccia ore type is more abundant (avg. around 45%), compared to other two ore types (massive sulphides approx. 9%, massive barite less than 2%). Pyrites textural characteristics, such as framboids, and colloidal texture were closely observed in dolomitic breccia ore type. Framboidal texture, with framboids grouped in spheres, or as individuals, are being suppressed by galena/barite/sulfosalts or quartz rich fluid (Figure 26. d-f). Colloidal texture of pyrite shows suppression by galena (Figure 26. g-i). Brecciated coarse grained pyrite grains (cataclastic texture) have fractures filled with sphalerite and barite rich fluid (Figure 26. a-c). Py 2 phase (xenomorphic) (Figure 26. g-i) associates with galena, tetrahedrite and chalcopyrite. Breakdown of pyrite to marcasite is dominant throughout the dolomite breccia samples (S 50-53 wt. %, Fe 45-48 wt. %). Further breakdown of pyrite into pyrrhotite evident (Fe - 60-63 wt. %, S - 37-39 wt. %), mostly in the colloform and framboidal textures, as outer rims tend to be more Fe rich, and inner rims more sulphur rich.

Quartz (O - 50-55 wt. %, Si - 44-48 wt. %) is a mineral phase first observed under optical microscope, but SEM-EDS confirmed its presence. Idiomorphic grains 50-200 μm in size are most related with the Gn+sulfosalts+Cpy+Py 1 complexes. It is suppressed by Cpy and the main ore bearing phase. Often observed as space filling, with it being overprinted by later ore stages. Commonly detected S (1-2 wt. %), Cu (1-2 wt. %), Sb (1-2 wt. %), K (< 1 wt. %) and Al (2-3 wt. %).

Hypidiomorphic grains of sphalerite often exhibit suppression by galena sulfosalts and later stage barite. Inclusions of idiomorphic quartz grains and chalcopyrite are observed (Figure 43, Appendix C). Cataclastic texture present, with fractures filled with quartz, barite, and pyrite. Within sphalerite, zinc (Zn) content ranges from 58 to 71 wt. %, sulphur (S) content spans between 25 and 30 wt. %, while iron (Fe) content varies from 1 to 4 wt. %. Minor amounts of Pb at 2 to 4 wt. %, Sr at less than 1 wt. %, As between 1-2 wt. %, Ba at less than 3 wt. % are detected in some samples. Furthermore, numerous instances also reveal the presence of inclusions comprising both chalcopyrite (Cpy) and pyrite (Py) 1.

Chalcopyrite associates with the sulfosalts phase, almost in every dolomitic breccia ore sample. Within chalcopyrite, Cu ranges from 38 to 41 wt. %, Fe from 37-41 wt. %, S from 19-23 wt. %. Barite and As are detected in traces (< 1 wt. %). Hydrothermal brecciation of Cpy grains by later stage Gn+Sulfosalt (Figure 26. j-l).

Galena is present as fracture filling, or in veins/veinlets, and having xenomorphic to idiomorphic habitus. Pb in galena is from 84-88 wt. %, while S is from 5-7 wt. %. Frequently detected elements are Cu (1-2 wt. %), Fe (1-6 wt. %) and Zn (2-6 wt. %). Late-stage galena observed as cement between the framboidal pyrite/marcasite grains (Figure 26. d-f).

Two types of sulfosalts are seen in the dolomitic breccia ore, tetrahedrite (subgroup – Freibergite), and bournonite. Dominant sulfosalt in the dolomite breccia ore type is bournonite, with sporadic occurrence of Ag-bearing Freibergite. Stoichiometry for bournonite is as follows: Pb, 40-43 wt. %, Sb, 22-25 wt. %, S, 18-20 wt. %, Cu, 12-14 wt. %. Closely related with the main ore stage, together with Py 1, Cpy and Gn(Figure 26. g-i). replacement of sulfosalts with pyrrhotite is observed, most likely a very late process (Figure 43, Appendix C).

Barite (Ba 55-58 wt. %, S 11-16 wt. % and O 24-28 wt. %) is mostly seen as space filling, overprinting the earlier stages of mineralisation. Idiomorphic barite blades inside the colloidal texture of pyrite have been recrystallised, with sulphide mineralisation overprinting the grains (Sph, Sulfosalts, Gn). Commonly detected with barite is Sr (1-6 wt. %), and rarely Cu (1-2 wt. %), Sb (< 1 wt. %) and Fe (1-3 wt. %).

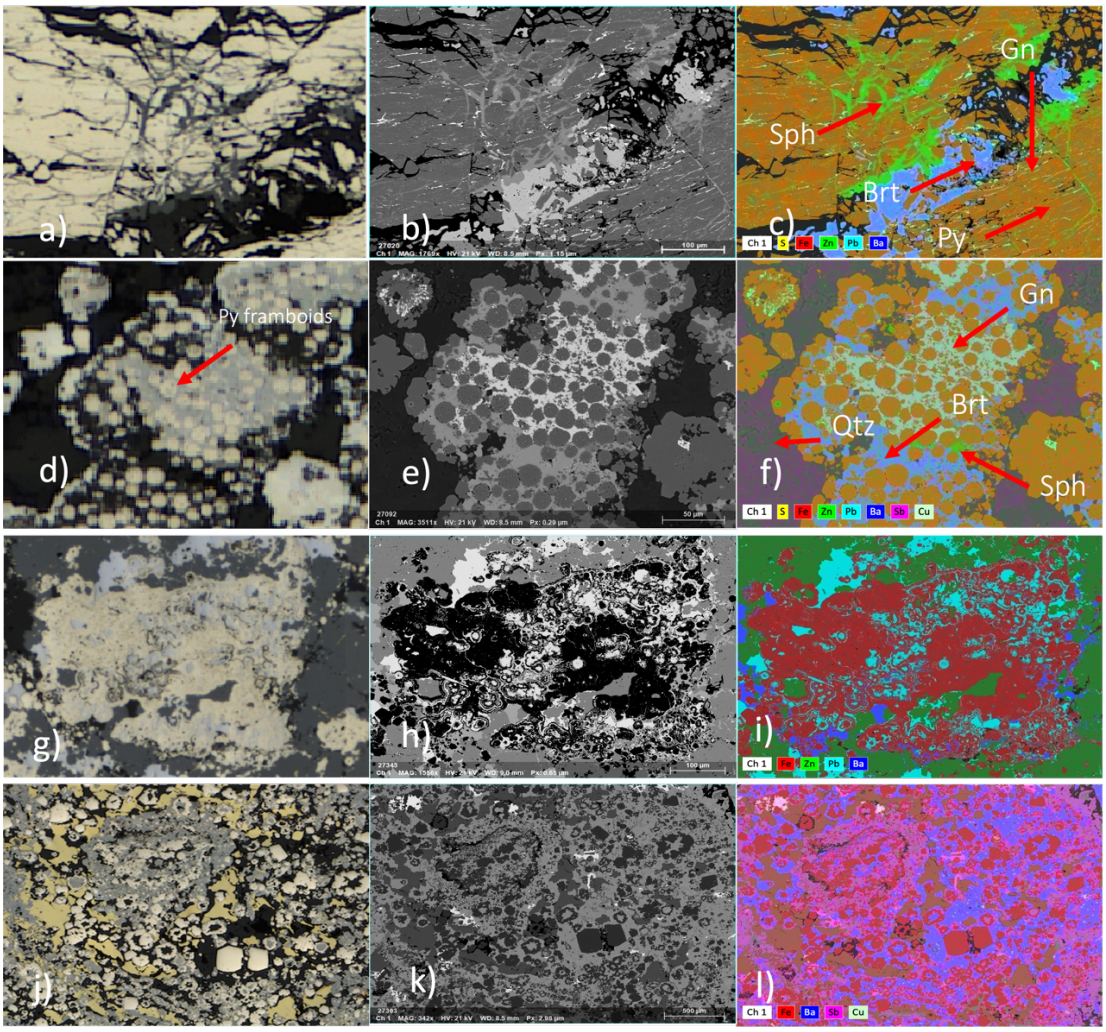

Figure 26. Dolomitic breccia sulphide ore type, Ore microscopy pictures (LEFT), SEM-BSE image (CENTRE), SEM-EDS elemental map (RIGHT).

LIBS

The following fifteen elements were detected in the 195-575 nm range of plasma emission: Zn, Pb, Si, Ag, Ba, Ca, Hg, Fe, As, Cu, Mg, Cd, P, Ge, Sb. The X and Y axis represent the sample size (in mm), while the Z axis shows the scale of intensity for each element. The distribution of Ba, Si and Zn is consistent with the delineation of barite, quartz, and sphalerite. The other elements observed are either trace elements or minor, or being shared between several mineral phases, such as the case of Pb (Figure 27). Other elements commonly detected in sulphide ore, such as: Co, Mo, Bi, Se, Te were not detected.

Since this LIBS prototype is currently not quantitative, the description of the samples and comparison of different elemental occurrences is theoretical. Looking at the elemental maps of the Figure 27., there is a positive correlation between Cd (and As) distribution in massive barite ore type. Zn and Pb are negatively correlated. Si and As counter each other out in sample BR-49-19-16. Occurrence of Ca and P can delineate the existence of apatite, as seen in several samples of the same ore type. Ge tends to occur closely related with Pb. Negative correlation between Mg, Fe and Ba is visible. Zn, Cd, As, P, Hg all seem to follow similar spatial distribution.

Massive sulphide sample, BR-11-22-16, is shown below. The fine-grained ore seems to cause an issue for the LIBS device, being able to have resolution from 100-200 µm, with a 0,1mm stop. However, some common traits are still observed. Cd and Zn are positively correlated, together with As and Hg, while Ba is negatively correlated with all those elements. Fe and Sb are positively correlated, with Cu, Ag and Ca seemingly coming along with them. Full list of samples analysed by LIBS can be found in the Appendix C.

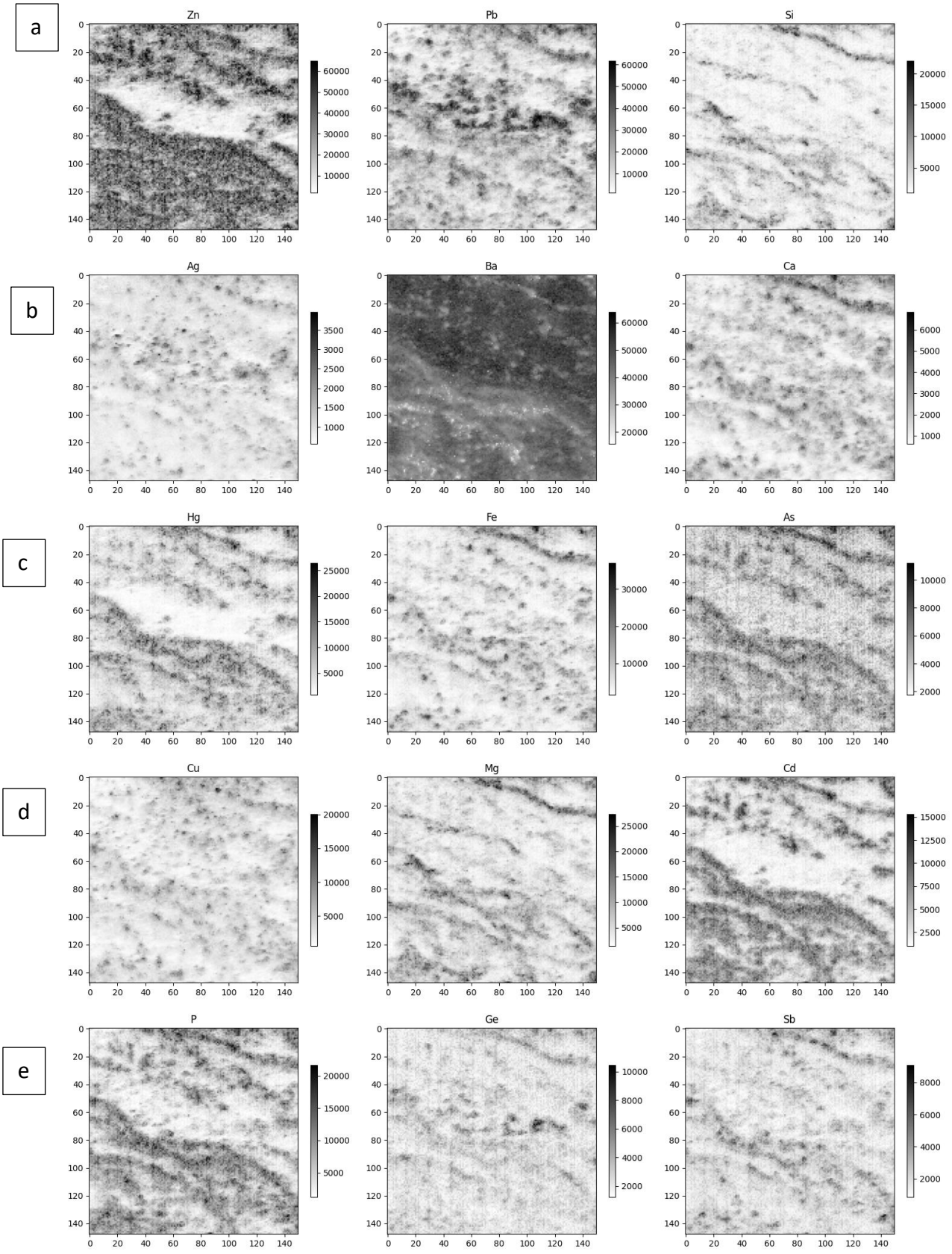

Figure 27. Elemental mapping for 15 elements, massive barite ore sample BR-49-19-16. a) Zn Pb Si, b) Ag Ba Ca, c) Hg Fe As, d) Cu, Mg, Cd, e) P Ge Sb

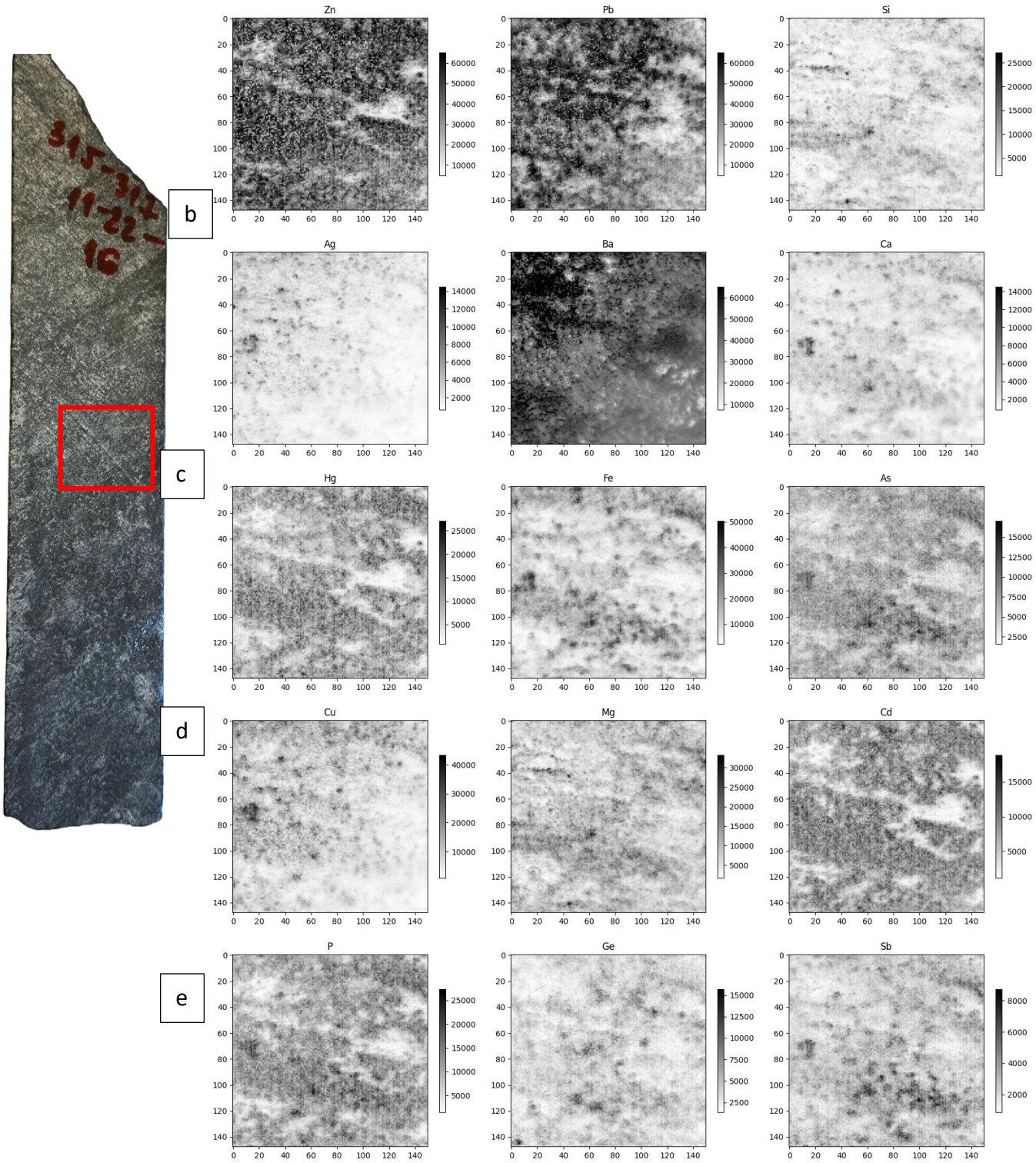

Figure 28. Massive sulphide sample BR-11-22-16. Macrophoto (LEFT), together with the analysed part of the sample (red square), RIGHT – elemental maps of the 15 elements, a) Zn Pb Si, b) Ag Ba Ca, c) Hg Fe As, d) Cu, Mg, Cd, e) P Ge Sb

Dolomitic breccia sample is shown below (Figure 30). Analysing the elemental maps reveals notable patterns and correlations within the dolomite breccia ore type. One significant observation is the positive correlation between the distribution of Cd and As in this ore type. Negative correlation is observed between Ba and Si. Notably, the presence and spatial distribution of Ca and P emerge as indicators of the possible occurrence of apatite (detected by SEM-EDS). This feature is consistently observed across several samples of the same ore type. In sample A, a positive correlation can be seen between Pb, Sb, and Ag, with these elements tending to localize almost precisely within the same region. This intriguing phenomenon could potentially signify the presence of a specific mineral phase within the Tetrahedrite group, such as Freibergite, known for its silver content. Furthermore, the data hints at the presence of a Ge-bearing phase, though further investigation is needed to confirm its identity and significance within the mineralogical context.

Combining the elemental maps and using convolutional neural networks for recognition and classification of different mineral phases present in the sample, joint elemental/mineral maps were created. Note that the sample picture was vertically rotated by 180 degrees due to processing difficulties. The X and Y axis correspond to the diameter of the analysed area of the sample, while the different lithologies delineate specific phases present in the sample.

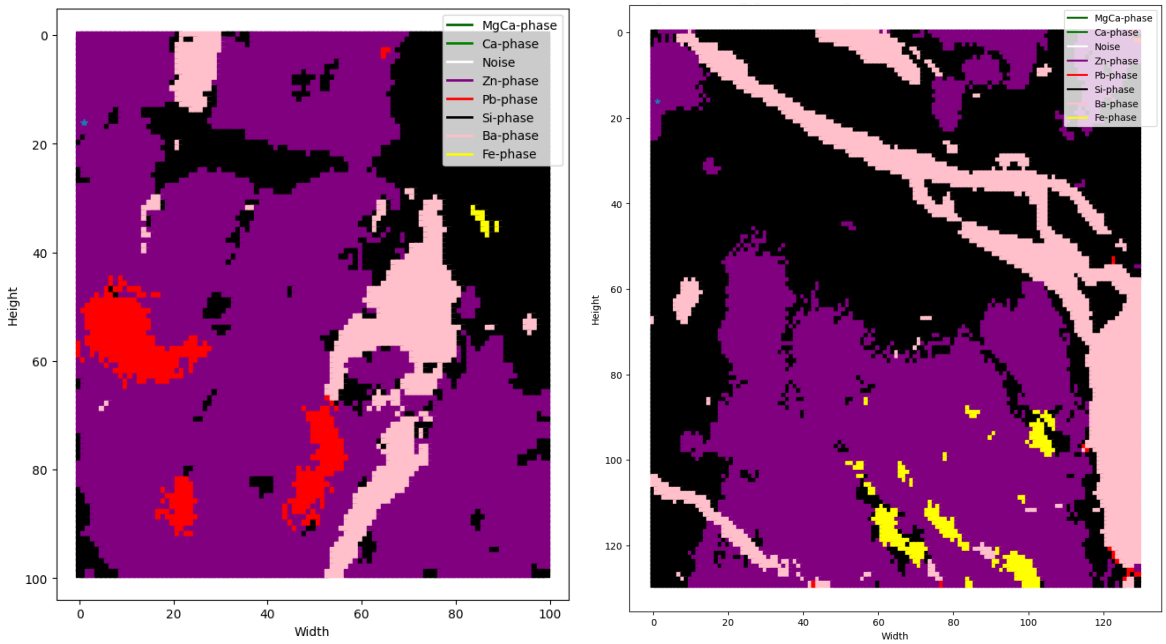

Figure 29. Combined elemental mapping of the BRD-27-22-20-A&B sample, using neural networks.

a

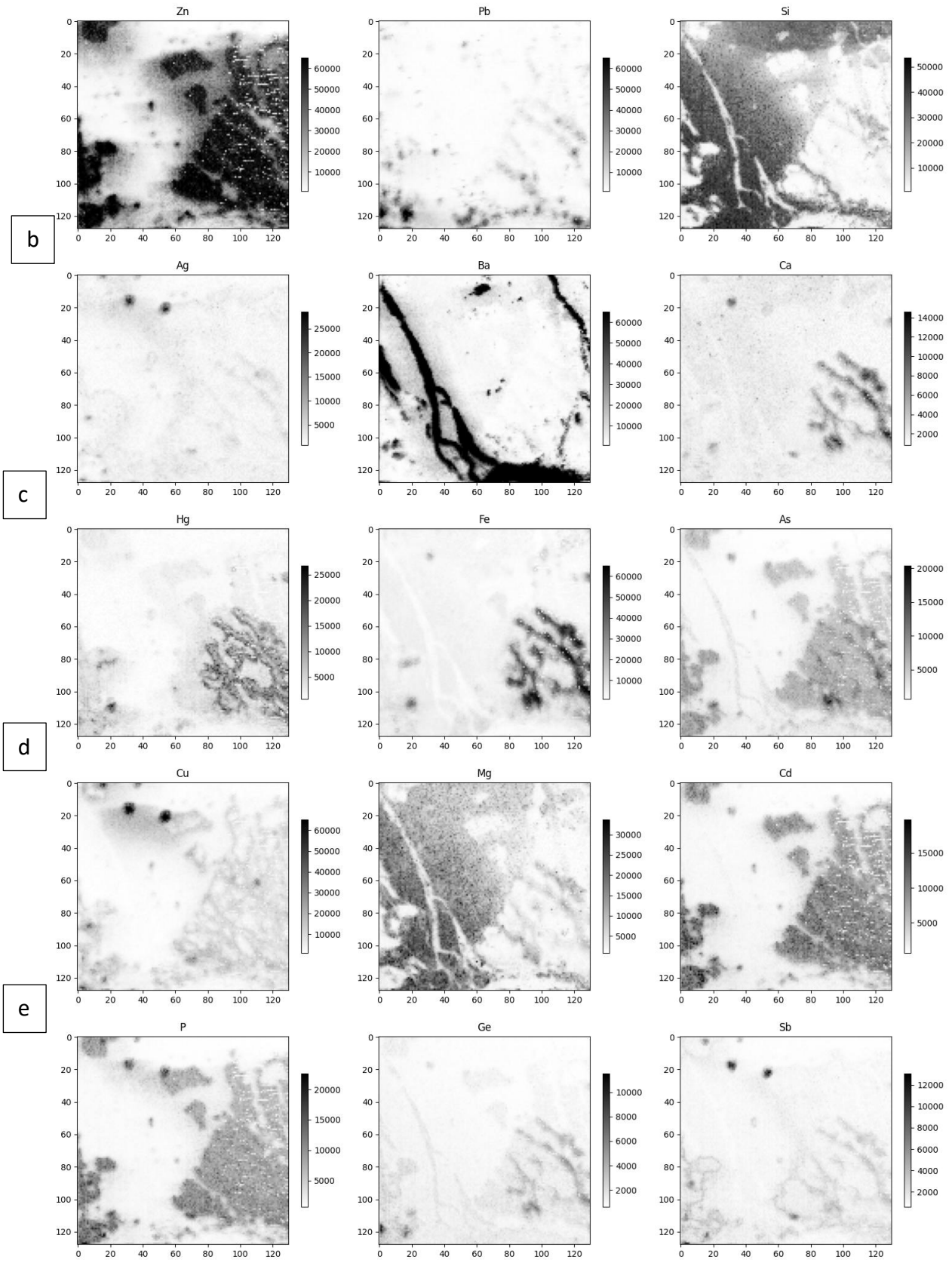

Figure 30- Elemental maps for the dolomite breccia ore type, sample BRD-27-22-13-A, a) Zn Pb Si, b) Ag Ba Ca, c) Hg Fe As, d) Cu, Mg, Cd, e) P Ge Sb

Automated mineralogy

Three composite samples undertook automated mineralogy analysis. IVC 1 represents massive barite ore, IVC 2 massive sulphide ore, and IVC 3 dolomitic breccia ore type. Total list of samples included in the analysis is shown in the table below.

Table 3. Automated mineralogy samples

COMPOSITES FOR THE AUTOMATED MINERALOGY AND XRD			
	Composite 1	Composite 2	Composite 3
Type of ore	Massive barite	Massive sulphide	Mineralised breccia
SAMPLE ID	NW-BR-49-19-16	NW-BR-21-22-04	MOB-BRD-27-22-21
	NW-BR-11-22-06	MOB-BR-49-19-14	MOB-BRD-27-22-22
	NW-BR-11-22-05	MOB-BR-49-19-15	MOB-BRD-27-22-23
	NW-BR-11-22-11	NW-BR-11-22-16	MOB-BRD-27-22-24
	MOB-BRD-27-22-20	NW-BR-11-22-17	MOB-BRD-27-22-25
		NW-BR-11-22-07	NW-BR-21-22-07

Bulk mineralogy, liberation data and association of liberated phases was analysed. The bulk mineralogy of each sample is shown in the graph below. Sulfosalts appear to be relatively more abundant in the dolomitic breccia ore type (2,4 %), compared to the first two ore types (0,6 % and 0,8 %), respectfully. Pyrite shows a similar trend, its abundancy is also the highest in the dolomitic breccia ore type, together with quartz and muscovite.

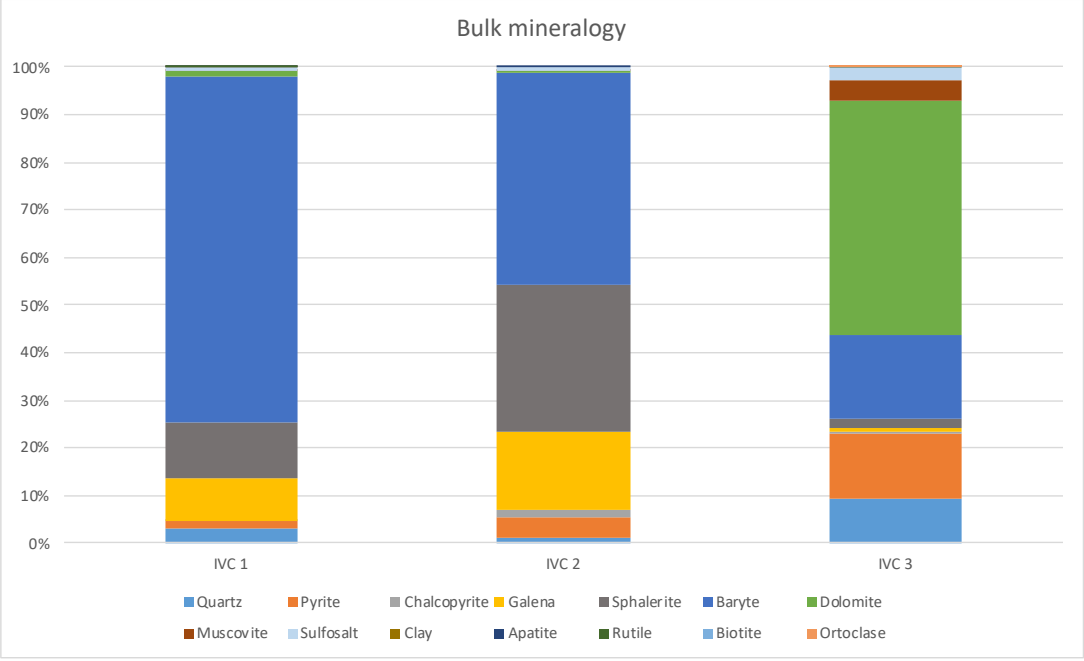

Figure 31. Bulk mineralogy for the three ore types

Liberation analysis was conducted for the three ore types, and all mineral phases present in them. Results are summarised below.

Massive barite

The primary objective of this analysis was to get a more comprehensive understanding in the liberation size of mineral phases. The samples were ground to <75 µm, as suggested by an independent analysis conducted by a contractor of Adriatic Metals Plc. results for the massive barite ore are shown below (Figure 32).

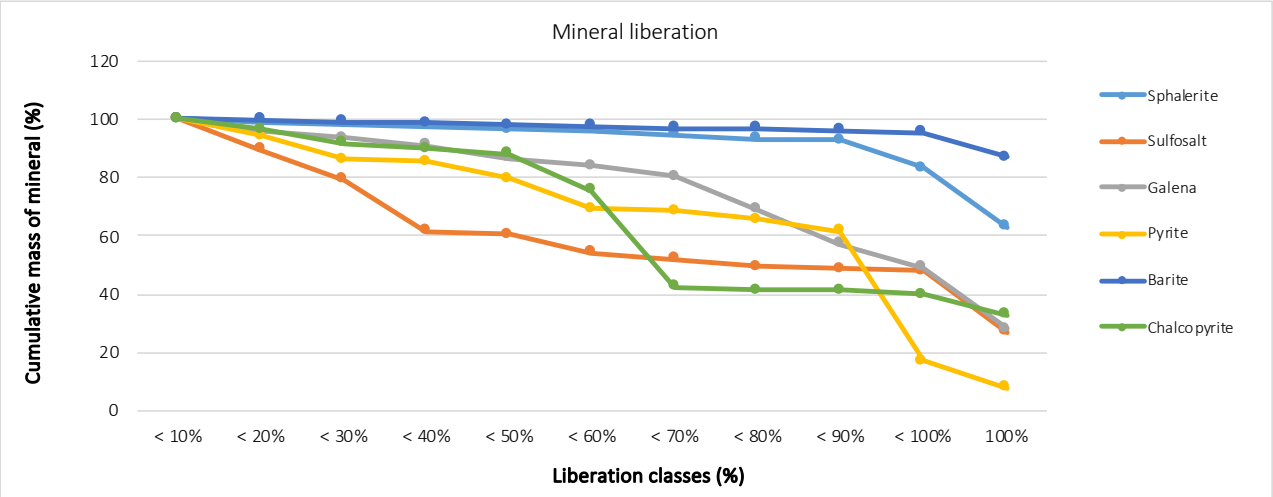

Figure 32. Mineral liberation for different mineral phases in massive barite ore

It is easily readable from the graph that there is a significant difference in cumulative mass of mineral liberated i.e. for the 100% liberation class. Looking at barite, 87 % if barite is completely liberated, sphalerite is 63 %, chalcopyrite galena and sulfosalts range around 33-37%, while the least liberated mineral phase is pyrite, with only 8 % being fully liberated. Substantial decrease in mass % of mineral liberated is noticeable in two places. Firstly, with chalcopyrite curve, going from the < 60 % to < 70 %, a drop from 75 % to 42 % of grains 70 % liberated is observed. Similarly, pyrite shows a larger drop in % liberated when going from lower than 90 % liberated, to lower than 100 %.

Massive sulphide

Massive sulphides show similar characteristics, when it comes to mineral liberation, as massive barite ore. Once again, barite has 83 % fully liberated particles (Figure 33), while the lowest is similarly pyrite, with 19 %. Significant decrease is observed comparing the sphalerite liberation, as sphalerite has 43 % of particles fully liberated, (compared to 63 % in massive barite).

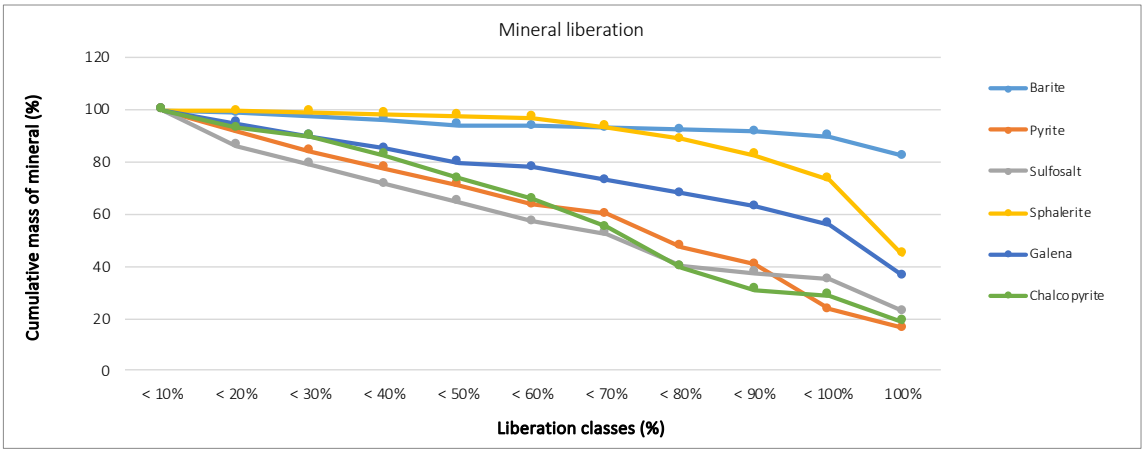

Figure 33. Mineral liberation for different mineral phases in massive sulphide ore

Dolomitic breccia

The liberation results for the dolomitic breccia are represented in the figure below. (Figure 34). Barite once again has the highest mass % fully liberated, with 79 %**.** Interestingly, chalcopyrite behaves almost identical going from the < 50 % liberated to fully, with its cumulative mass almost not decreasing at all. Galena has the lowest % of grains fully liberated, with 20 %.

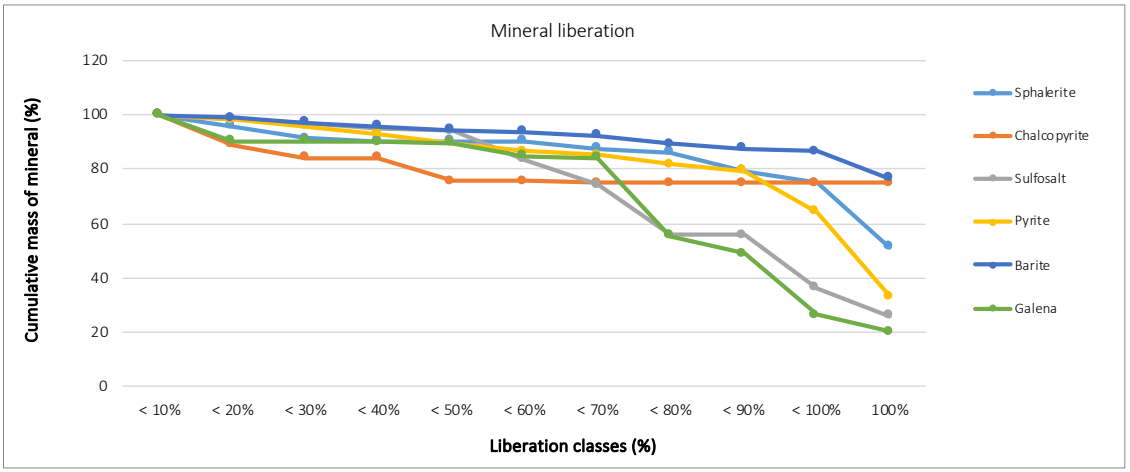

Figure 34 Mineral liberation for different mineral phases in dolomitic breccia ore

XRD

X-ray diffraction analysis was conducted for the three composite samples (APPENDIX C). The results are summarised in the figure below. IVC 1 represents massive barite ore, IVC 2 massive sulphide, and IVC 3 dolomitic breccia ore. Dolomite was detected in the massive barite ore, with 5 %. Galena and sphalerite are most abundant in the massive sulphide ore, as should be expected. Quartz is present in dolomitic breccia ore with almost 10 %, as well as massive barite (1,8%). Barite is most abundant in the massive barite ore, with 78 %, followed by 56 % in massive sulphide ore, and 17 % in dolomitic breccia ore. Muscovite is only detected in dolomitic breccia ore type, with 4,8 %.

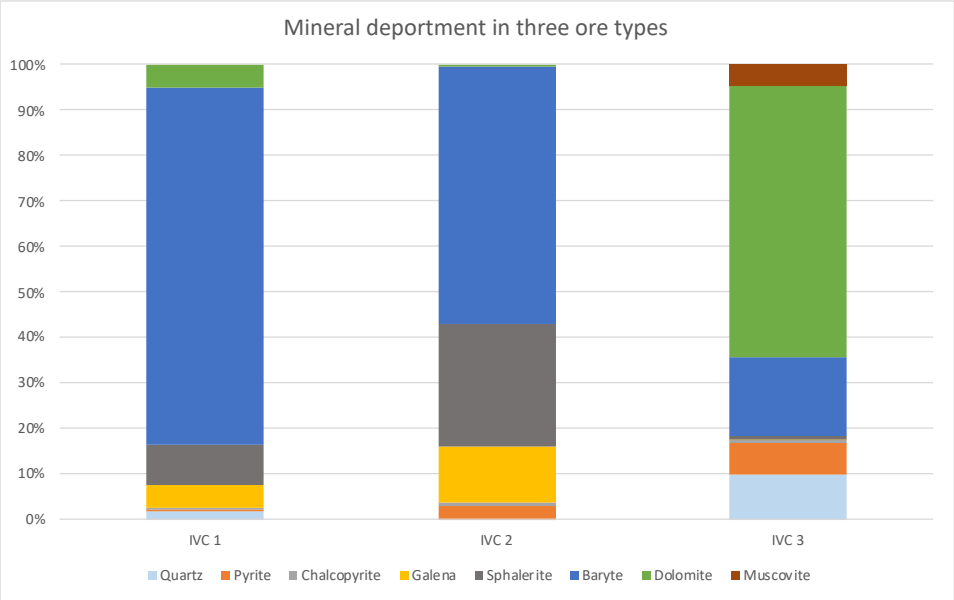

Figure 35. XRD results for the three composite samples.

5. Discussion

Macroscopic determination of the Rupice orebody

Three main ore types were delineated upon drill core mapping of the Rupice orebody. Massive barite ore is containing >80 % barite, with minor sulphide phases observed as veinlets. Most likely formed as a result of an overprinting of late barite stage of mineralisation. Mineralisation is fine grained (< 500 μm).

Massive sulphide ore type is characterised as fine grained, with a similar grain size as massive barite (Figure 18). Presence of barite is visible as space filling, partially overprinting the areas in samples closer to the massive barite ore (< 25 %). Upon closer inspection, several mineral phases are noted: galena, sphalerite, pyrite, and chalcopyrite.

Dolomitic breccia ore type is distinguished on the outer zones of the ore body and is represented by the dolomitic breccia with sulphide veins and veinlets. Multistage development of the mineralisation is evident, as overprinting stages make it difficult to distinguish the possible zonation, or sequence of mineralisation, at least not macroscopically.

Structural controlling factor is evident is almost every core that was mapped/analysed, as the mineralisation is bound by two sub-parallel faults. Tectonic activity is visible in the samples, macroscopically, as moving towards the faults zone brecciation and organic infill is more present in the samples. Brecciation and fracturing is most likely due to later stage tectonic activity, most likely corresponding to the Eocene tectonics and uplift od the Dinarides (L. A. Palinkaš et al., 2008).

Core scanning using the HySpex SWIR hyperspectral camera was conducted in order to observe the changes in mineralisation, and possible alteration patterns. The results showed decent correlation with the macro photo when it came to the coarser grained dolomitic breccia sulphide ore type. Difficulties arose when analysis the massive ore, due to their finer grain size. The cameras resolution was not optimised for the size of the core samples (3x10 cm on average), making the pictures grainy and losing the subjectivity of the resulting maps. One of the solutions would be to lower the camera closer to the conveyor belt, to try and obtain better resolution of the samples, and consequently, better, and highly delineated results, compared to the original ones.

Microscopic determination of the Rupice orebody

Massive barite ore type

Massive barite ore type is dominantly fine grained (< 200 µm). Its most abundant constituent is barite, averaging 70 %, when looking at all the samples. The sulphide phases tend to be hydrothermally brecciated, as a result of overprinting by the late barite stage.

Pyrite is present as idiomorphic and xenomorphic in habitus. Idiomorphic pyrite (Py 1) is commonly finer grained out of the two, with an average size < 50 µm. It is being suppressed by the quartz, sphalerite, chalcopyrite, galena, sulfosalts, making it genetically the oldest mineral phase observed in the samples. Occurs together with galena, sulfosalts and rarely chalcopyrite in massive barite ore. Xenomorphic pyrite is usually associated with galena and sulfosalts. It is being suppressed by the later barite, making its timeline of mineralisation related with the Gn+Sulfosalt ore phase. Pyrite in massive barite ore exhibits colloform texture, common for the massive sulphide ore in general (Hannington, 2014). Framboidal pyrite is another textural characteristic that can be seen in massive barite, with it representing an overprinting stage, most likely due to the low temperature emplacement and change in redox border (Liu et al., 2022), possibly related with the over thrusting processes in Late Jurassic (Palinkaš et al., 2008). SEM-EDS point analysis gives an insight in the framboidal pyrite texture. Framboids are characterised by different ordering stages, from completely disorganised, to fully spherical framboids. Agglomeration of framboids into colloform texture forms as a result of continuous growth of nuclei, with a stable redox environment (Wilkin et al., 1996; Wilkin & Barnes, 1997). Cementation with galena is observed. Conducting a sulphur isotope analysis using TOFL-SIMS or electron microprobe (EPMA) for the framboids and different pyrite phases could provide an insight in the movement of the redox boundary throughout the ore body, and consequently the spatial variability and placement of the deposit geotectonically (Liu et al., 2022). Breakdown of Py 1 to marcasite is evident in some grains. Sphalerite is the second most abundant phase in the massive barite ore, after barite. It has been hydrothermally brecciated by the younger barite phase. In many cases contains inclusions of Cpy and Py 1, suggesting that these two phases might be older. Chalcopyrite is rarely observed in massive barite ore. When it is seen, it associates with Gn, Py 1 and Sulfosalts. Suppression of the xenomorphic Cpy grains by sulfosalts and galena observed, suggesting that Cpy is older than the Gn+sulfosalt mineralisation stage. Galena is intergrown with sulfosalts +/- chalcopyrite, suppressing the earlier pyrite stage. Commonly seen as space and fracture filling. Sulfosalts are fine grained in massive barite ore (< 100 µm). SEM-EDS analysis delineated three probable main phases: bournonite, freibergite and tennantite (Tetrahedrite group). Freibergite is the main Ag-bearing mineral phase analysed and detected. Chemical zonation of the sulfosalt grains is visible (most notably observed with freibergite), which might be as a result of a difference in Ag-As-Sb ratio in the outer or inner part of the grain. SEM-EDS analysis indicated a possibility of a two-stage development of barite in massive barite ore type. Barite 1 is coarse-grained (>250 µm), present in samples as cavity fill, breccia infill of the earlier sulphide mineralization. It overprints all earlier mineral phases. Barite 2 (Fe-bearing reddish) can be described as cementing earlier, tectonically brecciated stages of mineralization, including brecciated Barite 1. It shows a banded texture with nanometre-scale intercalations of apatite. Two stage development is also a possible scenario for apatite, as both idiomorphic and xenomorphic habitus of apatite is notable, as well as associations with

younger/older phases. Idiomorphic grains show association with the main ore-bearing stage (Gn+Sulf.+Py1/Py2+Cpy), while the nanometre intercalations with Fe-bearing Barite 2 suggests a younger stage of development. Cinnabar is analysed in only one sample (BRD-27-22-20) and marks the area of contact between the two ore types, massive barite and massive sulphide. Its occurrence might be related with the mixing of two ore-bearing fluids, or simply a change in the chemistry of the fluid. Tectonic brecciation of the Fe-bearing barite 2 + apatite 2 veins is a likely result younger events in the Dinarides. The space between the brecciated parts of the vein was partially filled with cinnabar. This would indicate a low temperature emplacement, likely as a result of post-ore processes. Paragenetic sequence of the massive barite ore is summarised in the figure below (Figure 36).

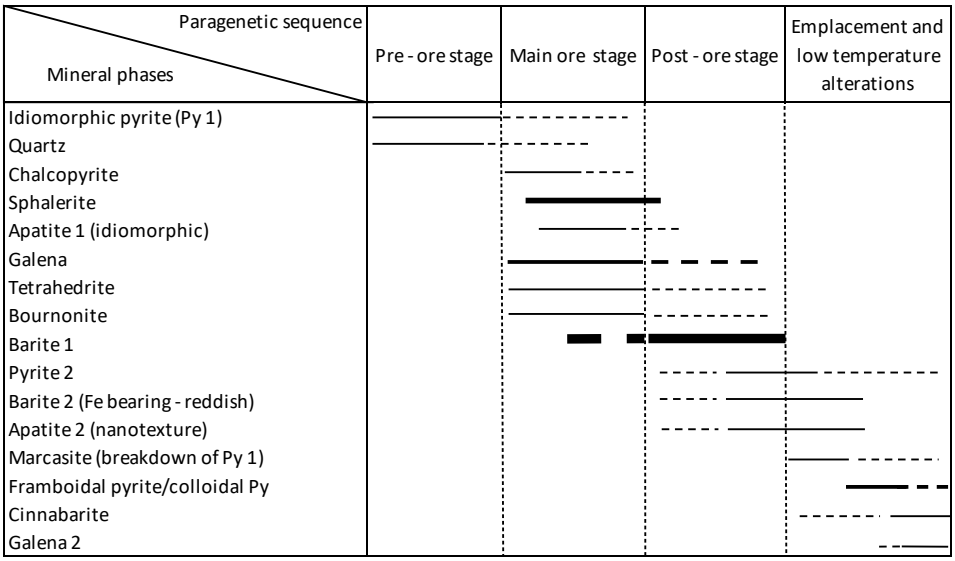

Figure 36. Paragenetic sequence of massive barite mineralisation

Massive sulphide ore type

Pyrite in massive sulphides shows similar characteristic as described above. Idiomorphic Py 1 represents pre-ore stage, as the main ore stage mineral phases (Sph+Gn+Sulfosalts+Cpy) suppress it. Py 1 exhibits framboidal and colloform texture. Framboids are observed in different stages of growth and order, going from nanocrystal to micron scale crystals. Framboidal pyrite is commonly formed in environments of euxinic seawater columns or shallow-marine sediments (Wilkin et al., 1996). Additionally, it could also be formed after the deposition of host rocks, occurring during phases of late diagenesis, low-grade metamorphism, and hydrothermal alteration (Liu et al., 2022; Wilkin & Barnes, 1997). The formation of framboidal pyrite is indicative of a shallow and a relatively low temperature setting (<200 ºC) (Wilkin & Barnes, 1997). Evidence of a change in depth or proximity to the redox border could be the change in mineralogy of the framboids, as four different mineral phases are detected by the SEM-EDS, greigite, marcasite, pyrite and pyrrhotite. Different authors stated the importance of specific precursors in the formation of framboids, such as greigite (Fe_3S_4) (Scott et al., 2009; Wilkin et al., 1996). However, the critical point of formation is high pyrite supersaturation (Wilkin & Barnes, 1997). Additional studies are needed in order

to investigate the difference in sulphur isotopes in different framboids, and their timeline in formation of the deposit. Liu et al., 2022, highlights the evolution stages of pyrite framboid formation, starting from the nanocrystals to micron size crystals, framboids, and colloidal and subhedral structures as final products.

Colloidal texture is commonly observed in massive sulphide samples. Breakdown of pyrite into pyrrhotite on the outer rims of the texture is evident, with galena commonly observed as cement in between the spheres and colloids. Quartz is rarely observed in massive sulphide samples. Idiomorphic grains are often < 20 µm and show suppression by Cpy and Sph, who are more abundant in the massive sulphide ore type, compared to massive baryte. Chalcopyrite is commonly observed in association with Gn+Sulfosalts+Py. Sphalerite is the most abundant mineral phase in massive sulphides and is present in samples as space filling. Inclusions of Cpy and Py 1 are often detected. Galena and sulfosalts tend to associate together. Galena is often observed as fracture filling of the brecciated coarse grains of sphalerite. Tetrahedrite (subgroup: Freibergite) and bournonite are main sulfosalt phases in massive sulphide ore type. Freibergite is the main Ag- bearing phase in the massive sulphide ore. It shows chemical zonation, with Ag-Sb-As ration differentiating the brighter and darker zones in the grain. Paragenetic sequence of the massive sulphide ore is summarised in the figure below (Figure 37).

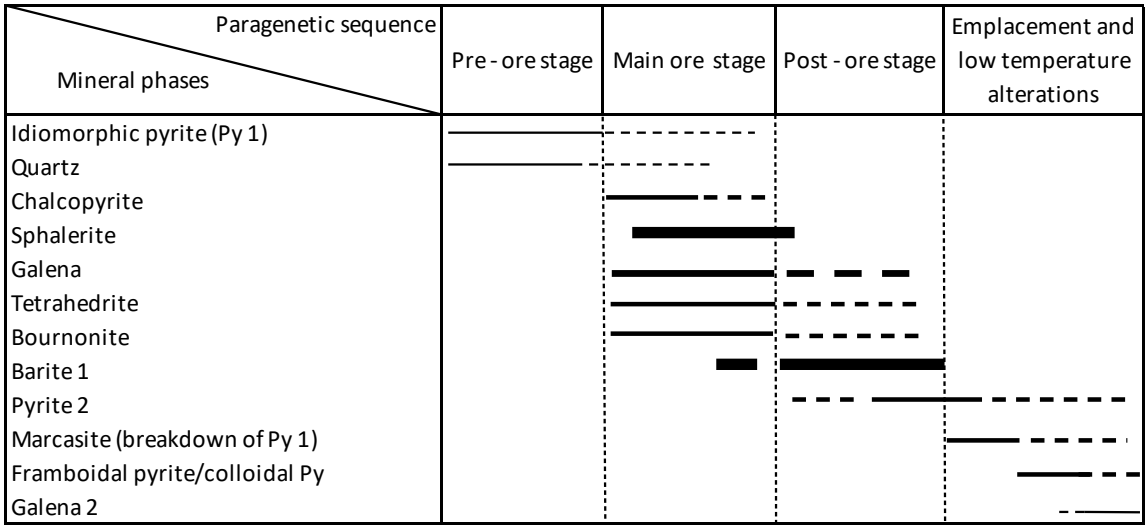

Figure 37. Paragenetic sequence of massive sulphide mineralisation, thickness of lines presence relative abundance in samples

Dolomitic breccia ore type

Pyrite is one of the most abundant mineral phases in the dolomitic breccia ore. It exhibits a variety of textural characteristics, such as framboidal and colloidal texture. Breakdown of pyrite into marcasite is observed in every sample, evident not only by the petrological characteristics of marcasite, but by volume change of the pyrite grains. Molar volume of pyrite is smaller (23.94 cm^3 mol^{-1}) than that of marcasite (24.58 cm^3 mol^{-1}) (Yao et al., 2020). The reduction in molar volume for the transformation from pyrite to marcasite is -2,6 %, which is clearly visible on the microscopical scale. Colloidal pyrite texture is heavily brecciated, which is likely a result of additional tectonic activity.

Mineralisation in dolomitic breccia is coarser grained (> 250 µm). Association of the Gn+Sulfosalt+Py 1+Cpy is not so clear, as in previous ore types. Cpy and Sulfosalts are commonly observed together, with Py 1, but Gn is rarely in association. Hydrothermal brecciation of Cpy is evident, as a result of later sulfosalt phase. Bournonite is the main sulfosalt mineral phase in dolomite breccia ore type. Late stage replacement of sulfosalts with pyrrhotite observed (Appendix C, Figure 43). Summarised paragenetic sequence of mineralisation is presented below (Figure 38).

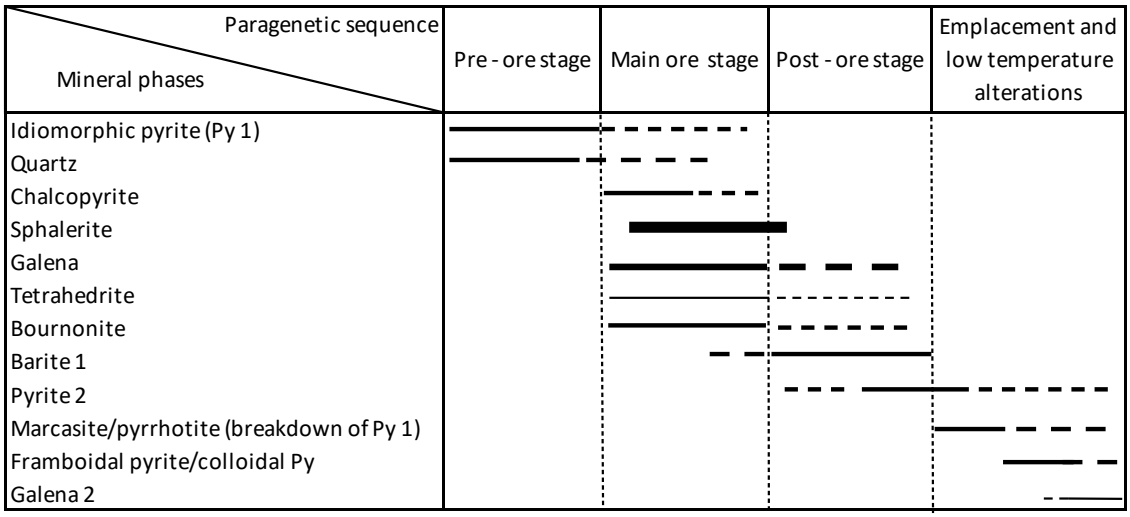

Figure 38. Paragenetic sequence of dolomitic breccia ore type. Thickness of lines presence relative abundance in samples

Automated Mineralogy

When comparing the three composite samples, and the specific liberation size of different mineral phases, several conclusions can be drawn.

Looking at the sulfosalts liberation in the three composite samples (Figure 39), there is a clear difference in the cumulative mass of the liberated class in IVC 3 all the way up to the < 80 % of the grains liberated. IVC 3 is the dolomite breccia ore type, with coarser grained sulfosalts. Mass of liberated grains is above 90 % up to the < 50 % liberation class, after which there is a downwards trend, when around 80 % liberation all three samples behave relatively similarly. The worst liberation is seen for the IVC 2 sample, which is the massive sulphide ore type, while the highest liberation is with IVC 3 composite sample.

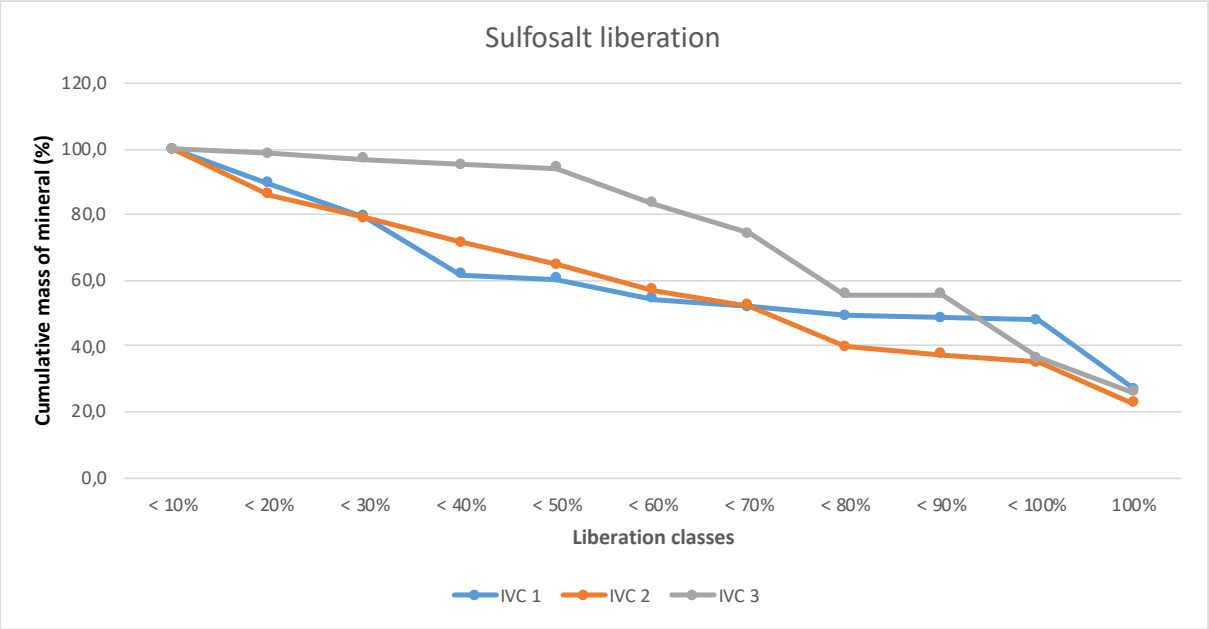

Figure 39. Comparison of sulfosalt liberation between the three composite samples

Sphalerite on the other hand, shows a different trend (Figure 40). Cumulative mass of liberated sphalerite is above 95 % almost throughout all the liberation classes. Mass of liberated sphalerite continues to be above 90 % for the massive baryte ore after the < 80 % liberation class, while the other two samples see a decrease in liberated mass of sphalerite.

The highest liberation is seen with the massive barite sample (IVC 1) (62 %), while the lowest is related with the massive sulphide ore (46 %).

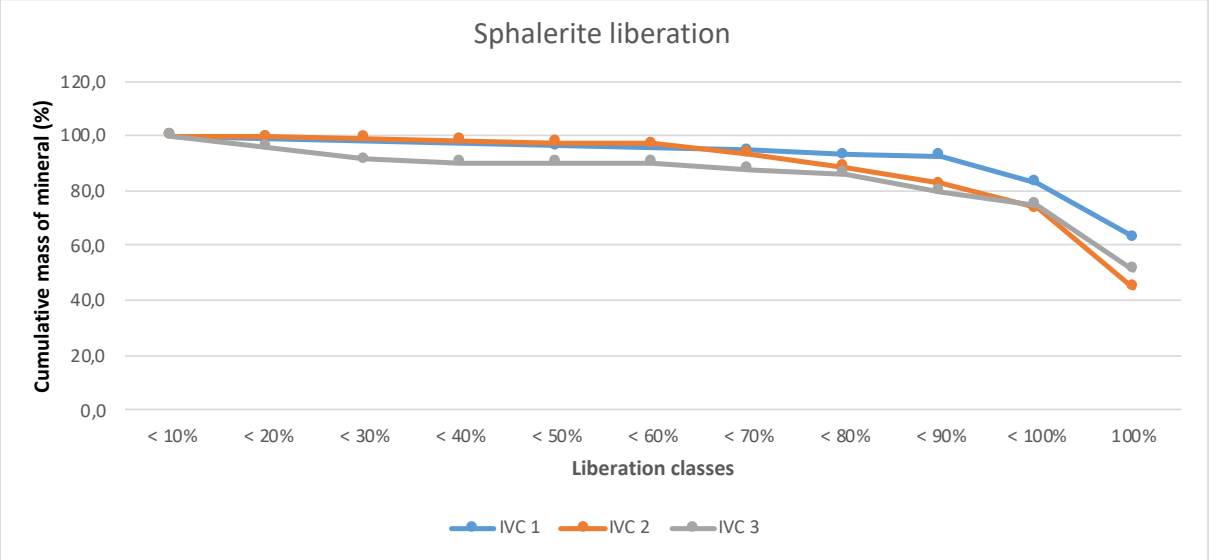

Figure 40. Comparison of sphalerite liberation between the three composite samples

6. Conclusion

Rupice deposit is a young prospect, currently owned by Adriatic Metals Plc. The mine is currently in the exploration stage, with plan of starting production in the winter of 2023. There is a lot of unknows, especially when talking about the genetic model of the ore deposit, or what kind of ore deposit it is.

Main objectives of this master thesis were to provide a comprehensive mineralogical analysis of the orebody, to get an insight in elemental deportments, as well as trace elements such as germanium, mercury, phosphorous and arsenic, and liberation analysis of the main ore-bearing and gangue phases.

The research was conducted partially at the Vareš locality in Bosnia and Herzegovina (as a part of the 2-month internship, hosted by the Adriatic Metals, Plc.), with analytical work taking place at University of Zagreb (Faculty of Mining, Geology and Petroleum Engineering) and University of Liege. The analytical techniques included: optical microscopy, core scanning (SWIR), SEM-EDS, LIBS, XRD, XRF, Automated mineralogy system (Mineralogic).

Mineralisation is presented by massive sulphides, with a high content of barite (avg. 40 %). Three distinct ore types were delineated based on optical observation, massive barite, massive sulphide, and dolomitic breccia ore type. Main ore-bearing mineral phases are galena, sphalerite, chalcopyrite, pyrite, cinnabar and sulfosalts (bournonite and minerals from tetrahedrite group, tennantite and freibergite), while the gangue is barite, dolomite, apatite, quartz, and muscovite. Pyrite exhibits several textural characteristics, such as framboidal and colloidal texture, specific to massive sulphide deposits (Hannington, 2014). Its late-stage breakdown to marcasite and pyrrhotite could be indicative of post-ore processes that affected the deposit and should be investigated in more details in the future research. Association of galena with sulfosalts and chalcopyrite and idiomorphic pyrite is commonly seen throughout the different ore types. Late stage overprinting with barite is evident in all ore types, in most cases causing hydrothermal brecciation of sulphides.

Trace elements, such as germanium, mercury, phosphorous and arsenic give valuable insight in the ore-forming processes. Hg-bearing mineral, cinnabar, formed most likely as a late-stage process, filling the previously brecciated cracks. Main phosphorous bearing mineral, apatite, is observed in two ore phases. Idiomorphic apatite (Apatite 1) is most likely related with the chalcopyrite-sphalerite ore-stage, while the Apatite 2 is visible as nanometre scale intercalation together with Fe - bearing Barite 2 (late). Arsenic is commonly detected with the sulfosalts, mostly freibergite. Germanium was described only with the LIBS device. While it is not a quantitative technique, a descriptive analysis was performed, with perspective conclusion about the Ge in the deposit. It was detected in most samples analysed by LIBS, and shows association with Pb and Sb.

Liberation analysis was conducted using the Mineralogic automated mineralogy system from Zeiss, for the three composite samples. Relatively low liberation can be concluded for the galena, sulfosalts and pyrite for all three ore types (20-40 %). In two cases pyrite had by far the worst liberation, which is definitely something to look into, when considering the mine tailing optimisation to prevent acid mine drainage.

Core-scanning and LIBS analysis showed promising results. Both techniques are currently in the development stage, and this work was one of the pilot tests for the future analysis. While there is still a lot of work to be done, especially in the improvements of resolution, detection limit and mapping, the current work done by the colleagues at the GeMME laboratory, and the Belgium Geological Survey is truly impressive.

This analysis was just a part of a much larger work to be done in the future. While this work was only focused on the orebody, trying to determine the paragenetic sequence of the mineralisation, a much wider analysis, involving alteration zones needs to be conducted in order to try and establish a genetic model of the deposit. Structural model is crucial in understanding the controls of the mineralisation, which are evident, even from the micro-scale. Furthermore, a more detailed work that involves electron microprobe (EPMA), together with TOFL-SIMS is suggested, to get conclusive evidence in the mineralogy of the mineral phases observed in the orebody.

Process-oriented approach is crucial for enhancing the understanding of the deposit and optimising the mining and processing methods, especially when dealing with penalty elements, such as cadmium, arsenic, mercury. integrates geological, mineralogical, metallurgical, and engineering aspects to optimize mining and processing methods, especially concerning penalty elements. This approach enables efficient resource utilization, minimizes environmental impacts, and enhances overall operational sustainability.

EIT CHAPTER

European Union has recently published a revised version of the critical raw materials assessment (CRM 2023.). in the revised version, several new minerals, including arsenic, copper, nickel, manganese, and helium were added (Figure 41).

Rupice deposit is a Ag-Zn-Pb deposit, with updated mineral resource estimation defined at 21.1 Mt at 156 g/t Ag, 1.2 g/t Au, 4.3% Zn, 2.8% Pb, 0.4% Cu, 27% $BaSO_4$. Baryte is currently being discarded as a by-product of processing, with the company stating that the current prices and volatility do not deem any profit. Baryte showed the best liberation, with almost 60 wt. % of grains fully liberated. This gives an insight that if opportunity arises, the processing of the baryte should not be overly complex.

Germanium is an element that has quite a potential for further research. Even though LIBS device isn't quantitative, Ge was present in all the samples analysed. The relationship with Pb and Sb means that the current processing scheme will extract it (the behaviour of Ge in the process flowsheet was not analysed).

Copper is under current flowsheet scheme going to the tailings, and while this is certainly not a Cu mine, the recent developments in the NW part of the orebody have seen substantial increase in Cu and Au content, which may give an opportunity for future process optimisation, if the resource estimation continues to increase.

Overall, Rupice polymetallic mine presents a significant prospect in the European Union, with a potential for further development and new prospects in the region.

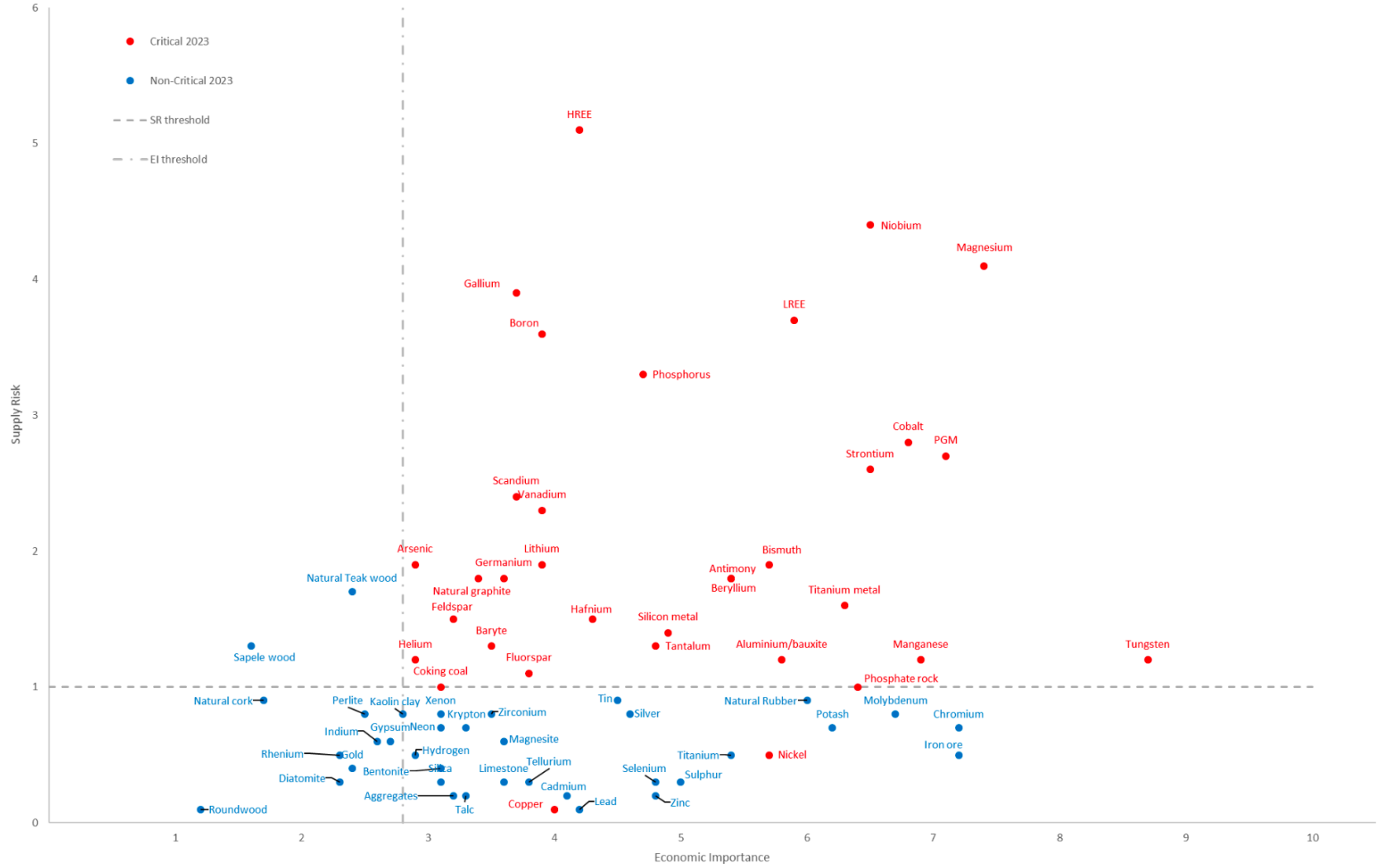

Figure 41. Critical Raw Materials, as of 2023.

References

Atanacković, M. ., Mudrenović, V. ., & Gaković, M. . (1968). *Geološka karta Područja Borovice = Carte géologique du terrain de Borovica*. Geoinženjering.

Balling, P., Tomljenović, B., Schmid, S. M., & Ustaszewski, K. (2021). Contrasting along-strike deformation styles in the central external Dinarides assessed by balanced cross-sections: Implications for the tectonic evolution of its Paleogene flexural foreland basin system. *Global and Planetary Change*, *205*, 103587. https://doi.org/10.1016/j.gloplacha.2021.103587

Borojević Šoštarić, S., Giannakopoulou, S., National Technical University of Athens, School of Mining & Metallurgical Engineering, Athens, Greece, Adam, K., National Technical University of Athens, School of Mining & Metallurgical Engineering, Athens, Greece, Mileusnić, M., & Faculty of Mining Geology and Petroleum Engineering, University of Zagreb, Croatia. (2022). The future of mining in the Adria region: Current status, SWOT and Gap analysis of the mineral sector. *Geologia Croatica*, *75*(Special Issue), 317–334. https://doi.org/10.4154/gc.2022.26

Borojević Šoštarić, S., Palinkaš, L., Strmić, S., & J.e, S. (2004). MVT-forming brines at Sv. Jakob, Medvednica Mt., Croatia. *Abstract Volume*, 183.

Hannington, M. D. (2014). Volcanogenic Massive Sulfide Deposits. In *Treatise on Geochemistry* (pp. 463–488). Elsevier. https://doi.org/10.1016/B978-0-08-095975-7.01120-7

Hrvatović, H. (2022). *Geološki vodič kroz Bosnu i Hercegovinu* (XC; 10). Akademija nauka i umjetnosti Bosne i Hercegovine. https://doi.org/10.5644/D2022.90

Hrvatović, H., & † Pamić, J. (2005). Principal thrust-nappe structures of the Dinarides. *Acta Geologica Hungarica*, *48*(2), 133–151. https://doi.org/10.1556/AGeol.48.2005.2.4

Katzer, F. (1903). *Geologischer Führer durch Bosnien und die Hercegovina*. Landesdruckerei.

Liu, K., Huang, F., Gao, S., Zhang, Z., Ren, Y., & An, B. (2022). Morphology of framboidal pyrite and its textural evolution: Evidence from the Logatchev area, Mid-Atlantic Ridge. *Ore Geology Reviews*, *141*, 104630. https://doi.org/10.1016/j.oregeorev.2021.104630

Mrinjek, E., Nemec, W., Pencinger, V., Vlahovic, I., Cosovic, V., Velic, I., & Maticec, D. (2012). *3. Topic Two: Promina Beds*.

Operta, M. (2006). Olovo, cink i barit u metalogenetskoj zoni Borovica-Vareš, VI Naučno-stručni simpozij sa meČunarodnim učešćem,„Metalni i nemetalni anorganski materijali “. *Zbornik Radova, Str*, 287–293.

Operta, M. (2014). *RUDNIRESURSIBOSNEIHERCEGOVINE-STANJE I PERSPEKTIVE perspektive MINING RESOURCES IN BOSNIA AND HERZEGOVINA-CONDITION AND PERSPECTIVES*.

Palinkaš, L. (n.d.). *Lead•Isotope Patterns in Galenas from some Selected Ore Deposits in Croatia and NW Bosnia*.

Palinkaš, L. A., Šoštarić, S. B., & Palinkaš, S. S. (2008). Metallogeny of the Northwestern and Central Dinarides and Southern Tisia. *Ore Geology Reviews*, *34*(3), 501–520. https://doi.org/10.1016/j.oregeorev.2008.05.006

Palinkaš, L. A., Strmić, S., Spangenberg, J., Prochaska, W., & Herlec, U. (2004). *Ore-forming fluids in the Grübler orebody, Idrija mercury deposit, Slovenia*.

Palinkaš, L., Bermanec, V., & Galović, L. (2016). The Alpine Wilson cycle and NW Tethyan Metallogeny. *Geologia Croatica*, *69*(1), 1–2. https://doi.org/10.4154/GC.2016.01

Pamić, J., Pamić, O., Olujić, J., Milojević, R., Veljković, D., & Kapeler, I. (1978). *Tumač osnovne geološke karte SFRJ M 1:100.000, list Vareš L 34-133 [Explanatory notes for basic geological map of SFR Yugoslavia in scale 1:100.000, sheet Vareš L 34-133 (in Serbo-Croatian)]. Institut za geologiju Sarajevo, Savezni geološki zavod Beograd*. 1–68. Scopus.

Ramović, M. (1955). Borovica kod Vareša, sedimentno leţište cinka, olova, barita i pirita. *Geološki Glasnik*, *1*.

Ramović, M. (1962). Studije metalogenetske zone Ozren-Vareš-Borovica tokom 1961. Godine. *Geološki Institut Sarajevo*.

Schmid, S. M., Bernoulli, D., Fügenschuh, B., Matenco, L., Schefer, S., Schuster, R., Tischler, M., & Ustaszewski, K. (2008). The Alpine-Carpathian-Dinaridic orogenic system: Correlation and evolution of tectonic units. *Swiss Journal of Geosciences*, *101*(1), 139–183. https://doi.org/10.1007/s00015-008-1247-3

Schmid, S. M., Fügenschuh, B., Kounov, A., Maţenco, L., Nievergelt, P., Oberhänsli, R., Pleuger, J., Schefer, S., Schuster, R., Tomljenović, B., Ustaszewski, K., & Van Hinsbergen, D. J. J. (2020). Tectonic units of the Alpine collision zone between Eastern Alps and western Turkey. *Gondwana Research*, *78*, 308–374. https://doi.org/10.1016/j.gr.2019.07.005

Scott, R. J., Meffre, S., Woodhead, J., Gilbert, S. E., Berry, R. F., & Emsbo, P. (2009). Development of Framboidal Pyrite During Diagenesis, Low-Grade Regional Metamorphism, and Hydrothermal Alteration. *Economic Geology*, *104*(8), 1143–1168. https://doi.org/10.2113/gsecongeo.104.8.1143

Trubelja, F. (1969). Petrološke karakteristike nekih tipova stijena na području Borovice kod Vareša. *Glasnik Zemaljskog Muzeja Sv*, *8*, 55–58.

Ustaszewski, K., Kounov, A., Schmid, S. M., Schaltegger, U., Krenn, E., Frank, W., & Fügenschuh, B. (2010). Evolution of the Adria-Europe plate boundary in the northern Dinarides: From continent-continent collision to back-arc extension: ADRIA-EUROPE PLATE BOUNDARY, DINARIDES. *Tectonics*, *29*(6), n/a-n/a. https://doi.org/10.1029/2010TC002668

Van Hinsbergen, D. J. J., Torsvik, T. H., Schmid, S. M., Maţenco, L. C., Maffione, M., Vissers, R. L. M., Gürer, D., & Spakman, W. (2020). Orogenic architecture of the Mediterranean region and kinematic reconstruction of its tectonic evolution since the Triassic. *Gondwana Research*, *81*, 79–229. https://doi.org/10.1016/j.gr.2019.07.009

Veljković, D. (1973). *Prilog poznavanju ležišta olovo-cinkamih ruda u zoni trijaskih sedimenata Borovica, Vareš, Čevljanovići*. *Geološki glasnik Sarajevo*(17), 269–291.

Veljković, D. (1989). Prilog poznavanju genetskih i paragenetskih karakteristika kompleksnih sulfidnih ruda olova, cinka i barita u zoni trijaskih sedimenata područja Vareša. *Zbornik Referata Naučnog Skupa" Minerali, Stijene i Izumrli Ţivi Svijet BiH", Sarajevo*, 73–85.

Wilkin, R. T., & Barnes, H. L. (1997). Formation processes of framboidal pyrite. *Geochimica et Cosmochimica Acta*, *61*(2), 323–339. https://doi.org/10.1016/S0016-7037(96)00320-1

Wilkin, R. T., Barnes, H. L., & Brantley, S. L. (1996). The size distribution of framboidal pyrite in modern sediments: An indicator of redox conditions. *Geochimica et Cosmochimica Acta*, *60*(20), 3897–3912. https://doi.org/10.1016/0016-7037(96)00209-8

Yao, X., Xia, F., Deditius, A. P., Brugger, J., Etschmann, B. E., Pearce, M. A., & Pring, A. (2020). The mechanism and kinetics of the transformation from marcasite to pyrite: In situ and ex situ experiments and geological implications. *Contributions to Mineralogy and Petrology*, *175*(3), 27. https://doi.org/10.1007/s00410-020-1665-4

Appendices

Appendix A

Table 4. Summarised descriptions of all samples prepared for microscopical analysis.

No	Sample ID	Lab-ID	Sample description - macroscopic	Mineral phases	Petrographical description - ore microscopy	Texture	Suppression	Ratios
1	NW-BR-21-22-04	2	Massive sulphides with coarse grained idiomorphic baryte blades	Galena, sphalerite, pyrite, sulfosalts, baryte	Fine grained masive sulphide mineralisation (<100µm). Py- multiple phases, idiomorphic grains (<50µm) suggest early crystallisation (Py1), colloform Py (>150µm) later stage, recrystalisation to Marcasite. Framboidal Py (<25µm) in veins and cavities, latest stage, overprinting. Gn - xenomorphic grains, <100µm. Also present as cavity infill , suggesting multiple stages of growth. Correlation with Py, sulfosalts, Sph "complexes" . Sph - hypidiomorphic to xenomorphic grains (100-200µm). Baryte - multiple stages present, from idiomorphic "blades" to massive xenomorphic grains suggesting a Baryte overprinting stage after massive sulphides crystallization. Idiomorphic blades present "inside" colloform pyrite, with Sulhpides crystalizing from the rim inwards the center of the blades, suggesting a recrystalizations of Brt. sulfosalts - xenomorphic grains, associated with Gn+Py1	Colloform Pyrite, Framboidal Pyrite	Gn+Sulph. Suppressing Py 1 (idiomorphic)	45% - Sph, 30%- Brt., 15%- Gn, 9%- Py, 1% -Sulph.
2	NW-BR-21-22-06	1	Dolomitic breccia with sulphide veins and veinlets	Galena, sphalerite, pyrite, sulfosalts, baryte, quartz	Massive baryte with coarse grained (>300µm) sulphide mineralisation and Qtz+Sph veins cross-cuting the primary mineralisation. Py - idiomorphic to xenomorphic grains, <200µm in size (around 50-85µm for idiomorphic, 100-200µm for xenomorphic). Gn - Hipdiomorphic to xenomorphic grains, 25-200µm in size. Association with sulfosalts and Py evident. Sph - 50-500µm hipidiomorhic to xenomorphic grains. Show association with Qtz in later stage overprinting veins. Shows inclusions of Brt, Py and Qtz. Sulhposalts - xenomorphic grains, associated with Gn+Py1	Colloform Pyrite, Framboidal Pyrite	Gn+Sulph. Suppressing Py 1 (idiomorphic). Gn suppressing Sph	40% - Brt, 25 %- Qtz, 15 % Sph, 10 % Py, 9% Gn, 1% sulfosalts

3	NW-BR-11-22-13	7	Upper zone of NW mineralisation, dolomitic breccia with sulphide veins	Pyrite, baryte, quartz, sphalerite, galena, sulfosalts, muscovite	Coarse grained (>1000µm) pyrite grains, idiomorphic to hipidiomorphic, dissolved with quartz rich fluid, with sulphide + baryte phases visible as the latest stage (Sph+Gn+ sulfosalts). Qtz grains xenomoprhic, with a size of around 50µm. Pyrite grains show signs of fracturing, with Brt as infill. Recrystallisation to marcasite is visible in almost every single pyrite grain (might be later stage). Gn and Sph rarely observed, grain size <40µm.	Colloform Pyrite, Framboidal Pyrite. Framboids may have formed as an earlier stage, with a progressive change in redox conditions causing the framboids to merge into colloids. Gn, Brt, and	Qtz suppressing Py 1, Gn+sph+Brt suppressing qtz and Py 1	50% - Qtz, 45% - Py, 2% - Brt, 2% - Sph, 1% - Gn
4	NW-BR-11-22-05	3	Massive mineralisation, baryte rich	Baryte, Cinnabar, Galena, Pyrite, reddish mineral (needs SEM-EDS)	Massive baryte sample, shows signs of multiple phases of growth (at least two). Idiomorphic to xenomorphic grains >200µm. Pyrite grains are xenomorphic, mostly <40µm. They show a connection with the later stage Brt phase, in the 1cm thich vein cutting across the whole sample. Heavy structural deformation observed, as the later stage baryte+ red mineral? grains completely brecciated. Cinnabar evident as xenomorphic grains, < 40µm in size.	Massive texture of Baryte. Sporadic framboids of pyrite present in the veins rich with baryte	Brt 1 suppressed by Brt 2 + Py 2	95% - Brt, 2 % - Cinnabar, 1% - Py,
5	NW-BR-11-22-06	4	Massive sulphides, with subordinate baryte	Baryte, sphalerite, galena, pyrite, sulfosalts	Massive baryte, xenomorphic to hipidiomorphic grains >200µm. Possible overprint of earlier massive sulphide mineralisation (Sph+Gn+Py+sulfosalts). Sph - grain size of 50-200µm, with xenomorphic to hipidiomorphic habitus. Compex intergrowth with Gn. Gn - hipidiomorphic to xenomorphic grains, ranging from 50-125 µm. Associated with Sph +/- Py. Py present in two phases, as framboidal and as idiomorphic grains, ranging from 20-80 µm.	Massive texture.	Sph+Gn suppressed by Brt 1	60% - Brt, 30% - Sph, 8% - Gn, 2% - Py, 1% - sulfosalts
6	NW-BR-11-22-16	11	Massive sulphides, minor baryte	Galena, sphalerite, chalcopyrite, pyrite, sulfosalts, baryte	Massive sulphides, with minor baryte. Baryte - xenomorphic to hipidiomorphic grains >200µm. Sph - grain size of 50-200µm, with xenomorphic to hipidiomorphic habitus. Complex intergrowth with Gn. Gn - hipidiomorphic to xenomorphic grains, ranging from 50-200 µm. Associated with Sph +/- Py. Py present in two phases, as framboidal and as idiomorphic grains, ranging from 20-80 µm, and exhibits colloform texture, with baryte inclusions (+/- sulfosalts, Sph, Gn) Cpy - fine grained (<50µm) xenomorphic grains, associated with Py1, Gn, sulfosalts.	Colloform pyrite, framboidal pyrite, massive texture	Gn and As-Sb-Ag sulfosalts, supressing Py1, Cpy, Sph	60% - Sph, 15% - Brt, 10% - Gn, 10% - Py, 5% - sulfosalts
7	NW-BR-11-22-10	5	Massive sulphides heavily tectonised and recrystalysed	Pyrite, marcasite, sphalerite, baryte, galena	Heavily tectonised sample, with cataclastic texture of pyrite grains, which are idiomorphic to hipidiomorphic (500-2000µm). Recrystallisation to marcasite evdent throughout the sample (pleochroism). Py 1 suppressed by the fluids rich in Brt+Sph (+/- Gn). Brt+Sph in veins most likely different times than Gn. Sph - hipidomorphic to xenomorphic grains 100-300µm. Baryte - hipidiomorphic to xenomorphic grains 50-250µm, with clear zonation of the veins, Sph internal, Brt external. Overprint of framboidal pyrite, with strict spatial distribution in the Brt-sulphide veins, later stage of crystalisation.	Cataclastic texture of Pyrite/marcasite grains, framboidal pyrite	Py 1 suppressed by Gn+Sph+Brt	95% - Py, 3% - Brt, 1% Sph, <1% - Gn
8	NW-BR-11-22-11	6	Coarse grained sulphide grains in shale matrix, heavily tectonised	Baryte, sphalerite, galena, pyrite, sulfosalts, chaclopyrite	Coarse grained Sph+Gn+Brt (> 500 µm), brecciated, infill with organic matter as a result of tectonic activity. Sph --- 200-2000 µm grain size, xenomorphic to hipidiomorphic habitus. Shows inclusions of Cpy, Py and Brt. Brt - grains 30-2000 µm size, showing signs of multi stage mineralisation, one coarser grained (500-2000 µm), one finer grained (30-200 µm). Gn - xenomorphic to hipidiomorphic grains 50-300 µm in size. Some grains showing signs of ductile deformation as a later stage. Py - idiomorphic to xenomorphic grains, multi stage development, with framobidal pyrite as a later stage (infill). Grain size - 20-100 µm. sulfosalts - 10-100 µm, xenomorphic grains, associated with Py1, Gn, Sph. Cpy - , 20 - 100 µm grain size, as inclusion in Sph.	Framboidal pyrite	Gn and As-Sb-Ag sulfosalts, supressing Py1, Cpy, Sph	75% - Brt, 15% - Sph, 7% - Gn, 2% - Py, 1% - sulfosalts

9	MOB-BRD-27-22-13	15	Massive sulphides with carbonate veins as overprints	Baryte, sphalerite, quartz, galena, pyrite, chalcopyrite, sulfosalts	Coarse grained sulfides Gn+Sph, minor Py, Cpy, Sulfosalts, (>1000 µm). Sample heavily brecciated, with all grains exibiting fractures. Gn - 500-2000 µm hipidiomorphic to xenomorphic grains, exhibiting trianuglar pits, and showing signs of ductile deformation, after the main mineralisation stage. Sph - 500 - 2500 µm xenomorphic grains, heavily brecciated. Inclusions of Brt present. Brt - 200 - 1000 µm xenomorphic grains, same stage as Sph, simultaneous. Qtz - infill between the grains, appears to be after the Brt + Sph stage. Xenomorphic grains ranging from 100-500 µm. Sulfosalts - hipidomorphic to xenomorphic habitus, 100-250 µm in size. Associated with Py1, Cpy, Gn, +/- Sph. Py - idomorphic to xenomorphic habitus, multi stage development. Idiomorphic appears to be the earliest, with framboidal being later stage. Framboids associated with veins and veinlets. Cpy - xenomorphic habitus, 50 - 200 µm. Rarely observed in the sample, associated with the Gn+Sulfos.+Py1+Sph "complexes". Observed as inclusions in Sph (< 50 µm).	Framboidal Pyrite, Brecciation	Gn and As-Sb-Ag sulfosalts, supressing Py1, Cpy, Sph	50% Sph, 20 % Brt, 15 % Gn, 10% Qtz, 2% Sulfosalts, 2 % Py, 1 % Cpy
10	MOB-BRD-27-22-20	8	Massive baryte, with minor sulphides	Baryte, sphalerite, quartz, pyrite, galena, chalcopyrite, sulfosalts	Massive sulfide sample, generally finner compared to previous samples (<200 µm). Py - multi stage development, idiomorphic to xenomorphic grains 50 - 350 µm in size. Idiomorphic grains appear to be an early stage of mineralisation, with colloidal and framboidal froms forming in a later stage (overprint). Gn - xenomorphic grains, 10-100 µm in size. Associated with sulfosalts, Py 1 (idiomorphic) +/- Cpy +Sph+Brt. Sph - 50- 300 µm grains, xenomorphic habitus. Appear to be formed in the same time as Brt phase	Massive texture, framobidal pyrite and colloidal pyrite.	Gn and As-Sb-Ag sulfosalts, supressing Py1, Cpy, Sph. Brt supressing Galena and sulfosalts,	60% Brt, 25 % Py, 8% Sph, 5 % Gn, 1 % Sulfosalts, 1% Cpy
11	MOB-BRD-27-22-23	16	Dolomitic breccia (clast supported) with massive sulphide mineralisation as stockwerk	Pyrite, marcasite, baryte, sphalerite, sulfosalts, chalcopyrite, galena,	Heavily structurally deformed sample, with coarse grained pyrite/marcasite grains (1000-2500 µm). Grains hipidomorphic to xenomorphic, with Py 1 exhibiting idiomorphic habitus. Gn+Sph+Cpy+Sulfosalts - complexes, usually found together. Idiomorphic Py 1 - grains ranging from 80 µm to 150 µm. Gn - ranges from 50 to 500 µm in size, with xenomorphic habitus. Sphalerite obsrved in association with Gn and Brt. Sulfosalts - idiomorphic to xenomorhic. Zonation present in sulfosalts.	Brecciation, colloidal pyrite, framobidal pyrite.	Gn and sulfosalts, supressing Py1, Cpy, Sph. Brt supressing Galena and sulfosalts,	50 % Py(Marc), Brt - 30 %, 8 % Sulfosalts, 8% Sph, 3% Gn, 4 %

12	MOB-BR-49-19-12	12	Dolomitic breccia with massive Py+sulfosalts	Sulfosalts, chalcopyrite, pyrite, galena, sphalerite, baryte, rhodocrosite	Massive sulphides with a rhodocrosite? Vein cross cutting the sample, most likely as a phase after the main mineralisation. Py - observed as idiomorphic to xenomorphic grains - 40- 2000 µm in size. Idiomorphic grains represrnt earliest stage of mineralisation, Py 1, while the colloidal and framboidal pyrites are most likely an after-event, not related with the main mineralising stage. Brecciation evident, likely the result of tectonic activity that hapened in the more recent geodynamic evolution. Cpy - xenomorphic grains 100-1000 µm in size. Associated with sulfosalts and rarely galena (different compared to previous samples). Sulfosalts - xenomorphic grains, massive, with a size of 80-1000 µm. Gn - xenomorphic habitus, 50-200 µm in size. Sph - xenmorphic, with a size of 50-150 µm.	Brecciation, massive texture, collodial pyrite, framboidal pyrite.	Gn and sulfosalts, supressing Py1, Cpy, Sph. Brt supressing Galena and sulfosalts	40 % Brt, 20 % Rhodo., 15 % Sulfosalts, 15 % Cpy, 5 % Py, 3% Gn, 2 % Sph
13	MOB-BR-49-19-13	9	Massive sulphides - Sph+Py+Gn+Cpy, minor Brt	Sphalerite, galena, baryte, chalcopyrite, pyrite, sulfosalts	Massive sulphide sample. Dominantly sphalerite rich, with lesser baryte, galena and cpy+sulfosalts+py. Sph - hipidiomorphic to xenomorphic habitus, with a size of 200-3000 µm. Gn - xenomorphic grains, mostly massive. Appears to fill in the space between Sph grains, with a size of 50-400 µm. Baryte - xenomorphic grains up to 1000 µm in size. Filling the space between massive sulphides. Sulfosalts - associated with Py 1+/-Cpy+Gn. Xenomorphic in habitus, 40-100 µm.	Massive texture	Gn and sulfosalts, supressing Py1, Cpy, Sph. Brt supressing Galena and sulfosalts	65 % Sph, 15 % Gn, 10 % Brt, 6 % Cpy, 3 % Py, 1 % Sulfosalts
14	MOB-BR-49-19-15	13	Massive sulphides - Sph+Gn+Py - increase of Brt	Sphalerite, galena, baryte, pyrite, chalcopyrite, sulfosalts	Massive sulphide sample. Dominantly sphalerite rich, but baryte content is increasing. Sph - hipidiomorphic to xenomorphic habitus, with a size of 50- 500 µm. Gn - xenomorphic grains, mostly massive. Appears to fill in the space between Sph grains. Py - idiomorphic to xenomorphic, with a size between 30-400 µm. Two generations of Py are observed, idiomorphic, Py 1, most likely earlier stage of mineralisation, and Py 2, xenomorphic, formed in as intergrowth with Cpy+Gn+Sulfosalts complexes. Also present as inclusions on Sph. Cpy - 50 - 200 µm, xenomorphic habitus. Sulfosalts - 10-50 µm in size, xenomorphic grains.	Massive texture, brecciation - hydrothermal, colloidal pyrite, framboidal pyrite	Gn and sulfosalts, supressing Py1, Cpy, Sph. Brt supressing Galena and sulfosalts	40 % Sph, 25% Gn, 20 % Brt., 10% Py, 3 % Cpy, 2 % Sulfosalts
15	MOB-BR-49-19-16	10	Massive sulphides - Sph+Gn+Py - baryte rich	Baryte, sphalerite, galena, chalcopyrite, pyrite, sulfosalts	Massive baryte dominated sample, with finer grained (<200 µm) sulphides. Baryte - massive, later stage of mineralisation, overprinting the massive sulphides. Sph - xenomorphic to hipidiomorphic habitus, 50-300 µm in size. Gn - 25 - 250 µm, xenomorphic to hipidiomorphic habitus. Associated with Sph+Cpy+Py+Sulfosalts. Possible zonation in a sulphide vein, going from Sph-Gn-Cpy+Py+Sulfosalts inwards. Py - possible two phasae development, with idiomorphic grains being earler, and xenomorphic being in the main ore phase, together with Gn+sulfosalts (+Sph?). Generally <100 µm in size.	Massive texture	Gn and sulfosalts, supressing Py1, Cpy, Sph. Brt supressing Galena and sulfosalts	50 % Brt, 40 % Sph, 5 % Gn, 3 % Py, 1% Cpy, <1% Sulfosalts
16	MOB-BR-49-19-17	14	Massive sulphides, baryte rich, fine grained	Baryte, sphalerite, galena, chalcopyrite, pyrite, sulfosalts	Massive sulphides, with minor baryte. Baryte - xenomorphic to hipidiomorphic grains >200µm. Sph - grain size of 50-200µm, with xenomorphic to hipidiomorphic habitus. Complex intergrowth with Gn. Gn - hipidiomorphic to xenomorphic grains, ranging from 50-200 µm. Associated with Sph +/- Py. Py present in two phases, as framboidal and as idiomorphic grains, ranging from 20-80 µm, and exhibits colloform texture, with baryte inclusions (+/- sulfosalts, Sph, Gn) Cpy - fine grained (<50µm) xenomorphic grains, associated with Py1, Gn, sulfosalts. Sulfosalts - fine grained, xenomorphic (20-150 µm)	Massive texture	Gn and sulfosalts, supressing Py1, Cpy, Sph. Brt supressing Galena and sulfosalts	40 % Sph,35 % Brt., 20% Gn, 5% Py, <1% Sulfosalts

Appendix B

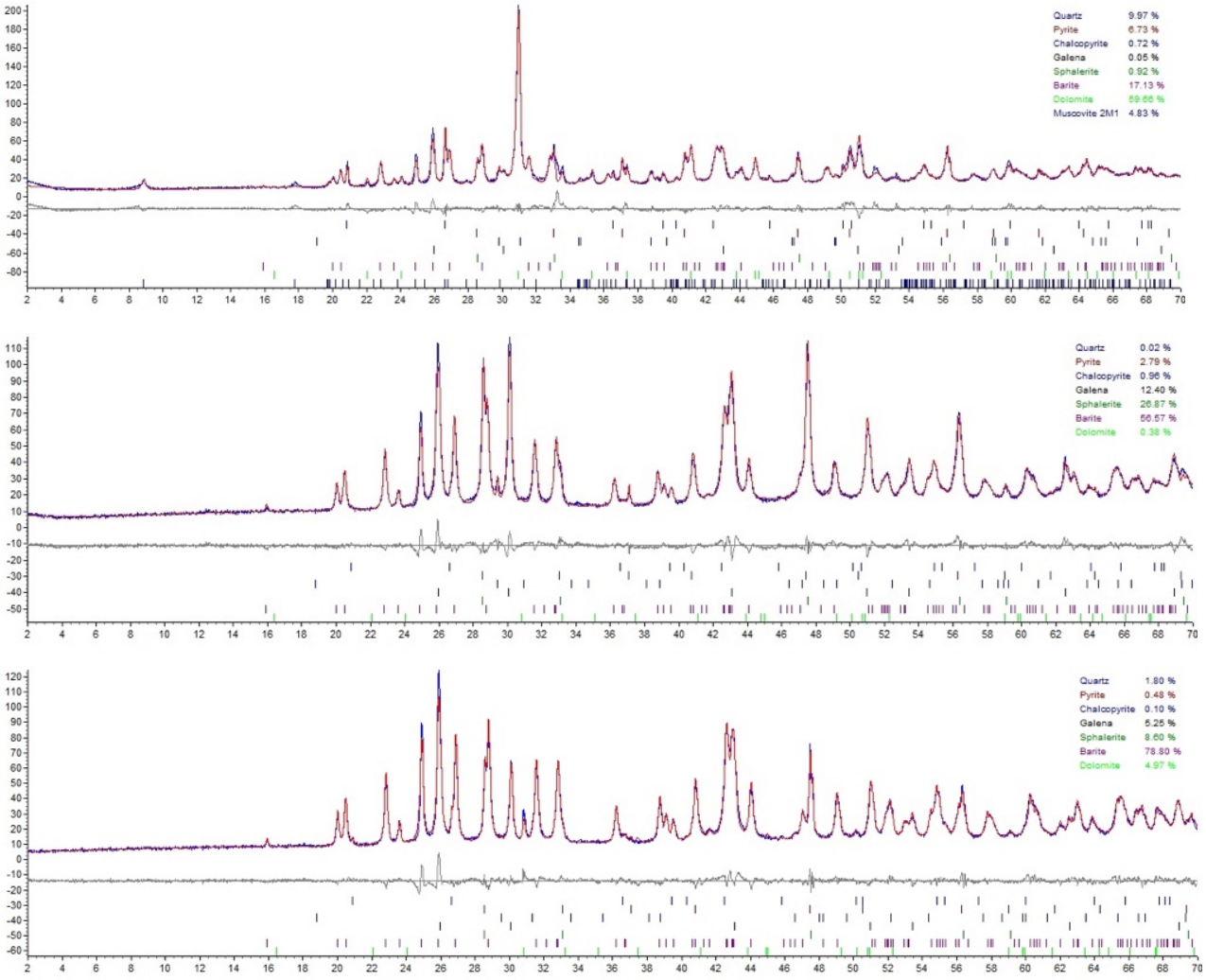

Figure 42. XRD spectra for three composite samples, IVC 1 (TOP), IVC 3(BOTTOM)

Appendix C

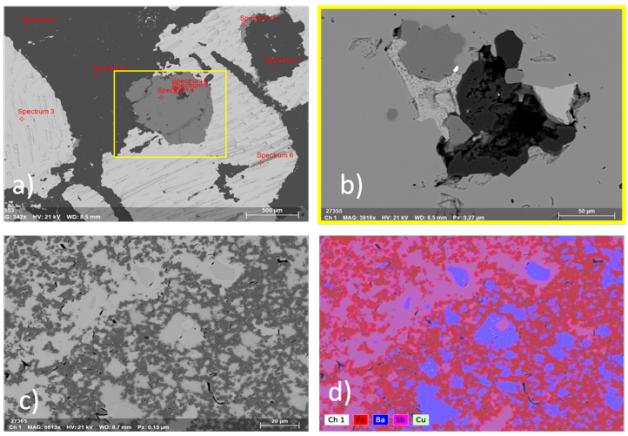

Figure 43. Dolomitic breccia sulphide ore type, Ore microscopy pictures (LEFT), SEM-BSE image (CENTRE), SEM-EDS elemental map (RIGHT).

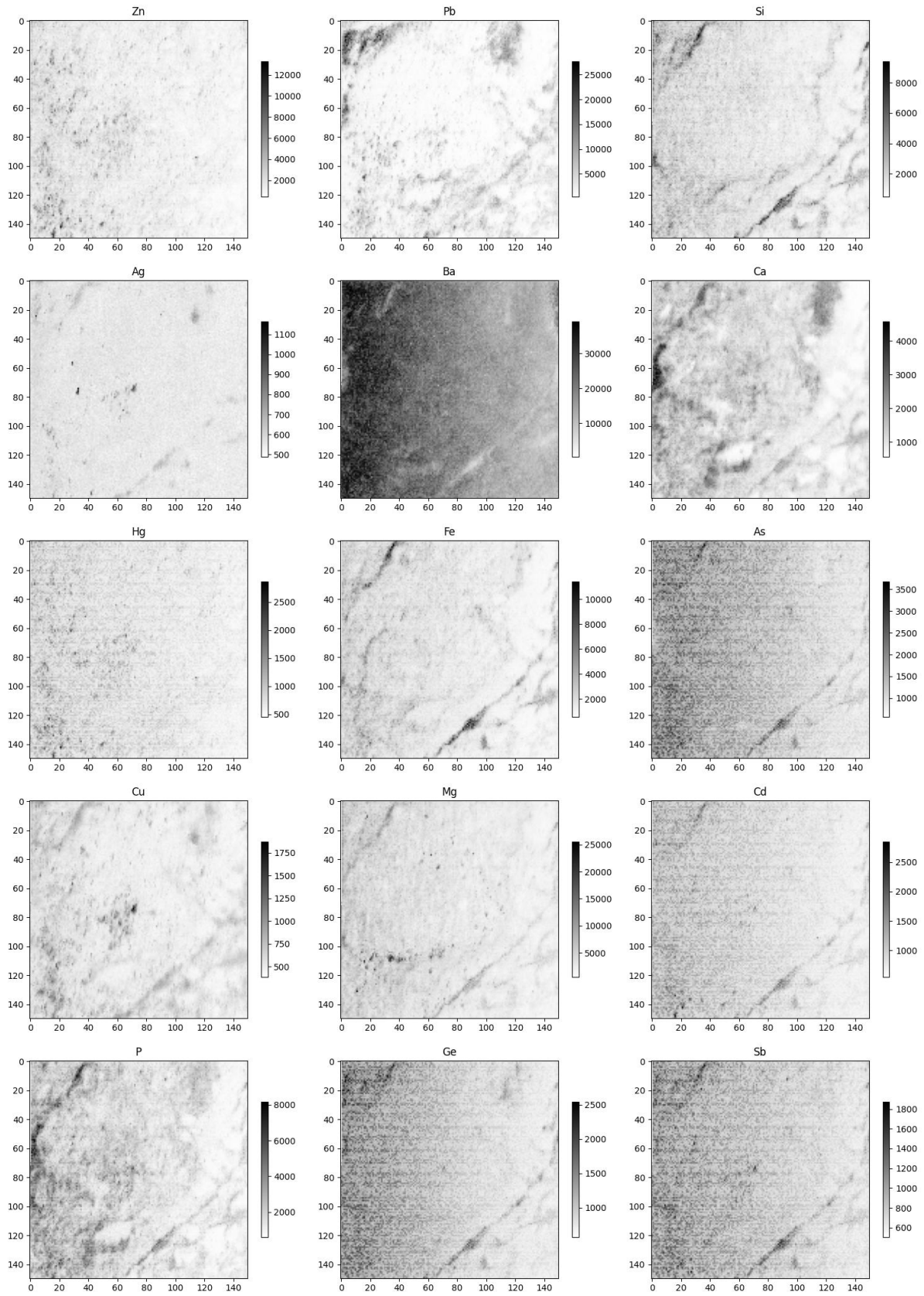

Figure 44. Elemental maps for the dolomite breccia ore type, sample BRD-27-22-20, a) Zn Pb Si, b) Ag Ba Ca, c) Hg Fe As, d) Cu, Mg, Cd, e) P Ge Sb

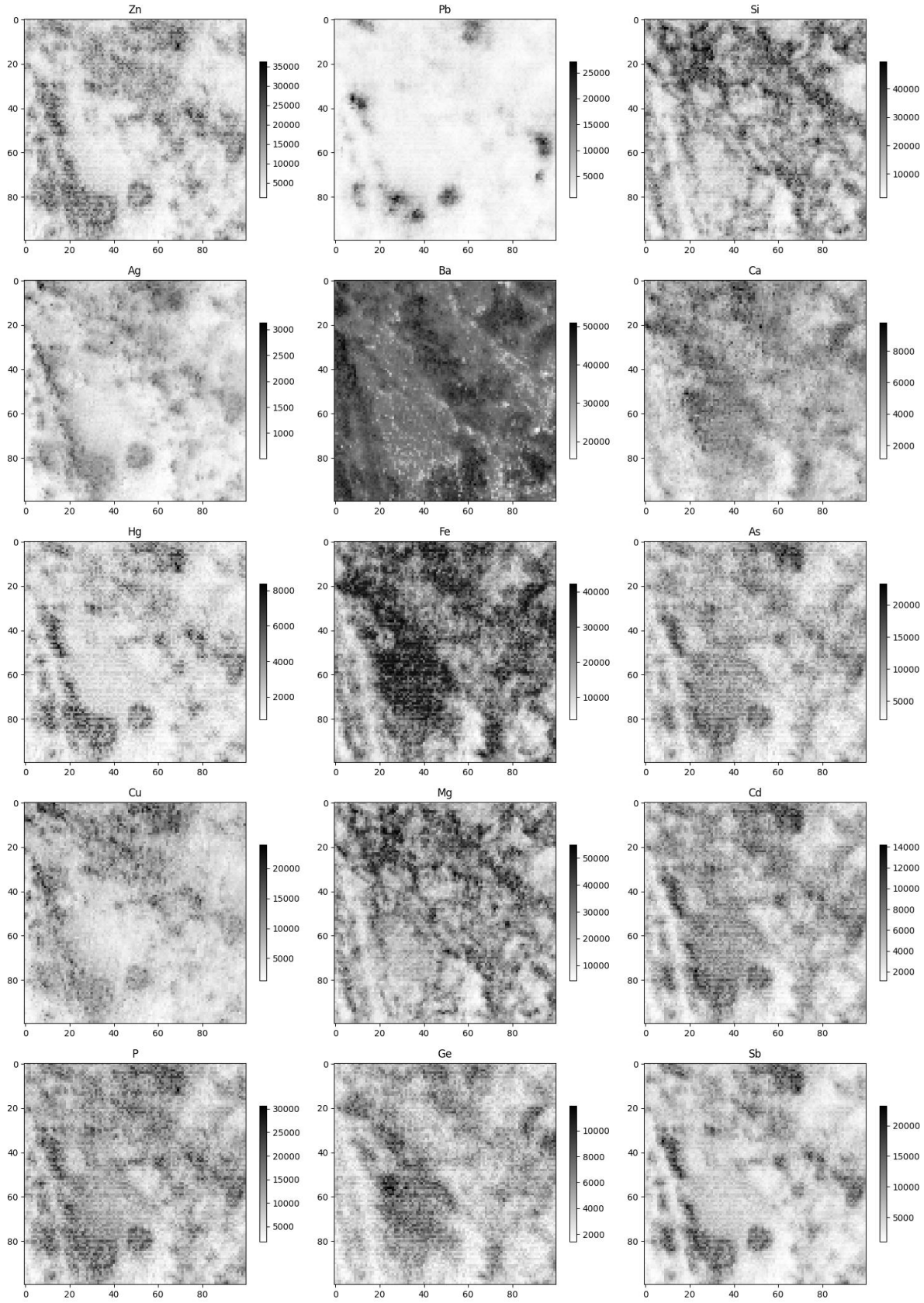

Figure 45. Elemental maps for the dolomite breccia ore type, sample BRD-27-22-21, a) Zn Pb Si, b) Ag Ba Ca, c) Hg Fe As, d) Cu, Mg, Cd, e) P Ge Sb

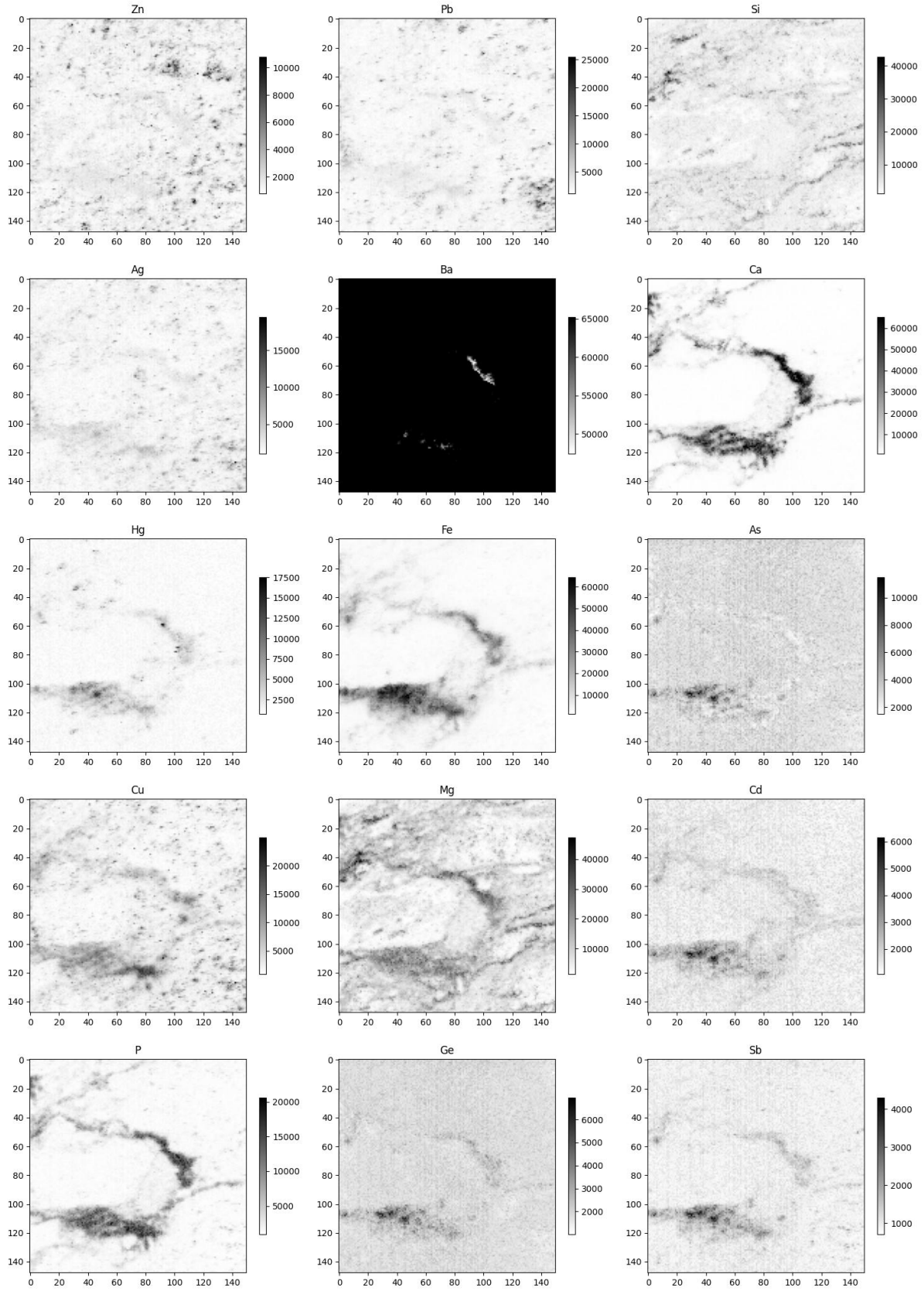

Figure 46. Elemental maps for the dolomite breccia ore type, sample BR-11-22-05, a) Zn Pb Si, b) Ag Ba Ca, c) Hg Fe As, d) Cu, Mg, Cd, e) P Ge Sb

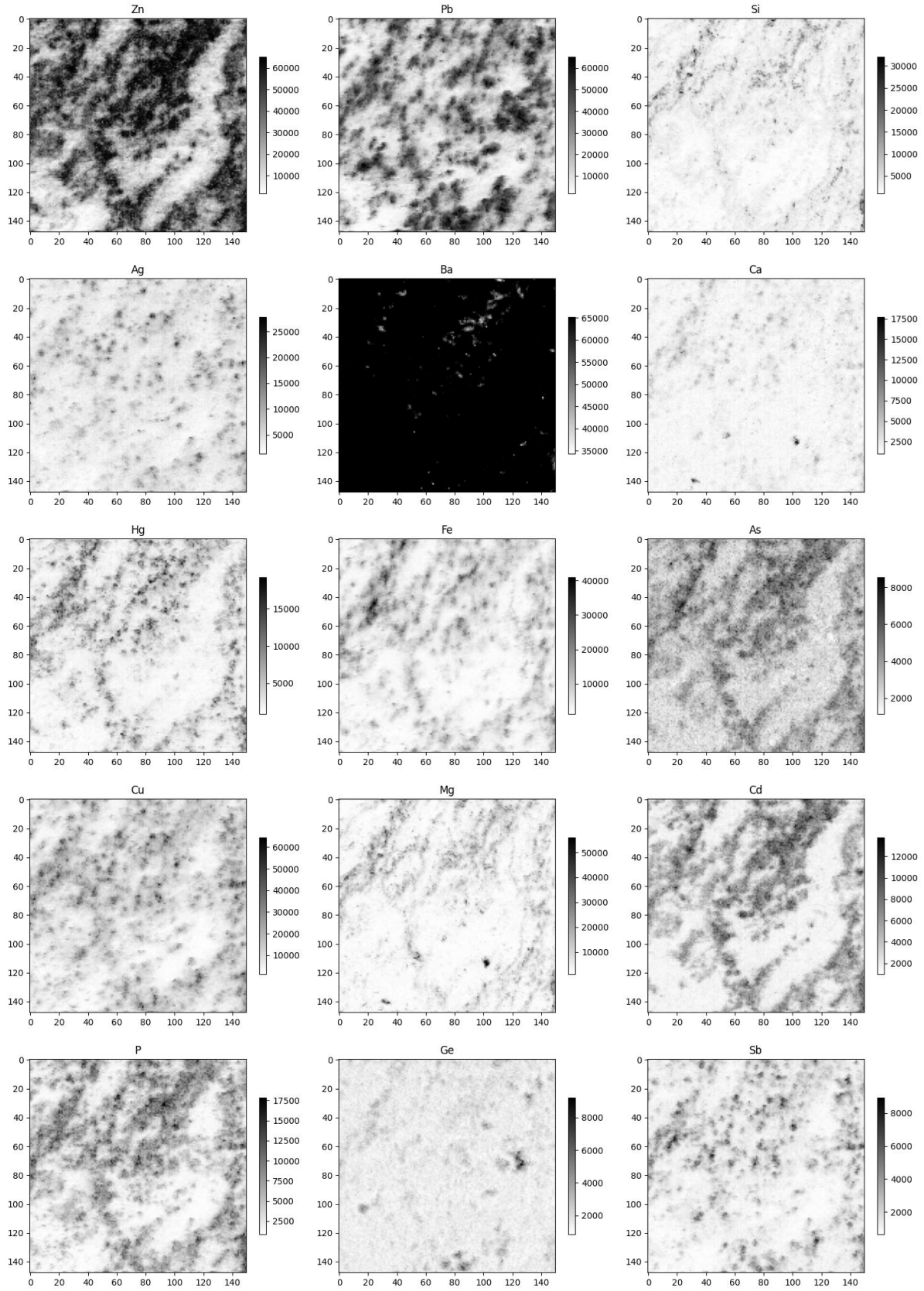

Figure 47Elemental maps for the dolomite breccia ore type, sample BRD-11-22-06, a) Zn Pb Si, b) Ag Ba Ca, c) Hg Fe As, d) Cu, Mg, Cd, e) P Ge Sb